Snow Accumulation in a Distributed Hydrological Model

by

Bruce Davison

A thesis
presented to the University of Waterloo
in fulfillment of the
thesis requirement for the degree of
Master of Applied Science
in
Civil Engineering

Waterloo, Ontario, Canada, 2003

I hereby declare that I am the sole author of this thesis. This is a true copy of the thesis, including any required final revisions, as accepted by my examiners.

I understand that my thesis may be made electronically available to the public.

Bruce Davison

ABSTRACT

The cryosphere is defined as the portions of the earth where water is in solid form. It represents a very important part of the hydrologic cycle, affecting ecological, human and climate systems. A number of component models describing the energy and mass balances of a snowpack have been developed and these component models are finding their way into watershed models and land surface schemes. The purpose of this thesis is to examine the incorporation of a number of snow processes in the coupled land-surface-hydrological model WATCLASS.

The processes under consideration were mixed precipitation, variable fresh snow density, maximum snowpack density, canopy interception and snow-covered area (SCA). The first four of these processes were based on similar work done by Fassnacht (2000) on a watershed in Southern Ontario. In the case of this thesis, the work was completed on a basin in Northern Manitoba. A theory of the relationship between snow-covered area and average snow depth was developed and an algorithm was developed to implement this theory in WATCLASS. Of the five snow processes considered, mixed precipitation was found to have the greatest impact on streamflow while the new canopy interception algorithm was found to have the greatest impact on sensible and latent heat fluxes. The development of a new relationship between SCA and average snow depth was found to have a minimal impact in one study case, but a significant impact on the sensible and latent heat fluxes when snow fell on a pack that had begun to melt and was partially free of snow. Further study of these snow processes in land-surface-hydrologic models is recommended.

ACKNOWLEDGEMENTS

To the sculptors of the world

Ozymandias

I met a traveller from an antique land
Who said: "Two vast and trunkless legs of stone
Stand in the desert. Near them on the sand,
Half sunk, a shattered visage lies, whose frown,
And wrinkled lip, and sneer of cold command,
Tell that its sculptor well those passions read
Which yet survive, stamped on these lifeless things,
The hand that mocked them, and the heart that fed.
And on the pedestal these words appear:
'My name is Ozymandias, King of Kings:
Look upon my works, ye Mighty, and despair!'
Nothing besides remains. Round the decay
Of that colossal wreck, boundless and bare
The lone and level sands stretch far away."

Percy Bysshe Shelley

TABLE OF CONTENTS

LIST OF FIGURES

LIST OF TABLES

LIST OF EQUATIONS

1. Introduction

This thesis is a modelling study of snow representation in a distributed hydrological model. Chapter 1 provides a context for the thesis modelling study by introducing the hydrologic cycle, hydrological modelling, and the significance of snow. The importance of snow in ecological, climate and human systems is discussed. Chapter 2 examines the mathematical water and energy balance models developed to describe physical snow processes. Chapter 3 examines the effects of a number of new snow process component models in the physically based land-surface-hydrological model. Due to the nature of the model used, the modelled watershed responses are examined in greater detail than previously possible. Chapter 4 examines one particular snow process –the relationship between average snow depth and snowcovered area– in detail. A new method of handling this relationship is developed and analyzed. Chapter 5 provides some conclusions and recommendations.

1.1 The Hydrologic Cycle

The hydrologic cycle is a complex process involving the storage and movement of water. Ocean-currents carry water around the globe. The sun's energy evaporates water from water bodies and the land surface, transporting it to the atmosphere where air currents carry it around the globe. Snow falls in the mountains, and northern and southern latitudes. Glaciers run like slow rivers across the continents. Rain percolates into the ground, joining huge underground reservoirs in their slow march through the soil. Icicles form and melt from their precipices. Rivers fill with groundwater, interflow and overland flow from the rain or snowmelt, running to lakes, seas and oceans with their loads of sediment carved from the landscape. Living organisms consume water, transporting it through their stems or bodies for use in their cells. The consumed water is then expelled mainly through transpiration. Some water stays in one location for long periods of time, other water is transported across vast areas, moving relatively quickly, changing form time and time again. Figure 1-1 illustrates the water cycle with a special emphasis on snow and ice processes.
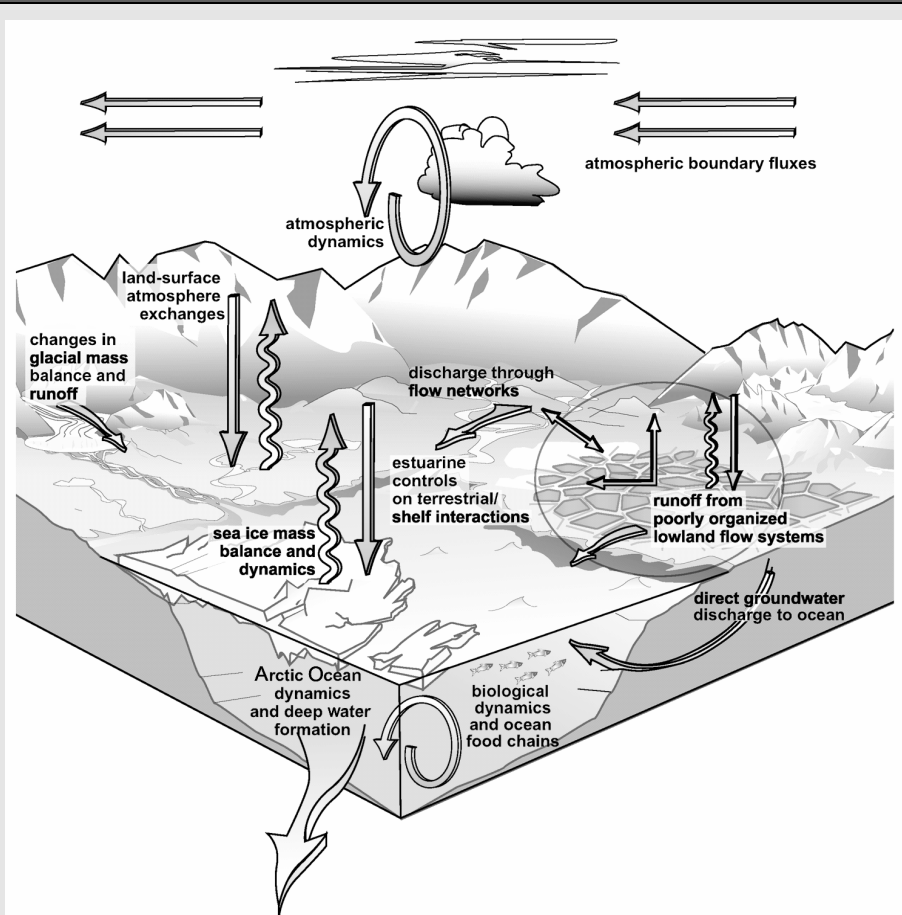
Figure 1-1: The water cycle emphasizing snow and ice processes. (Vörösmarty *et al.* 2001)

One of the main driving forces behind the movement of water is the energy from the sun, which causes water to evaporate and snow to melt and sublimate. The energy cycle is inextricably linked with the water cycle because gaseous, liquid and solid water store energy as latent heat. The hydrologic cycle is constantly changing as the energy cycle changes across geological time-periods. When the earth is warmer, more energy permeates the system and a greater amount of liquid water is moving around the globe. When the earth is cooler, ice-sheets cover the land, tying up water and slowing the entire cycle. It is speculated that the amount of water on the earth is constantly increasing as snow from space enters the atmosphere (Frank and Sigwarth 2001), adding an estimated two to three centimeters of water over the entire earth every twenty thousand years (Kluger 1997).

The current balance of water on Earth --the world's water stocks-- have been estimated by Shiklomanov (1993). According to these calculations, the oceans contain 96.54% of the Earth's water, while the remaining 3.46% can be found in glaciers and permanent snowcover, groundwater, ground ice and permafrost, lakes, soil moisture, atmosphere water vapor, marshes, wetlands, rivers, and biota. Glaciers, permanent snowcover and groundwater contain 98.76% of the fresh water, leaving 1.24% for the land-surface and atmosphere. Table 1-1 shows the breakdown of the planet's water stocks.

Table 1-1: The Earth's Water Stocks (Shiklomanov 1993)

	Volume (100 km^3)	Percentage of Total Water	Percentage of Total Fresh Water
Salt water stocks			
Oceans	1,338,000	96.54	
Saline/brackish groundwater	12,870	0.93	
Saltwater Lakes	85	0.006	
Freshwater Stocks			
Glaciers, permanent snowcover	24,064	1.74	68.70
Fresh groundwater	10,530	0.76	30.06
Ground ice, permafrost	300	0.022	0.86
Freshwater lakes	91	0.007	0.26
Soil moisture	16.5	0.001	0.05
Atmospheric water vapor	12.9	0.001	0.04
Marshes, wetlands [a]	11.5	0.001	0.03
Rivers	2.12	0.0002	0.006
Incorporated in biota	1.12	0.0001	0.003
Total Water on Earth (1000 km^3)	1,386,000	100	
Total Fresh Water on Earth (1000 km^3)	35,029		100

[a] Marshes, wetlands, and water in biota are often mixed salt and fresh water.

Physically, chemically and biologically interacting with the environment, water has an enormous impact on many aspects of life. The physical structure of the earth is altered as water moves through the landscape. Chemical reactions result when water inter-mingles with other matter. Biological communities live, adjust and die depending on the water cycle. Human economies are strongly dependent on the movement, or lack of movement, of water. The impact of irrigation and electrical generating capacity has changed the way many of us live (Reisner 1986, Postel 1999). Floods and droughts can cause havoc for human societies. Conflict and tension over water resources has a long history, even in recorded history (Gleick 2002). Recent fears of climate change have implications for the hydrologic cycle, and the biologic communities that depend on the current nature of the water cycle. Humans have been studying and altering the

hydrological cycle for centuries. A number of publications can be found on the history of ancient and modern land-surface hydrology. (Meinzer 1949, Rouse and Ince 1957, Krynine 1960, Jones *et al.* 1963, Biswas 1970, Nace 1974, Singh and Woolhiser 2002) and a number of texts also include a brief history (Dingman 1994, Viessman and Lewis 1996).

1.2 Hydrologic Modelling

Traditionally, different groups of scientists and practitioners have modelled different aspects of the water cycle, focusing on the atmosphere, oceans, watersheds and groundwater. These groups have been developing their models relatively independently of one-another. Due to the natural integration of the hydrological cycle, each group has needed to develop methods of characterizing the hydrology at the "boundaries" of their specific field. These boundaries tend to overlap from one discipline to the next and much of the recent activity in these communities has revolved around working together to integrate the modelling efforts. One difficulty with this approach, however, has resulted from the fact that the different communities have developed different languages to describe the same natural hydrologic boundaries. The resulting confusion has made it difficult to integrate the models effectively. This sub-section is meant to provide some background to hydrologic modelling, focusing on physically-based watershed modelling, touching on physically-based atmospheric modelling, and briefly discussing current trends in coupled land-surface-atmospheric modelling. Figure 1-2 (Chow *et al.* 1988) presents one classification of hydrologic (watershed) models.

Figure 1-2: A Classification of Watershed Hydrologic Models

4
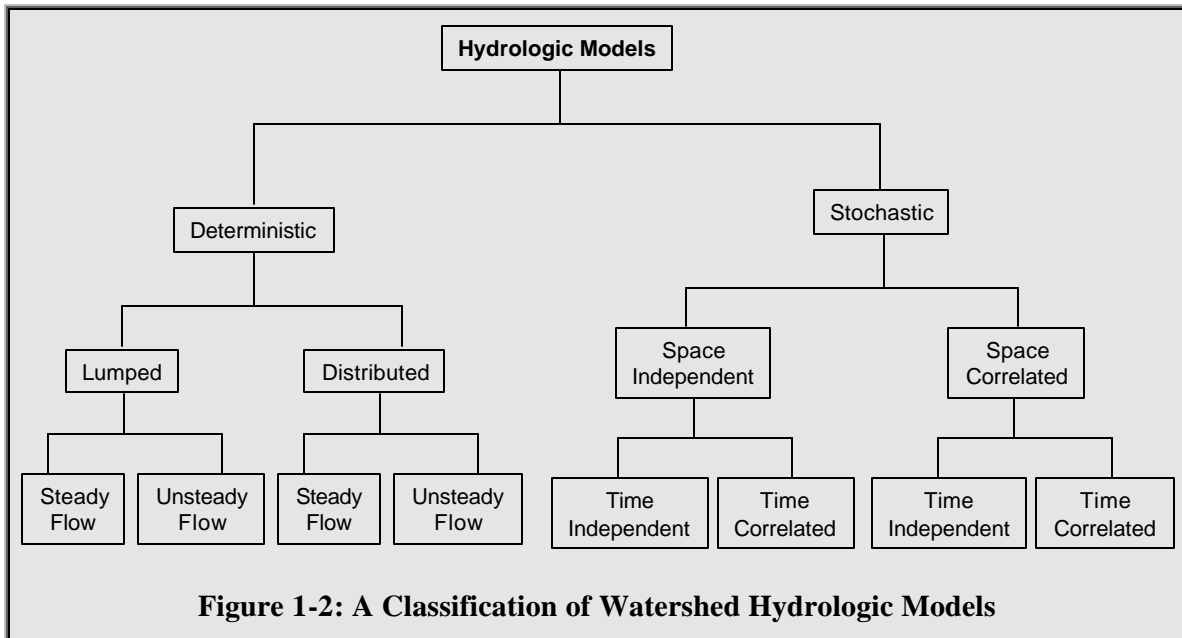
The first level of separation between the watershed models depends on whether or not the model includes randomness in its calculations. A given deterministic model will always produce the same output given a particular input. Stochastic models, however, incorporate the statistical nature of hydrology in their analysis. The second level of separation splits the models based on their ability to handle spatial variation. Lumped models spatially average the variables while distributed models consider the spatial distribution of the variables. The third level of separation considers the handling of time variation within a model. Deterministic watershed models consider whether or not the flow changes with time (unsteady) or not (steady). Stochastic model output always varies with time, but time-dependent models consider that one event is correlated with the nearby events (temporally speaking), while time-independent models do not make such a consideration. In the field of deterministic modelling, recent efforts are focused towards developing physically-based models, which try to mimic natural processes as closely as possible. Lumped models are limited in their ability to achieve this physically-based goal because of the spatial averaging necessary for the variables.

In the movement towards physically based models, scientists first developed mathematical component models in the late 1800s and 1900s, describing very specific parts of the hydrologic cycle at the land surface and in the atmosphere. These component models provided a solid base for the more comprehensive computer-based watershed and global circulation models beginning to appear in the 1950s and 60s. The first computer model of the atmosphere arrived in 1950 through the efforts of John von Neumann and Jule Charney (Stevens 2001). The first computer watershed model came on the scene in 1966, with the work of Crawford and Linsley and the Stanford Watershed Model (Singh and Woolhiser 2002).

These computer models were the earliest attempts to combine different components of the water-cycle into a more comprehensive deterministic framework. The result was a series of computer models that simulate different sub-cycles of the water cycle, such as groundwater, ocean-currents, global atmospheric circulation and land-surface watershed hydrology. The current status of computer modelling of the overall hydrologic cycle still falls short of bringing these models together into an overall, comprehensive and global representation of the water cycle.

1.2.1 Watershed Modelling

The use of mathematical hydrologic models is relatively recent, beginning late in the nineteenth century and derived out of a need of the civil engineering challenges of industrialized societies (Singh and Woolhiser 2002), just as the earliest water management structures were built in response to the engineering challenges facing agricultural societies. Early hydrologic models considered individual components of the water cycle. The first such empirical model was the rational method, developed by Mulvany (1850) for estimating peak runoff. This model is still in use today. In the years and decades that followed, a multitude of mathematical models were developed to describe specific components of the hydrologic cycle.

Computer development in the 1960's revolutionized hydrologic modelling and made it possible to integrate component models into more comprehensive watershed models. The resulting boom in computer-based mathematical hydrologic modelling lead to a plethora of models, too numerous to describe in this introduction. Singh and Frevert (2002[a,b]) describes a multitude of these models in two large volumes, 'Mathematical Models of Large Watershed Hydrology' and 'Mathematical Models of Small Watershed Hydrology Applications.' One Canadian hydrologic model is WATFLOOD, developed at the University of Waterloo (Kouwen and Mousavi 2002).

1.2.2 Atmospheric Modelling

The first to attempt a numerical prediction of the weather was done by Lewis Fry Richardson around 1920. The lack of computational power at the time secured the failure of Richardson's attempt, but he laid the groundwork for computer modelling of the atmosphere. Richardson's failure dissuaded others from following the same path until John von Neumann and Jule Charney teamed up to produce the first computer simulation of the weather in 1950, sparking a revolution in weather prediction that still permeates operational meteorology today.

The first Global Circulation Models (GCMs) created by the atmospheric community needed some representation of the land and ocean to provide the appropriate inputs to simulate atmospheric hydrology. These early representations of non-atmospheric hydrologic sub-cycles first appeared in the late 1960s (Manabe 1969) and were very simple for computational efficiency. In the 1980s, most GCMs had a representation of the land surface as described by Carson (1982). The soil heat capacity was zero while the ground heat flux was equal to a constant fraction of the net surface radiation. Soil heat storage took after Deardorff (1978) and the surface moisture took after Manabe's bucket model (1969). Vegetation was not separate from the soil, except that it altered the surface roughness and albedo. Snow was also lumped with the soil; with the added

characteristics of providing extra water storage and altering the energy balance through differing albedo and surface heat capacity. These land surface schemes (LSS's) are often referred to as the first generation LSS's.

1.2.3 Coupled Land-Atmosphere Modelling

The limitations of the first generation LSS's were becoming apparent in the 1980s. Studies by Dickenson (1984), and later by Verseghy (1996), illustrated some of these problems, especially in the handling of evaporation and transpiration. GCMs were also finding a new utility in longer-term climate change studies which were often focused on the implications of climate at the land surface (e.g. Boer *et al.* 1992). The desire to improve atmospheric simulations has motivated further improvements in computer modelling, specifically in relation to the handling of the land surface. The response was to develop second generation LSS's with improved physical representations of the soil water and energy budgets, as well as better vegetation models. The first two models to incorporate these improved physics were the Biosphere-Atmosphere Transfer Scheme (BATS) (Dickenson *et al.* 1986) and the Simple Biosphere scheme (SiB) (Sellers *et al.* 1986).

In Canada, the development of a second generation land surface scheme began in 1987 with the Canadian Land Surface Scheme (CLASS) (Verseghy 2000). CLASS is characteristic of a sophisticated second generation LSS's, incorporating a more detailed physical representation of the vertical energy and water budgets on the land surface. The original framework for CLASS was incorporated into the Canadian GCM. This would improve the vertical water and energy budgets for the GCM, while still ignoring the horizontal land surface water budget. To fill this gap, the hydrologic model WATFLOOD, with its lateral surface and sub-surface water flows, was included in the overall modelling strategy for Canada.

Figure 1-3 illustrates the overall strategy with respect to the coupling of land surface models with GCMs. This strategy has four levels. Level zero is the one-way forcing of WATFLOOD directly with the output from two Canadian GCMs, the Global Environmental Multi-scale Model (GEM) and the Regional Climate Model (RCM). Level one is the use of the coupled CLASS-GCM models to provide WATFLOOD with precipitation. Level one would presumably produce better results than level zero because feedback would be incorporated into the coupled atmospheric, land surface model. Level two is the use of a coupled WATFLOOD-CLASS model, also known as WATCLASS, forced by the output from the CLASS-GCM models. Level three would be the coupling of all three model types to incorporate feedback throughout the system.

Figure 1-3: Canada's Model Coupling Strategy
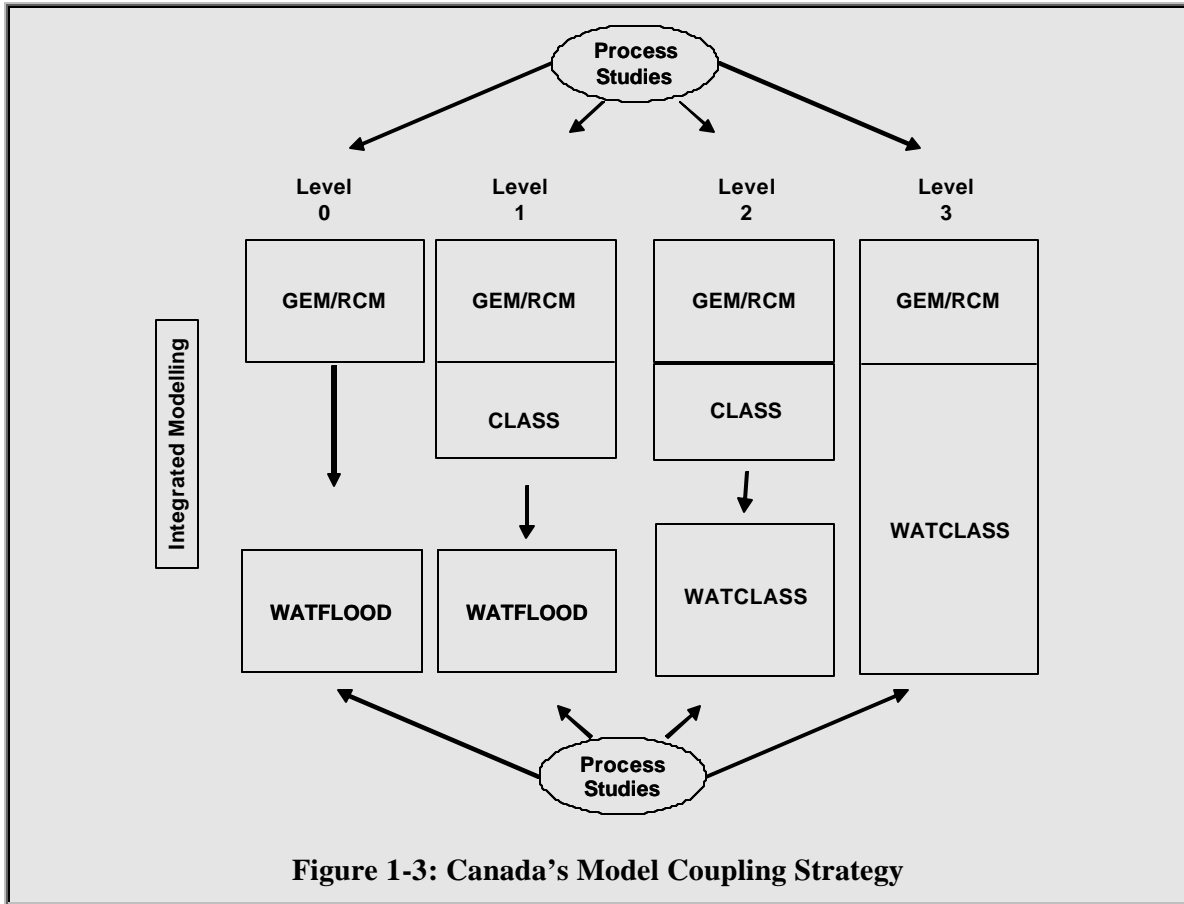
The feedback incorporated into the models is an important concept that requires some elaboration. Studies have shown that land surface hydrology can have an impact on atmospheric hydrologic processes (e.g. Betts *et al.* 1994). An atmospheric model that provides one-way input to a land-surface model would fail to predict atmospheric responses to the land-surface. Betts *et al.* (1994) illustrated that evaporative feedback from the land, if properly incorporated into a Numerical Weather Prediction (NWP) model, can have a re-enforcing effect on the weather by causing additional precipitation. This additional precipitation would cause more evaporation which would continue to feed the atmosphere with moisture for even more precipitation, resulting in an on-going positive feedback loop. This kind of feedback can best be incorporated into the modelling framework by coupling models of hydrologic sub-cycles, as is the plan with Canada's modelling strategy. In addition to the coupling of GCMs with land surface schemes, work is continuing in the area of coupling GCMs with fully-circulating ocean models.

Ultimately, the coupling that has been discussed so far is limited to the water and energy cycles. Much work is needed to improve the physical modelling of these cycles, but other

possibilities are on the horizon for expanding the cycles being modelled in a movement towards true Earth System Models (Vörösmarty *et al.* 1993). The atmospheric community is particularly interested in the incorporation of the carbon cycle to these models. The addition of phosphorus and nitrogen also has implications for our society, particularly water and agricultural managers and people concerned about water quality issues. Ecological modelling can also benefit from an improved understanding of, and ability to predict, the water, energy, and constituent components of the Earth. Linking these physical models with economic models can also have an impact on society.

1.2.4 Error Sources in Hydrological Modelling

Error sources in land-surface-hydrological modelling are depicted in Figure 1-4.

Figure 1-4: Error Sources in Land-Surface-Hydrological Modelling
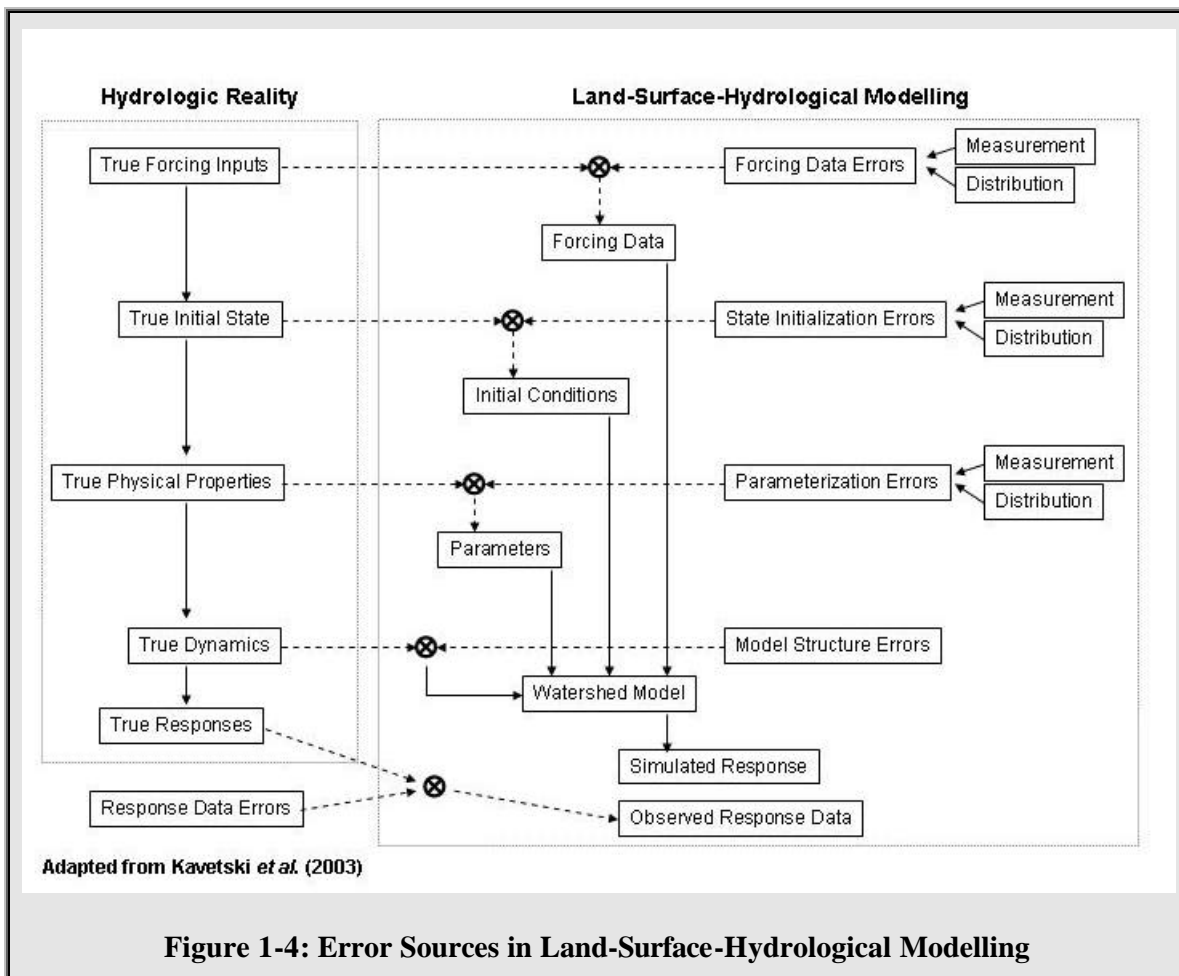
Many potential error sources exist when attempting to evaluate the efficacy of a watershed model. Simply comparing the simulated response to observed data fails to answer the

question of which error sources are the most important. The lack of error source recognition is compounded by the possibility of one error being offset by another error in terms of any given simulated response. For example, too much initial snow in the model could be offset by too little initial soil moisture, resulting in a reasonable runoff volume. The close match between the simulated and observed response hides the fact that both the initial soil moisture and snow water equivalent are wrong.

It has been argued that the problem of identifying a model for a specific purpose can be boiled down to parameterization (Gupta *et al.* 2003 – p 10), which presumably includes the forcing data and initial conditions as well as the parameters. Gupta *et al.* (2003 – p 21) also states that any effective model identification should involve a comprehensive evaluation of *all* sources of uncertainty characterized by the five error sources. Although the model identification problem may boil down to the calibration of parameters, initial conditions and forcing data in many situations; in the case of WATCLASS, the problem also includes model structure. Due to the research nature of the model, cold-soil and snow processes are two areas of research affecting the model structure.

1.2.5 Process Hydrology and Hydrological Modelling

This thesis represents the author's first attempt at linking the worlds of process hydrology and land-surface-hydrologic modelling. In an effort to weave a story of scientific engineering, the document touches on many aspects of snow process hydrology as well as the challenges associated with modelling. Figure 1-5 illustrates the interplay between process hydrology (science)
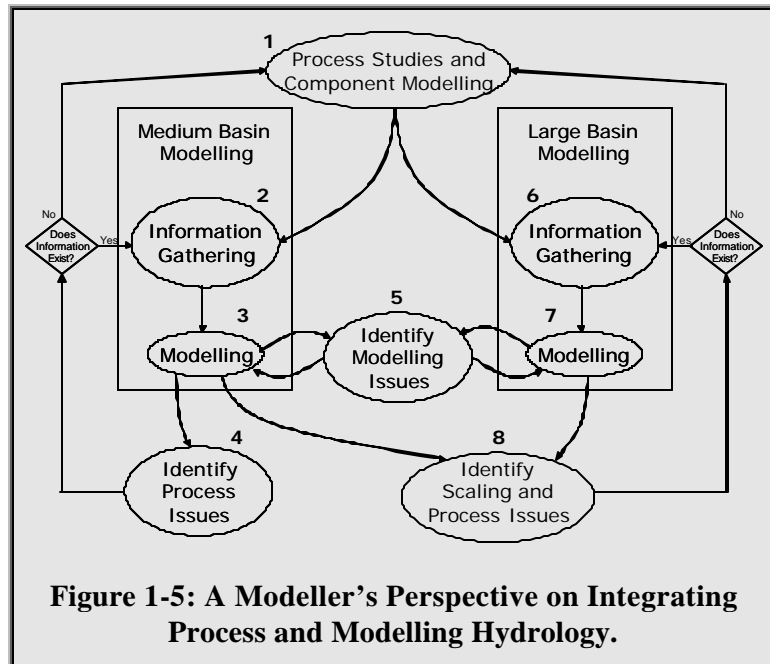
Figure 1-5: A Modeller's Perspective on Integrating Process and Modelling Hydrology.

and basin modelling (engineering). (Recognizing that "medium" and "large" are qualitative descriptors for basins, medium basins are defined as between 100 km^2 and 10,000 km^2. Large

basins are defined as greater than 10,000 km^2.) The first step in basin modelling is the development of a strong base of scientific knowledge and component models describing various aspects of the hydrologic cycle. This base of information has been developing for many years, as described in section 1.2.

Using the scientific knowledge as a base, both medium and large-basin modelling begins with the collection of information and culminates in the development and testing of watershed models. The component modelling essentially lies in the realm of the scientific community while the watershed modelling lies within the domain of the engineering community. The benefit of the modelling exercise to the scientific community is the identification of process issues that need further study, which in turn can benefit the modelling community. The engineering community benefits from the identification of modelling and scaling issues. Figure 1-5 illustrates this process at a high level. The contributions described in this thesis fit into step 4 in Figure 1-5.

1.3 Snow

The cryosphere is defined as the portions of the earth where water is in solid form. It represents a very important part of the hydrologic cycle, impacting ecological, human and climate systems. Cryosphere studies encompass a number of research areas, including snow, permafrost, sea ice, lake ice, river ice, glaciers, ice sheets, ice caps and ice shelves. This section is intended to give a brief overview of our understanding of the importance of snow processes in areas where the snow is not permanent; focusing on the relevance of snow in ecological, human and climate systems.

The ecology in areas where snow occurs is intricately tied to the nature of the snowpack. A sufficient pack will provide insulation for plants, protecting their root systems, and cover for mammals that are unable to migrate far from their homes (Groisman and Davies 2001). Many microorganisms such as bacteria, algae and fungi have adapted to the extreme fluctuations of energy, water and nutrients often found in snow environments, setting the stage for nivian food webs and other biogeochemical processes (Hoham and Duval 2001). All animals that come into contact with snow are affected by the physical, chemical and microbiological processes of the snow, possibly influencing the ability of many animals to survive (Aitchison 2001).

Human society is also affected by snow. Urban and rural communities are susceptible to immobilization from large snow storms which can disrupt power and transportation services. Snow removal is a prominent feature in many municipal budgets. Spring flooding can also cause

problems for many communities, exemplified by the 1999 record snowfalls in Toronto (Tieri 1999). Snow loads on buildings can have disastrous results, as occurred in February 2003 when a rain on snow event caused several roofs to collapse in Maryland and Virginia (Manning 2003). Heart attacks while shoveling snow are estimated to cause 1,200 deaths annually (Franklin *et al.* 1996).

Snow is a prominent feature in many agricultural settings. Snow is estimated, on one hand, to supply at least one third of water for irrigation around the world in the 1970s, and on the other hand, to cause considerable damage to agricultural productivity in floods (Steppuhn 1981). Snow is also a source of water in many non-irrigated areas and enough snow insulates the soil and underlying seeds from the diurnal variations in air temperature (Steppuhn 1981). Livestock can be threatened by snow storms and many crops can be damaged by heavy snow loads or abrasive blowing snow (Steppuhn 1981).

The productivity of a number of industries is also directly related to snow. The oil and gas and pulp and paper industries relied on ice roads for their winter operations in the 1970s (Adam 1981). The first recorded attempt to predict snowmelt runoff for hydro-electric and flood control purposes was performed by a power company in Nevada in 1909 (Male and Gray 1981). The company correlated spring lake levels with the snow water equivalent on a nearby mountain and adjusted their operations accordingly.

A significant recreational industry has also built-up around snow. Downhill skiing, cross-country skiing and snowmobiling are popular sports across Canada. Although these sporting activities have significant economic impacts, certain recreational activities are suspected to have detrimental environmental impacts. One Canadian Geographic article by Payton (2003) highlights some of the concerns with heli-skiing and snowmobiling in the Canadian Rockies. These activities may be further damaging the endangered mountain caribou population by limiting their travel patterns and providing snow-packed trails for predators to travel deeper into the mountain caribou habitat (Payton 2003). The same may be true for many animals in snow environments.

In addition to the impacts on local ecology and human society, snow is intricately linked with the global water and energy cycles, having important implications for areas that never experience snow. One study has linked delayed or weakened Indian summer monsoons with higher than normal snowcover in Eurasia and/or the Tibetan plateau (Jones 1999). These same Eurasian and Tibetan snowcovers are partially responsible for very large-scale waves in the atmosphere, affecting the climate in the tropical Pacific and North America (Barnett *et al.* 1989). Large scale snowcover in parts of the world are also linked to the El Niño Southern Oscillation

(ENSO), a significant five to seven year low frequency variation of atmospheric pressure, wind, and surface temperature fields in the tropical Pacific (e.g. Li 1989; Groisman *et al.* 1994).

All snow is not the same. The impact of snow on local ecology, human endeavors and global climate depends on the physical, chemical and biological properties of the snow environment. A number of efforts to classify the physical nature of the seasonal snowcover have been undertaken by Formosov (1946), Richter (1954), Benson (1969), McKay and Gray (1981), Pruitt (1984), and Sturm, Holmgren and Liston (1995). Church (1974) has also classified Northern hydrological regimes based on the source and timing of run-off. Table 1-2 lists the classification of Sturm *et al.* (1995) as shown by Groisman and Davies (2001).

Table 1-2: Description of Snow Classes (Sturm *et al.* 1995)

Snowcover Class	Description
Tundra	A thin, cold, windblown snow. Maximum depth, ~75 cm. Usually found above or north of tree line. Consists of a basal layer of depth hoar overlain by multiple wind slabs. Surface zastrugi common. Melt features rare.
Taiga	A thin to moderately deep low-density cold snowcover. Maximum depth 120 cm. Found in cold climates in forests where wind, initial snow density, and average winter air temperatures are all low. By late winter consists of 50-80% depth hoar covered by low-density new snow.
Alpine	An intermediate to cold deep snowcover. Maximum depth, ~250 cm. Often alternate thick and thin layers, common as well as occasional wind crusts. Most new snowfalls are low density. Melt features occur but are generally insignificant.
Maritime	A warm deep snowcover. Maximum depth can be in excess of 300 cm. Melt features (ice layers, percolation columns) very common. Coarse-grained snow due to wetting ubiquitous. Basal melting common.
Ephemeral	A thin, extremely warm snowcover. Ranges from 0 to 50 cm. Shortly after basal melting common. Melt features common. Often consist of a single snowfall, which melts away; then a new snowcover re-forms at the next snowfall.
Prairie	A thin (except in drifts) moderately cold snowcover with substantial wind drifting. Maximum depth, ~100 cm. Wind slabs and drifts common.
Mountain, special cases	A highly variable snowcover, depending on solar radiation effects and local wind patterns. Usually deeper than associated type of snowcover from adjacent lowlands.

The classification in Table 1-2 is derived from an analysis of snowcover and meteorological conditions in Alaska. The approach was validated with Russian data. A map was then developed for the northern hemisphere using world-wide wind, temperature and precipitation data (Groisman and Davies 2001).

The work undertaken for this thesis involved the snow processes within the hydrologic-land-surface model WATCLASS. The classification of continental snowcover is an important consideration for large domain watershed models. Model domains often encompass these areas, providing insight into the appropriateness, or lack of, in using particular snow models for the areas of interest. A number of watersheds modelled using WATFLOOD and WATCLASS --in Southern Ontario, Northern Manitoba, Central Saskatchewan, British Columbia, the Yukon and the North-West Territories-- experience snow as classified in Table 1-2. The representation of snow in these models could be more appropriate for certain classifications, leading to a physical justification for altering modelled snow parameters in certain areas. For example, reducing the snow present in a WATFLOOD model area that experiences high sublimation rates could be a possible application of this procedure.

This introduction to snow is meant to highlight the importance of snow in ecological, human and climate systems. Understanding the physical processes of snow is important for predicting how these systems will react under different circumstances. Scientists have studied the formation, accumulation, movement and ablation of snow, and much still needs to be learned surrounding these physical processes. Part of the emphasis of this ongoing research is to develop the mathematical and computer models that can be used to predict the impact of snow on the various cycles - energy, water, nutrient, ecosystem - operating in the biosphere.

1.4 Component Snow Modelling

A survey of the literature (Gray and Male 1981; Male 1980; Dingman 1994; Prowse and Ommanney 1990; Woo *et al.* 2000; Essery and Yang 2001; Pomeroy and Brun 2001), shows that the most common modelling of snow processes relate to the energy cycle. Very few equations describing the mass balance of a snowpack were encountered. The exceptions were a very simple mass balance model (Essery and Yang 2001), a conceptual model for the canopy mass balance (Pomeroy and Brun 2001), and a mathematical model for blowing snow (Pomeroy and Brun 2001). Much work is needed to develop some fundamental models of the energy and mass balance components that involve snow.

1.5 Snow in Hydrologic and Land Surface Modelling

Despite the effort that is needed to develop the component models describing snow processes, many hydrologic and land surface models incorporate snow into their algorithms. The approaches to modelling snow in these algorithms range from the very simple to the very complex, depending on the respective purposes of the models. The author is aware of two inter-comparison projects that are underway to examine the relative effectiveness of different models in various scenarios involving snow. The PILPS 2e Arctic Model Intercomparison is specifically designed to compare cold-region modelling of twenty-one land surface schemes (Bowling, *et al.*, In Press [a]). In addition, the SnowMIP (Model Inter-comparison Project) is a comparison of atmospheric general circulation models, hydrologic snowmelt models, numerical weather prediction models, and detailed avalanche and snow physics models (Essery and Yang 2001). A total of twenty-four models are being compared for the SnowMIP project. The reader is referred to Etchevers *et al.* (2002), Nijssen *et al.* (In Press) and Bowling *et al.* (In Press [b]) for preliminary results on these model comparison projects.

This thesis is concerned with the snow processes of WATCLASS, the coupled hydrologic model WATFLOOD with the Canadian Land Surface Scheme (CLASS). WATFLOOD was first developed in 1972 by Dr. Nicholas Kouwen and, facilitated by the work of several Masters and PhD students, has been improving ever since (Kouwen and Mousavi 2002). It is a good example of an integration of components of the hydrologic cycle to produce a comprehensive watershed model. CLASS was first developed in 1989 as a response to the desire for a second-generation land-surface scheme in the Canadian Global Climate Model (GCM). Second-generation land-surface schemes were designed to improve the representation of the vertical land surface water and energy budgets in global climate models. Since 1989, a number of improvements have been made to the model, culminating in version 2.6 in August 1997 (Verseghy 2000). WATCLASS is the coupling of these two models, joining a number of components of WATFLOOD and CLASS (Soulis *et al.* 2000, Snelgrove 2002). In addition, Fassnacht (2000) and Fassnacht and Soulis (2002) have implemented and analyzed a number of improvements of the CLASS representation of snow in WATCLASS, studying the Upper Grand River watershed in south-western Ontario. As of the final stages of writing this thesis, CLASS 3.0 had been released and WATCLASS 3.0 was in the early stages of development.

1.6 Objectives

This thesis has two objectives. The first objective is to further analyze the relative importance of various model structure uncertainties with respect to snow in a spring-melt model domain. The second objective is to develop and analyze a fresh snow accumulation algorithm.

1.6.1 Investigating Aspects of Model Structure

A number of potential error sources exist in hydrologic-land-surface models. These include forcing data errors, state initialization errors, parameterization errors, model structure errors and response data errors. This thesis quantitatively examines the relative importance of certain aspects of the model structure. The model structure components considered are mixed precipitation, variable fresh snow density, maximum snowpack density, canopy snowmelt interception and fractional SCA-hysteresis .

1.6.2 Developing and Analyzing an Algorithm for the Relationship between Snow Depth and Fractional Snowcovered Area

CLASS and WATCLASS currently use a snowcover depletion curve (SDC) to calculate fractional snowcovered areas and average snow depths in the grid-squares. The SDC is used for both snowmelt and snow-accumulation. Snow accumulation, however, is a different process than snowmelt and, although the SDC is ideal for use in melt scenarios; it fails to adequately describe the fresh snow-accumulation process. This thesis describes the theory behind, and analyzes, a newly developed algorithm representing the hysteretic relationship between snow depth and fractional snowcovered area.

2. Background

This chapter provides a description of the snow processes as they are represented in models. A brief overview of some important snow processes during the lifecycle of a snowpack is described, specific energy and mass component models are presented, and the models relevant to this study are described. Special attention is directed towards the representation of snowcovered area and the interpretation of land surface heterogeneity in the pertinent models.

2.1 Snow Processes

At the most basic level, seasonal snow falls, stays on the ground until it ablates and the ground remains bare until the next year. The cycle can be broken into two main periods; the accumulation period and the melt period. The melt period can be further categorized into the phases of warming, ripening, and output.

The accumulation period is characterized by a general increase in the water equivalent, and a decrease in the temperature and net input of energy (Dingman 1994). Snow first forms in the atmosphere, the individual crystals growing in the clouds and taking on a variety of shapes that depend on temperature and humidity. As these flakes fall to the ground, they can grow or break apart, depending on the temperature, humidity and wind conditions. Vegetative canopies intercept snow before it reaches the ground, affecting the overall mass, energy and nutrient balances. Once on the ground, the matrix of snow particles undergoes different metamorphic processes depending on whether the pack is wet or dry. The accumulation period is generally dominated by dry snow conditions, in which case the metamorphic processes depend on whether the pack is isothermal or exhibits a temperature gradient (Male 1980).

Blowing snow is an important process as the main force for redistribution. The resulting spatial variability of the snow affects other processes such as the sensible and latent heat fluxes. The three main mechanisms of snow transport by the wind are creep, saltation and turbulent diffusion (Pomeroy and Brun 2001). Creep is the rolling motion of the snow particles that are too heavy to be lifted by the wind (Pomeroy and Brun 2001). Saltation is the process of snow particles moving close to the pack, up to a few centimeters from the surface. Wind dislodges a particle and carries it in a curved trajectory based on gravity and the drag from the relative velocity between the particle and the wind (Male 1980). If the wind is strong enough, turbulent diffusion will cause the particles to remain suspended in the air (Male 1980). With redistribution,

sublimation can be dramatically increased, accounting for a 16-49% loss of snow water equivalent in prairie environments (Pomeroy and Li 1997).

The melt period generally begins when the net energy is positive (Dingman 1994). The main mechanisms of melt depend on the location. In temperate regions, radiation is the main source of energy for melt, followed by the turbulent fluxes of sensible and latent heat. The energy added by warm rain is generally disregarded, but the ground heat flux has a role to play in both temperate and arctic environments. In temperate regions, the ground heat flux is small and often neglected, but it tends to always be positive, having a cumulative effect on the seasonal energy balance (Male 1980). In arctic environments, the ground heat flux is large enough to warrant special attention (Marsh 1990).

Water generated from the snow surface melt, or input from rainfall, results in wet snow, which causes different metamorphic processes than dry snow. The presence of water causes smaller snow particles to disappear and larger particles to grow, resulting in a pack with less structural strength between the particles and a higher density (Wakahama 1968). The following loss in surface area causes a drop in capillary potential and may be the reason that a pack can be observed to release a lot of water very quickly in the early stages of melt (Colbeck 1978).

The warming phase represents the period in which the snow temperature is increasing to zero degrees Celsius, the ripening phase represents the melting of the pack until it can no longer hold any more water, and the output phase occurs when the pack releases water (Dingman 1994). The distinction between the warming, ripening and output phases is not always straightforward. Large energy gradients between the atmosphere, snow and ground can cause snow to melt and refreeze until the pack reaches a stage of isothermal energy. In many cases, snow will accumulate and melt several times in one season, occasionally re-accumulating on a pack that has partially melted. These scenarios can cause problems in predicting the net snow water equivalent (Rango *et al.* 1983).

2.2 Component Snow Models

Many snow process components have mathematical representations. These mathematical relationships can be used to describe energy, mass or nutrient cycling as well as other ecosystem functions. This section of the thesis will focus on the mathematical models that describe the author's understanding of the energy and mass components.

2.2.1 Energy Balance Components
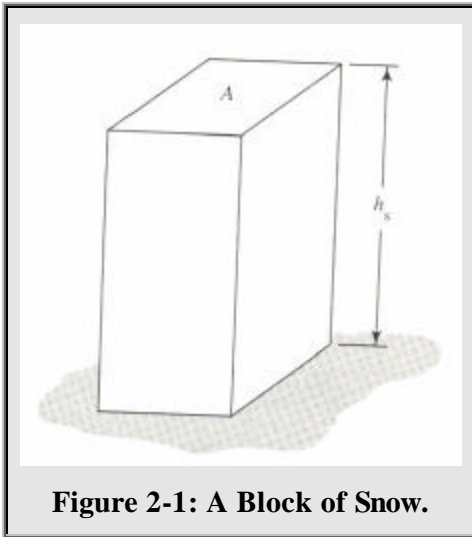
Figure 2-1: A Block of Snow.

A number of different energy balance models exist for snow. The differences between these

$$(\Delta t)S = \Delta Q$$

Equation 2-1: Snow Energy Balance (Dingman 1994)

models are subtle. The following is a discussion of these mathematical models. In Equation 2-1, Dingman (1994) describes the energy balance of an element of snow of surface area A and height h_s, shown in Figure 2-1. S $[EL^{-2}T^{-1}]$ is the net rate of energy exchanges into the element by all processes over a time period Δt [T], and ΔQ $[EL^{-2}]$ is the change in heat energy absorbed by the snowpack during Δt.

The net rate of energy exchange is represented by Equation 2-2, where K is the shortwave (0.2 to 3 µm) radiation input, L is the long-wave (3 to 30 µm) radiation exchange, H is the sensible heat exchange

$$S = K + L + H + LE + R + G$$

Equation 2-2: Net Rate of Energy Exchange into a Snow Element

with the atmosphere, LE is the latent heat exchange with the atmosphere, R is the heat input by rain, and G is the sensible heat exchange with the ground.

Shortwave radiation input

The shortwave radiation input is described by Equation 2-3. K_{in} is the incoming shortwave radiation, K_{out} is the outgoing shortwave radiation and a is albedo, which represents the fraction of radiation reflected from the snow surface.

$$K = K_{in} - K_{out} = K_{in}(1-a)$$

Equation 2-3: Shortwave Radiation Input

Longwave radiation exchange

The longwave radiation exchange is described as Equation 2-4. L_{in} is the incoming long-wave radiation, L_{out} is the outgoing long-wave radiation, e_{ss} is the emissivity of the snow surface, e_{at} is the integrated

$$L = L_{in} - L_{out} = e_{ss}e_{at}sT_{at}^4 - e_{ss}sT_{ss}^4$$

Equation 2-4: Longwave Radiation Exchange

effective emissivity of the atmosphere and canopy, and s is the Stefan-Boltzmann constant ($s =$

5.67×10^{-8} W m^{-2} K^{-4}), T_{at} is the effective radiating absolute temperature of the atmosphere and canopy, and T_{ss} is the absolute temperature of the snow surface. The emissivity of snow is often assumed to be 1. According to Dingman (1994) "The major problem in applying [Equation 2-4] is to find expressions for e_{at} and T_{at} or, equivalently, to estimate the value of L_{in} under various conditions of cloudiness and forest cover." He then goes on to discuss some methods for estimating L_{in}.

Sensible Heat Exchange with the Atmosphere

Sensible heat is transferred to the atmosphere when turbulent eddies exist in tandem with a vertical temperature gradient. The expression developed for sensible heat transfer, for the purposes of calculating a

$$H = \frac{D_H}{D_M} c_a r_a \frac{k^2 u_m}{\left\{ \ln\left[(z_m - z_d)/z_0 \right] \right\}^2} (T_s - T_m)$$

Equation 2-5: Sensible Heat Exchange with the Atmosphere (Dingman, 1994)

value from measurements, is shown in Equation 2-5. H is the upward flux of sensible heat, D_H is the diffusivity of sensible heat, D_M is the diffusivity of momentum in turbulent air, c_a is heat capacity of air at constant temperature, r_a is the mass density of air, k is a dimensionless constant, u_m is the wind velocity at height z_m, z_d is the zero-plane displacement, z_0 is the roughness height, T_s is the temperature of the surface and T_m is the temperature at the measurement height.

Latent Heat Exchange with the Atmosphere

Latent heat (water vapor) is transferred to the atmosphere when turbulent eddies exist in tandem with a vertical pressure gradient. The expression dev-

$$LE = \frac{D_{WV}}{D_M} l_v \frac{0.622 r_a}{P} \frac{k^2 u_m}{\left\{ \ln\left[(z_m - z_d)/z_0 \right] \right\}^2} (e_s - e_m)$$

Equation 2-6: Latent Heat Exhcange with the Atmosphere (Dingman, 1994)

eloped for latent heat transfer, for the purposes of calculating a value from measurements is shown in Equation 2-6. D_{WV} is the diffusivity of water vapor in turbulent air, D_M is the diffusivity of momentum in turbulent air, l_v is the latent heat of vaporization, r_a is the mass density of air, P is the air pressure in mb, 'k' is a constant (0.4), u_m is the wind velocity at height z_m, z_d is the

zero-plane displacement, z_0 is the roughness height, e_s is the vapor pressure at the surface and e_m is the vapor pressure at height z_m.

Heat Input by Rain

Two equations are provided for heat input by rain. Equation 2-7 is for rain on a pack that is at freezing temperature. r_w is the density of water, c_w is the heat capacity of water, r is the rainfall rate and T_r is the temperature of the rain.

$$R = r_w c_w r (T_r - T_m)$$

Equation 2-7: Heat Input by Rain for Snow at Zero Degrees Celsius

The second equation is for rain on snow that is below freezing. The only new term is l_f, which is the latent heat of fusion.

$$R = r_w c_w r (T_r - T_m) + r_w l_f r$$

Equation 2-8: Heat Input by Rain for Sub-zero Snow Temperatures

Sensible Heat Exchange with the Ground

When temperatures in the soil increase downwards from the snowpack, due to summer storage of thermal energy, heat is conducted to the base of the pack at a rate described by Equation 2-9, where k_G is the thermal conductivity of the soil and dT/dz is the vertical temperature gradient in the soil. Dingman (1994) states

$$G = k_G \frac{dT}{dz}$$

Equation 2-9: Sensible Heat Exchange with the Ground

that G is usually negligible during a snowmelt season, but can be significant during the accumulation season. Marsh (1990) notes that ground heat fluxes can be considerably more important in northern climates.

A Comparison of Energy Balance Models

Marsh (1990) describes the energy balance as Equation 2-10, where Q_M is the energy available for melt, Q* is net all-wave radiation, Q_H is the

$$Q_M = Q^* + Q_H + Q_E + Q_R + Q_G - \frac{du}{dt}$$

Equation 2-10: Snow Energy Balance (Marsh 1990)

sensible heat flux, Q_E is the latent heat flux, Q_R is the flux of heat from rain, Q_G is the ground heat flux at the snow-soil interface, and du/dt is the rate of change of internal energy.

Male (1980) describes two common equations for the energy balance, illustrated in Equation 2-11 and Equation 2-12. In Equation 2-11, Q_i [kW/m^2] is the energy flux due to radiation, sensible and latent heat flux, and heat

$$\Sigma Q_i + \Sigma (mh)_i = 0$$

Equation 2-11: Snow Energy Balance 1 (Male 1980)

transfer from the lower layers of the snowpack. $(mh)_i$ is the energy transfer due to precipitation, m [kg/m^2 sec] with an associated specific enthalpy, 'h' [KJ/kg].

For Equation 2-12, dU/dt [kJ/sec m^2] is the change in internal energy of the pack, Q_i includes the ground heat flux, and $(mh)_i$ includes the melt-water draining from the bottom of the pack. According to Male (1980, p 349),

$$\frac{dU}{dt} = \Sigma Q_i + \Sigma (mh)_i$$

Equation 2-12: Snow Energy Balance 2 (Male 1980)

Equation 2-11 is suitable for deeper snowpacks as it only needs measurements at or near the upper surface. Equation 2-12 describes the entire thermal regime of the pack and is practically usable for shallow packs of less than 40cm. Neither equation is considered valid for situations where horizontal advection is substantial (i.e. not near open water, nor a patchy cover).

Of the four models presented, the simplest is the first model presented by Male (Equation 2-11). Equation 2-1 includes the internal energy of the pack, while the second model presented by Male (Equation 2-12) and the model presented by Marsh (Equation 2-10) also include melt energy. In Marsh's model, the energy is presented as melt energy, while in Male's model; it is presented as melt-water from the bottom of the pack. The models presented by Male are solely focused on the melt phase, while Dingman and Marsh present the models in a manner that includes the accumulation phase as well as the melt phase. The models presented by Male are also suitable for the accumulation phase, assuming the conditions of negligible horizontal advection are met.

2.2.2 Mass Balance Components

Due to the limited availability of common mass balance models, the mass balance components considered in Equation 2-13 are specific to an idealization of WATCLASS that incorporates all

$$\frac{dM}{dt} = P + E + B + C + R + P_f$$

Equation 2-13: Suggested GRU Snow Mass Balance Model

snow mass components. Within this context, the description of the snow mass balance is complicated by the lack of a clear distinction between snow properties for an entire grouped response unit (GRU) and the internal variability within a GRU. For the purposes of this thesis, the following mass-balance model is suggested for a GRU. M is the mass of snow per unit surface

area, P is precipitation rate, E is the sublimation or condensation, B is the snow blown into the GRU, -C is the interception by the canopy, -R is the rate of runoff from the bottom of the pack, and P_f is the amount of ponded water that freezes. Equation 2-13 does not address the issues of within-GRU variability of density, depth, snowcovered area and snow water equivalent. It also does not consider the mass balance of snow in a canopy, which, with the exception of canopy interception's impact on the underlying snowpack, is not discussed in this thesis. The remainder this section considers our understanding of the components of Equation 2-13 as well as the components that would affect within-GRU variability of snow properties.

Precipitation

Snow forms in the atmosphere where cloud temperatures are below zero degrees Celsius. The variety of temperature and humidity conditions possible during crystal formation results in a phenomenal diversity of initial snow shapes. As the snow falls through the atmosphere, the changes in temperature and humidity that the crystals encounter alters their form, compounded by collisions that further modify their structure (Male 1980). The multiplicity of factors that affect snow from formation to deposition produce an even more phenomenal diversity of deposited snow types. Precipitation can come in the form of rain or snow, or as a mixture of rain and snow, depending on the meteorological conditions as precipitation falls through the air.

Evaporation and Condensation

Water will either sublimate from, or condense on, the pack. This process is driven by the vapor pressure gradient between the surface and the atmosphere. If the vapor pressure above the surface is greater than the vapor pressure at the surface, moisture will condense on the snow. If the vapor pressure above the surface is smaller than the vapor pressure at the surface, moisture will sublimate from the snowpack.

Canopy Interception

Snowfall canopy interception is the process of snowfall being caught by the branches and foliage of the canopy. This snowfall may or may not reach the ground. Some of the snow may blow off the trees and

$$I = c_{suc}\left(I^* - I_0\right)\left(1 - e^{-\frac{C_{can}R_s}{I^*}}\right)$$

Equation 2-14: Snowfall Canopy Interception

reach the ground, but much of it sublimates back into the atmosphere. Snowfall canopy interception is an important process because of its impact on the water balance. Hedstrom and Pomeroy (1998) estimated snowfall canopy interception (I) with Equation 2-14. c_{suc} is a dimensionless snow unloading coefficient, I^* is the maximum snow load in kg/m^2, I_0 is the initial snow load in kg/m^2, R_s is the snowfall for a unit of time in mm SWE or kg/m^2, and C_{can} is the canopy coverage fraction.

Hedstrom and Pomeroy (1998) estimated c_{suc} to be 0.697 and the maximum snow load with Equation 2-15. S_p is a tree species coefficient, LAI is the leaf area index, and $r_s(fresh)$ is the fresh snow density in kg/m^3.

$$I^* = S_p LAI\left(0.27 + \frac{46}{r_s(fresh)}\right)$$

Equation 2-15: Maximum Snow Load

Runoff from the Bottom of the Pack

The runoff from the bottom of the pack is driven by the energy balance.

Freezing Ponded Water

If the surface temperature is below zero degrees Celsius, ponded water will freeze, releasing latent heat.

Density

Snow density varies depending on the meteorological conditions during crystal formation, descent and deposition; and the metamorphic pro-cesses crystals undergo while on the ground. Fresh snow density has been found to vary from 70 to 100 kg/m^3 by Goodison, Ferguson and McKay (1981). Male (1980, p 308) reported that fresh snow density can vary from 10 to 500 kg/m^3. La Chapelle (1961) derived Equation 2-16 relating fresh snow density to

$$r_s(fresh) = 50 + 1.7(T_a + 15)^{1.5}$$

Equation 2-16: Fresh Snow Density (La Chapelle 1961)

$$r_s(fresh) = 67.92 + 51.25e^{\left(\frac{T_a}{2.59}\right)}$$

Equation 2-17: Fresh Snow Density (Hedstrom and Pomeroy 1998)

air temperature from data collected at the Alta Avalanche Study Center. Hedstrom and Pomeroy (1998) have examined the work of Diamond and Lowry (1953) and Schmidt and Gluns (1991) to

derive Equation 2-17 for fresh snow density. In both equations, $r_s(fresh)$ is the fresh snow density in kg/m^3, and T$_a$ is the air temperature in degrees Celsius. Snow density increases exponentially with time, as wind, sublimation, gravity and warm periods change the internal structure of the pack. The maximum density of a snowpack depends on its location, land cover and other factors (Fassnacht 2000. p22).

Snowcovered Area and Depth

Equation 2-13 does not consider the snowcovered area or snow depth of a GRU and a distinct method must be employed to calculate these terms. The second objective of this thesis is directly concerned with these components and will be discussed in detail in the next section.

Snow Water Equivalent

The snow water equivalent can be calculated from snowcovered area, snow depth and snow density. The within-GRU variability of SWE would therefore be a function of the variability of area, depth and density.

2.3 Snowcovered Area (SCA)

The second objective of this thesis is to develop and analyze a fresh snow accumulation algorithm. The current method of accumulating fresh snow in CLASS fails to accurately represent the SCA, accumulating fresh snow in the same manner as mature snow is depleted. This incorrect accumulation of fresh snow results in excessive bare ground being predicted, with implications for the energy and mass balances of the pack. Bare ground is generally darker than snow, absorbing more incoming shortwave radiation and releasing some of the absorbed energy as sensible and latent heat (Shook 1995). Bare ground turbulent heat is transferred downwind, increasing the melt rate at neighboring snow patches (Shook 1995). Although horizontal advection is not currently in CLASS or WATCLASS, properly determining the amount of bare ground will be especially important when horizontal advection is incorporated into the models. In the meantime, correctly assessing the SCA has implications for the energy balance. In this section, some current approaches to SCA, and the problem with fresh snow, will be explained.

2.3.1 Current Approaches to Snowcovered Area

A number of different approaches exist for illustrating partial snowcovers. In all cases presented in this thesis, the methods use the terminology of "snowcover depletion curves" (SDCs). The terminology is the same, but the representation of SCA is different, resulting in the potential for confusion. It is worth noting that, of the variety of SDCs found in the literature, the first two depletion curves by Rango *et al.* (1983) and Luce *et al.* (1999) are watershed based. The third depletion curve, by Donald (1992) is land-cover based. The first depletion curve varies from year to year, the second depletion curve is a property of the watershed, and the third depletion curve is a property of the GRU.

In their discussion of the necessary resolution for the remote sensing of snowcover, Rango *et al.* (1983) present a depletion curve (Figure 2-2) where the percentage of snowcovered area is on the y-axis and time is on the x-axis. Conceptually, this approach is very easy to understand. In seasonal snowpacks, the trend is for snowcovered area to decrease from one hundred percent to zero percent over a period of time. Plotting

Figure 2-2: SCA vs. Time SDC

this depletion curve with sufficiently regular satellite overpasses can result in an accurate calculation of the evolution of basin-wide SCA.
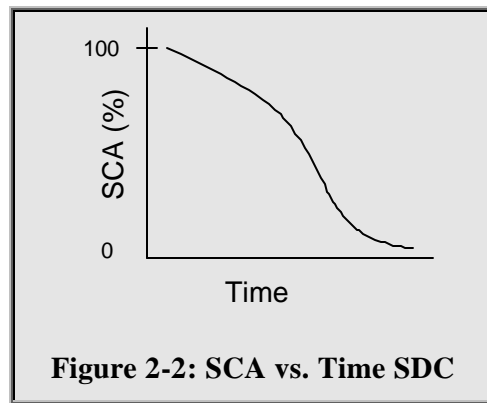
In work concerning the sub-grid parameterization of snow distribution for a lumped model, a second basin-wide SDC (Figure 2-3) is presented by Luce *et al.* (1999). In this SDC, the y-axis is the SCA fraction and the x-axis is basin or element average SWE. The SCA fraction is assumed to be 1 at maximum SWE for the season. As a result, the SDC varies from year to year and from basin to basin with maximum seasonal SWE. Annual variability is

Figure 2-3: SCA vs. SWE SDC

addressed through the development of a dimensionless depletion curve by dividing the SWE by the maximum seasonal SWE. This assumes that the shape of the dimensionless curve is consistent for different values of maximum seasonal SWE. No validation data were provided to justify the shape of the SDC.
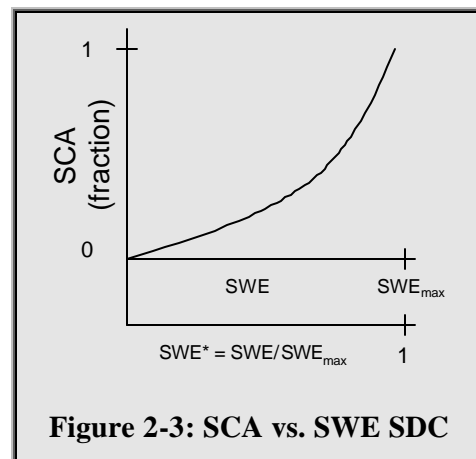
The third method of representing snowcover depletion is described in detail by Donald (1992). One significant difference with this kind of SDC is that it is land-cover based. The y-axis is average snow depth for the element and the x-axis is SCA (Figure 2-4). The theory behind the curve begins with the pre-melt snowcover profile of a particular land-class (Figure 2-5a). The ground is 100% covered at 1 in Figure 2-5a. As the snow melts from 1 through to 5, bare ground first appears just after 3 and increases until there is no more snow on the ground.

Figure 2-4: Snow Depth vs. SCA SDC
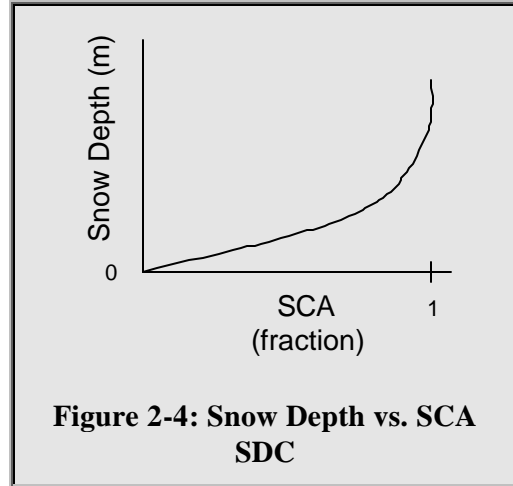
The assumption is that the snow depth profile is log-normally distributed. Donald (1992) showed that this assumption is reasonable for a watershed model. As the snow melts from 1 to 5, the assumed log-normal distribution shifts as shown in Figure 2-5b. The areal distribution curve of Figure 2-5c represents the cumulative distribution of Figure 2-5b. Each curve on Figure 2-5c represents a point on Figure 2-5d, with the depth at each point being equal to the average snow depth and the SCA percentage being equal to the total amount of snowcovered area at this average depth. The land-class dependence of this SDC assumes that each land-class has a characteristic depth at which bare ground begins to appear during

Figure 2-5: Snow Depth vs. SCA SDC theory development (Donald, 1992)

snowmelt. This depth is referred to as the D100 value. It is likely that the D100 is also dependent
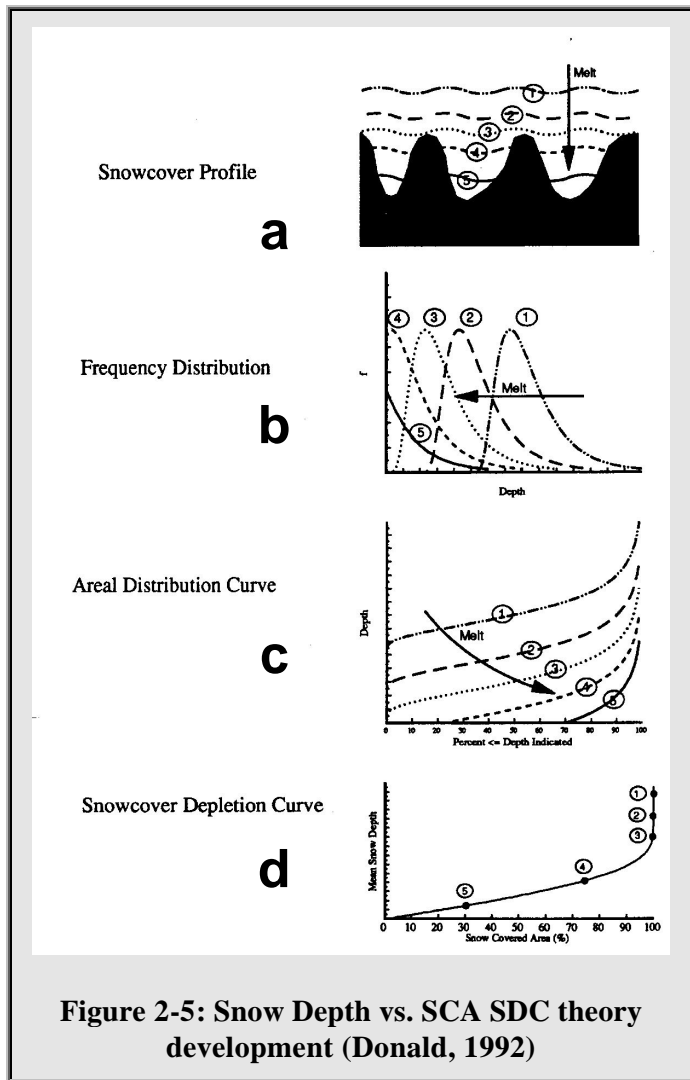
on the local meteorological conditions, topographic influences and land-class distribution. The D100 for a bare field GRU would likely be quite different if small fields were interspersed between clumps of forest, rather than one field next to one forest.

2.3.2 The Problem with Fresh Snow

Snow-accumulation is often discussed in the context of all the processes that lead to maximum accumulation, including interception, blowing snow and redistribution, densification, sublimation fluxes, and spatial variation of SWE and SCA (e.g. Pomeroy *et al.* 1998; Woo *et al.* 2000), rather than accumulation as a specific process on its own. Considering all of the processes affecting a snowpack, fresh snow accumulation should be treated separately from the other processes occurring during the snowpack's life.

A number of sources corroborate this argument. Kung *et al.* (1964) avoided studying the snowpack until a few days after a snowfall because the fresh snow would have biased the albedo measurements they were taking. Donald (1992 pp.113) found that fresh snow had an impact on the brightness-depth relationships developed from 1987 satellite images and snow course data. He found that the brightness-depth relationship developed for a mature pack was different than for a fresh pack. A snowcover that clearly covered most of Southern Ontario was the result of a series of snow storms on February 28th and 29th, 1990. Comparing the snow course depth measurements to the reflectance illustrated that reflectance was not dependent on snow depth as it was with the 1987 mature pack. The lack of correlation between snow depth and reflectance is an indication that fresh snow behaves differently than snow in a mature pack, at least in terms of the albedo, and therefore fraction of bare ground, associated with the pack.

Rango *et al.* (1983) also highlight the distinctive nature of a fresh snowfall, which can result in erroneous assumptions if handled incorrectly. In their case, a graph of snowcovered area versus time can be distorted if a summer snow storm occurs and the frequency of observation is inadequate. The key point in presenting the information from Kung *et al.* (1964), Donald (1992) and Rango *et al.* (1983), is to provide evidence that fresh snow accumulation is different than snow ablation and should be treated as such.

One way of dealing with fresh snow was developed by Luce *et al.* (1999), who incorporated a hysteretic-type relationship, between fractional snowcovered area and element average snow water equivalence, into a physically-based lumped snowpack model. The model was a modification of the Utah Energy Balance snowpack energy and mass balance model. Luce

et al. (1999) dealt with fresh snow accumulation by creating a dimensionless snowcover depletion curve and re-scaling it to 100% coverage when fresh snow fell, resulting in the hysteretic relationship.

This SDC must be used appropriately. If the SCA fraction is assumed to deplete to less than 1 as soon as SWE begins decreasing, then the assumption is that bare ground begins appearing at the beginning of the depletion phase. This may be an appropriate assumption at a basin-scale or for a grid-square of variable topography and land-class, but is not likely appropriate for a typical GRU. Donald's approach is likely better for the GRU. Donald (1992), however, does not develop a framework for dealing with the effects of fresh snow. Piersol (2000) developed a method within a point version of WATCLASS to deal with fresh snow on a partial pack.

2.4 The Models

As this thesis is concerned with the modelling of snow in WATCLASS, a description of the pertinent components of WATFLOOD, CLASS and WATCLASS is warranted.

2.4.1 WATFLOOD

The hydrologic components that WATFLOOD integrates are: interception, infiltration, surface storage, evapotranspiration, snow accumulation and ablation, interflow and depression storage, recharge, baseflow, overland routing and channel routing. Figure 2-6 shows a conceptual model of the processes included in the model.
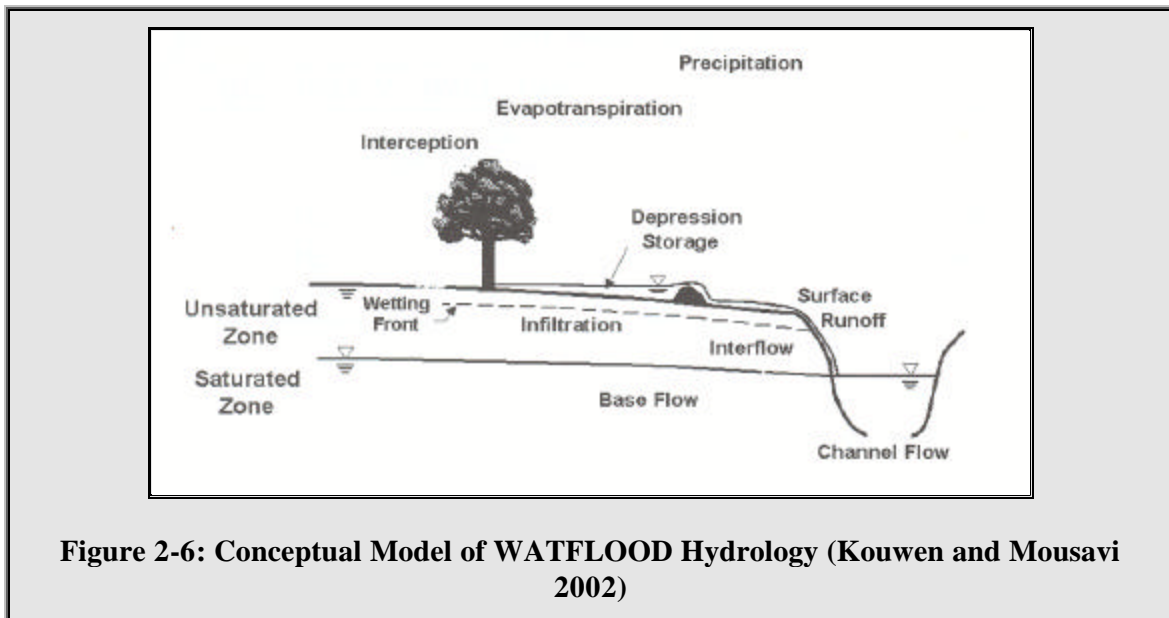
Figure 2-6: Conceptual Model of WATFLOOD Hydrology (Kouwen and Mousavi 2002)

WATFLOOD is described in detail by Kouwen and Mousavi (2002) and the following section describes the channel routing coupled into WATCLASS. The WATFLOOD snowmelt model is also briefly described.

Channel Routing

The routing of water through channels in WATFLOOD is modelled using a simple application of the continuity equation, shown in Equation 2-18. $I_{1,2}$ is the inflow to the reach from all sources (baseflow, interflow, overland flow, upstreamflow) in m^3/s, $O_{1,2}$ is the outflow from the reach in m^3/s. $S_{1,2}$ is the

$$\frac{I_1 + I_2}{2} - \frac{O_1 + O_2}{2} = \frac{S_2 - S_1}{\Delta t}$$

Equation 2-18: Channel Routing in WATFLOOD

storage in the reach in m^3, and t is the time step of the routing in s. The outflow is calculated from the storage based on Manning's equation.

Snowmelt

WATFLOOD models snowcovered and snow-free areas separately. Deep packs will have a 100% snowcover with fractional coverage appearing with time according to a snowcover depletion curve. The depletion of a pack is calculated based on a temperature index algorithm.

2.4.2 CLASS 2.6

The soil thermal regime, energy regime and snow model for CLASS 2.6 are described in detail by Verseghy (1991). The vegetation thermal and energy regimes for CLASS 2.6 are also described in detail by Verseghy *et al.* (1993). Figure 2-7 illustrates the energy and water cycle components modelled by CLASS 2.6.
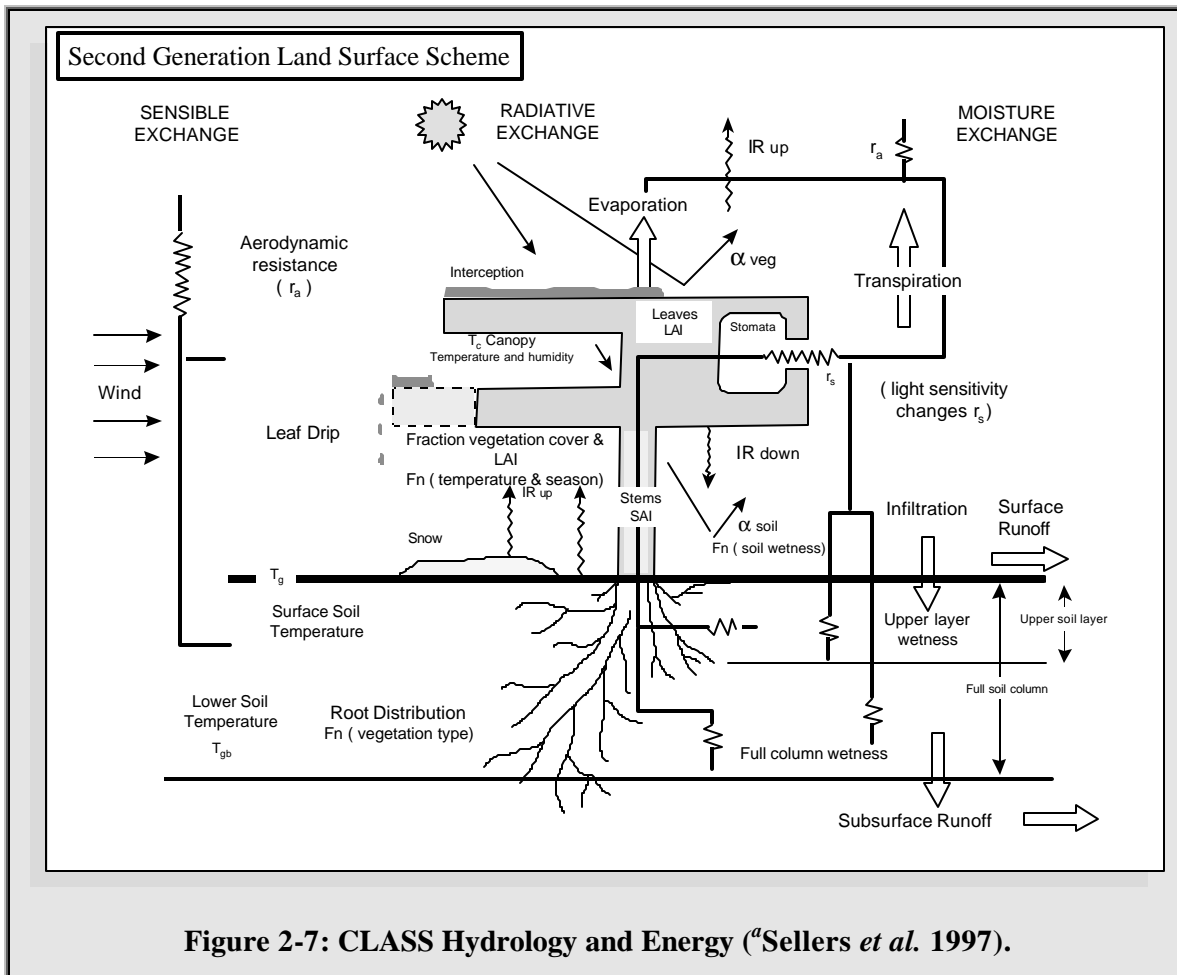
Figure 2-7: CLASS Hydrology and Energy ([a]Sellers *et al.* 1997).

CLASS 2.6 handles snow in the following manner: at the beginning of the first time-step, snow-water equivalent (SWE) is specified in an initialization file. This SWE, coupled with a user specified snow-density, is used to calculate the average snow depth. This snow depth is then used to determine the fractional snowcovered area based on a SDC. The fractional sub-areas of canopy over bare ground, bare ground, canopy over snow, and snow are adjusted accordingly. Snowfall that is not intercepted by the canopy is added to the snowpack and the snow depth within the four sub-areas is adjusted for frost formation, sublimation, snowmelt, new snowfall, rain melting snow, freezing ponded water, and snow aging. The overall average snow depth for the grid square is then recalculated and carried forward to the next time step. This process is illustrated in Figure 2-8.

Figure 2-8: CLASS Snow Processing for One Time Step.
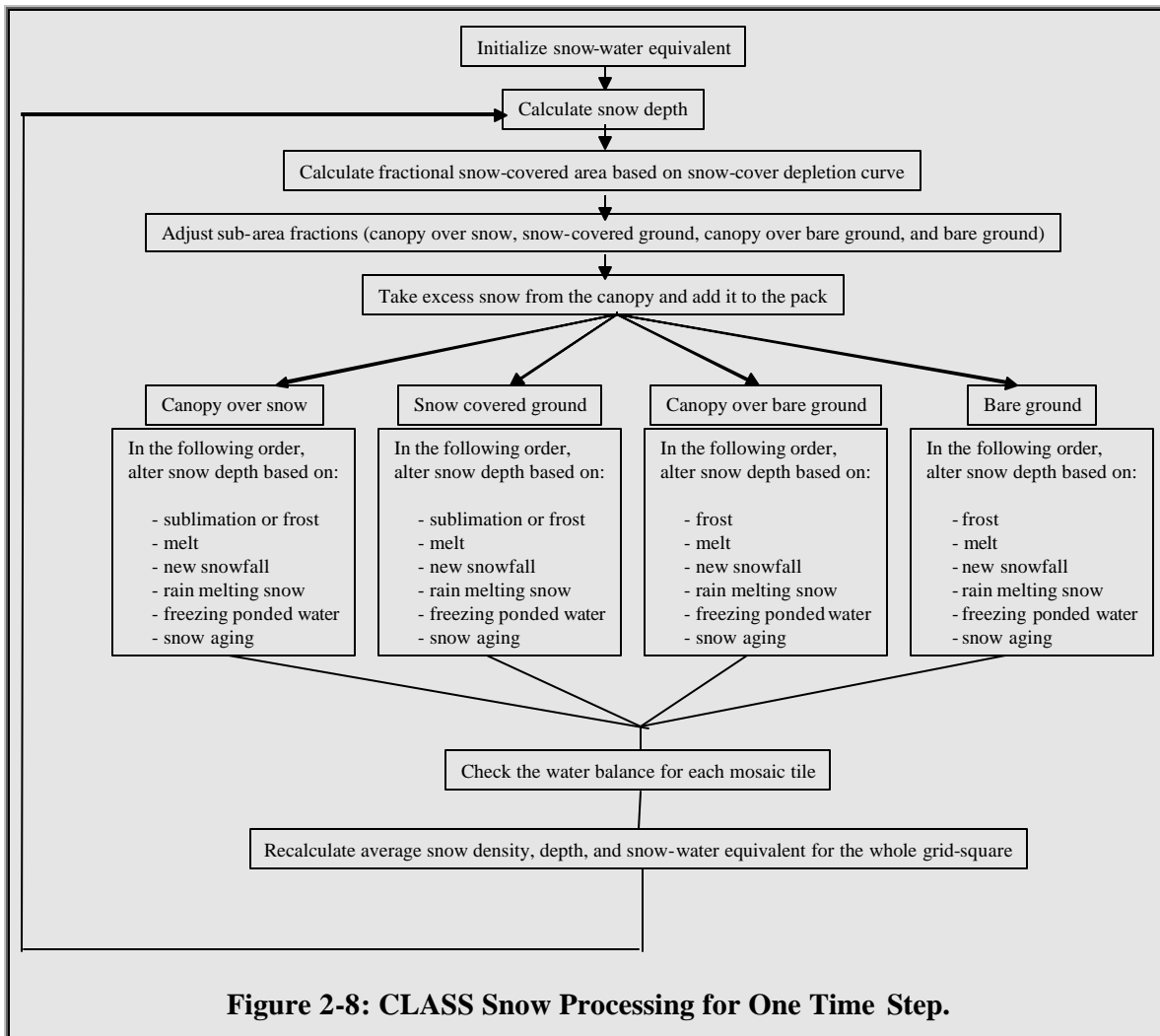
A number of the variables are averaged between the four mosaic tiles of canopy over snow, snowcovered ground, canopy over bare ground and bare ground. These variables are calculated individually over the four mosaic tiles, averaged at the end of the time step and then split evenly between the mosaic tiles at the beginning of the time step. The variables that are averaged, in terms of the snowpack, are snow albedo, snowpack temperature, snow density, snow depth and snow water equivalent.

In reality, the energy and mass balances are intricately intertwined. For the purposes of discussion, however, the snow processes discussed here are split into the categories of energy and mass.

2.4.2.1 Energy Balance Model

The energy balance for snow in CLASS is handled as if it were a variable-depth soil layer. There is no horizontal heat flow. The one dimensional heat conservation equation (Equation 2-19) is applied to each layer to calculate the temperature changes in the three soil layers and snow layer. $\overline{T}_i(t)$ and $\overline{T}_i(t+1)$ are the soil layer temperatures at the beginning and end of

$$\overline{T}_i(t+1) = \overline{T}_i(t) + \left[G(z_{i-1},t) - G(z_i,t)\right]\frac{\Delta t}{C_i \Delta z_i} \pm S_i$$

Equation 2-19: One-Dimensional Heat Conservation Equation for CLASS

$$G(z) = -l(z)\frac{dT}{dz}\bigg|_z$$

Equation 2-20: Soil Layer Heat Flux

the time step, Δt, $G(z_{i-1},t)$ and $G(z_i,t)$ are the downward heat fluxes at the top and bottom of the layer, C_i is the volumetric heat capacity of the soil, Δz_i is the layer depth, and S_i is a correction term applied in the case of freezing or thawing, or the percolation of ground water. G and z are both considered to be positive downward. If the surface temperature is known – regardless of whether or not there is snow on the ground– the soil layer heat fluxes can be calculated by Equation 2-20, where l is the thermal conductivity. Assuming that dT/dz is zero at the bottom of the lowest soil layer produces a system of three linear equations in the three unknown G's and an unknown surface temperature. If the surface temperature can be found, the fluxes can be computed.

When there is no snow, the surface temperature is calculated by iteratively solving a non-linear representation of the surface energy balance. K* is the net shortwave radiation, L* is the net longwave radiation, Q_H is the sensible heat flux, Q_E

$$K_* + L_* + Q_H + Q_E = G(0)$$

Equation 2-21: Surface Energy Balance

is the latent heat flux, and G(0) is the surface heat flux. Each of the terms in Equation 2-21 can be represented as a function of the surface temperature T(0), except for net shortwave radiation which is calculated as a function of albedo and the incoming shortwave radiation. The result is an equation that can be solved to find T(0), which can then be substituted back into the original equations to calculate the energy balance, heat flux, and layer temperature terms for the next time step. Equation 2-21 is the implementation of the energy balance, similar to the energy balance models described earlier, only for a surface without snow.

When snow is present, the same approach is used, with one more heat conservation equation (Equation 2-19) and one more unknown flux between the soil and snow. The inclusion of melting snow brings Equation 2-21 into line with Equation 2-10 and Equation 2-12. To gain a more in-depth understanding of how CLASS handles the snow energy balance, each of the components of the balance is considered individually in Appendix A.

2.4.2.2 Mass Balance Model

Precipitation

Ideally, atmospheric models would provide detailed information about the form of the precipitation, but this is not yet possible. In the meantime, the land surface model must decide how to deal with mixed precipitation. CLASS 2.6 turns all precipitation into snow if the near-surface air temperature is zero degrees Celsius or lower, and rain if the temperature is above zero degrees.

Canopy Interception

CLASS 2.6 treats snowfall canopy interception similarly to rainfall canopy interception, allowing for a maximum interception of 20% of the Leaf Area Index (LAI).

Runoff from the Bottom of the Pack

The runoff from the bottom of the pack is driven by the energy balance and has already been described in the melt energy subsection of the energy balance section.

Freezing Pond Water

If the surface temperature is below zero degrees Celsius, pond water will freeze, releasing latent heat causing the pond temperature to rise. The frozen water is then treated as snow in the model. If liquid water is still present in the pond, the temperature will increase to zero degrees Celsius, after which the energy losses will be used to cool the snowpack.

Density

Fresh snow is assumed to have a density of 100 kg/m^3. The density is assumed to be constant with depth and it increases with time to 300 kg/m^3, according to an equation formulated by Longley

$$r_s(t+1) = [r_s(t) - 300]\exp\left[\frac{-0.01\Delta t}{3600}\right] + 300$$

Equation 2-22: CLASS Density Calculation

(1960) and Gold (1958).

Snowcovered Area and Depth

The snowcovered area (SCA) is assumed to be one hundred percent unless the average snow depth is less than 10cm, in which case SCA is proportional to the depth, as described by the snowcover depletion curve. The current implementation of this relationship is able to represent sub-grid variability within a CLASS grid-square.

At first, the previous statement is not obvious. Without an SDC in the model, the snowcover in a model grid-square is uniform. Upon completion of melt under an SDC-free model, the grid square would instantly go from 100% covered to 0% covered. As described by Donald (1995) and Donald *et al.* (2000), observations clearly illustrate that a grid square would not become instantly bare. A number of sources illustrate the work being done to characterize patchy snowcovers (e.g. Cox and Zuzel 1976; Weisman 1977; Liston 1995; Essery 1997; Liston 1999; Neumann and Marsh 1998; Marsh *et al.* 1999). Thus, basin-wide and land-cover based SDC's represent a form of sub-grid variability within a grid-square. Donald (1995) provides a strong statistical indication that land-cover based SDC's can accurately represent the melt-cycle of a log-normal distribution of snow depths found in one type of land-cover.

Snow Water Equivalent

The snow water equivalent within a GRU is calculated as a multiplication of fractional snowcovered area, snow depth and density.

2.4.3 WATCLASS 2.7

Coupling WATFLOOD and CLASS has resulted in three major modelling improvements (Soulis *et al.* 2000). First, the GRU approach and stream routing of WATFLOOD enables WATCLASS to model the energy and water balances in a semi-distributed manner. Second, the improvement of interflow, with the incorporation of an internal slope and improved physics, increased the temporal resolution of modelled evaporation and latent heat. Third, channel routing allows CLASS physics to be used in the context of watershed modelling. In addition, a number of improvements have been made to the snow mass balance model (Fassnacht 2000; Fassnacht and Soulis 2002).

2.4.3.1 Interflow and Channel Routing

Hydrologically speaking, the coupling has introduced horizontal water fluxes, specifically through a mechanism for interflow and channel routing. Figure 2-9 illustrates a conceptual model of the coupled surface and sub-surface water budget.
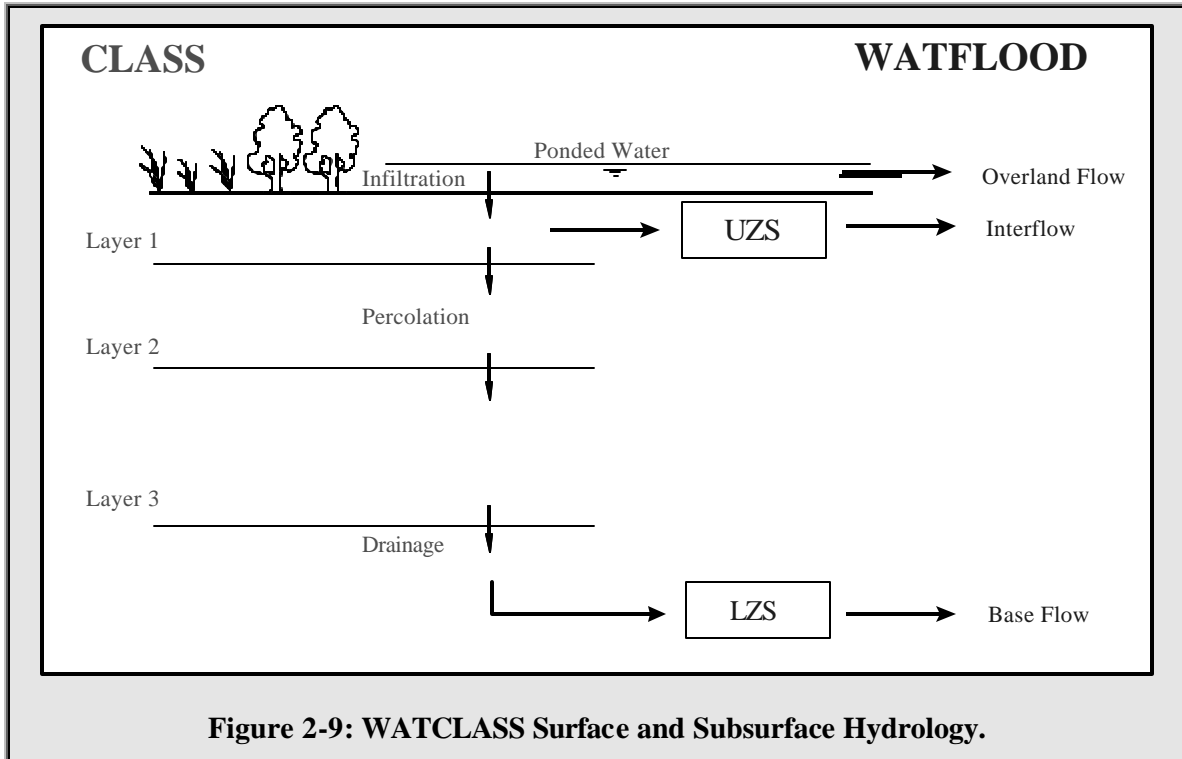
Figure 2-9: WATCLASS Surface and Subsurface Hydrology.

Saturated and unsaturated flow through the top layers of soil contributes significantly to streamflow, especially characterizing the recession limb of the hydrograph. The internal slope provides more interflow to the stream network. In CLASS 2.6, the soil would stay too wet during, and immediately after, a storm. One result would be an overestimation of evaporation and latent heat flux during this time (Soulis *et al.* 2000).

Figure 2-10 illustrates the internal slope and Figure 2-11 shows the interflow components included in the model.

Figure 2-10: Interflow from a Grid Cell (Soulis *et al.* 2000).

Figure 2-11: Interflow Components (Soulis *et al.* 2000).
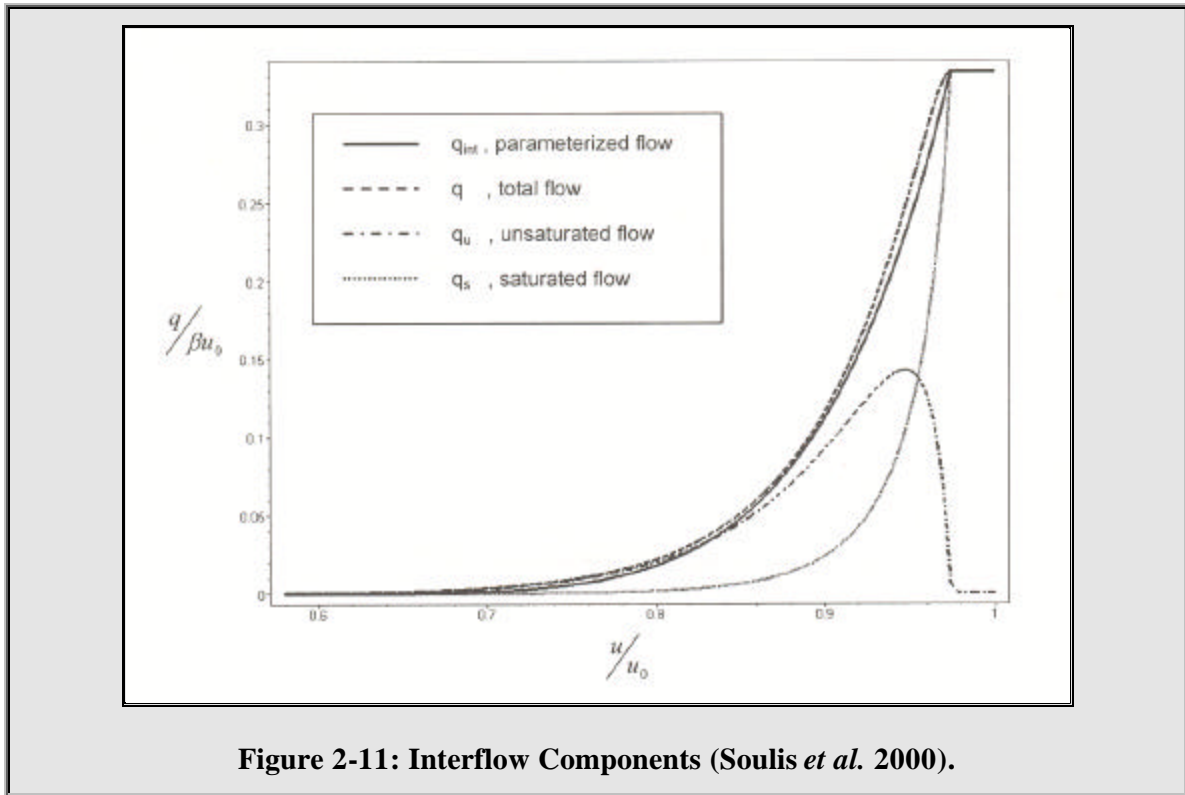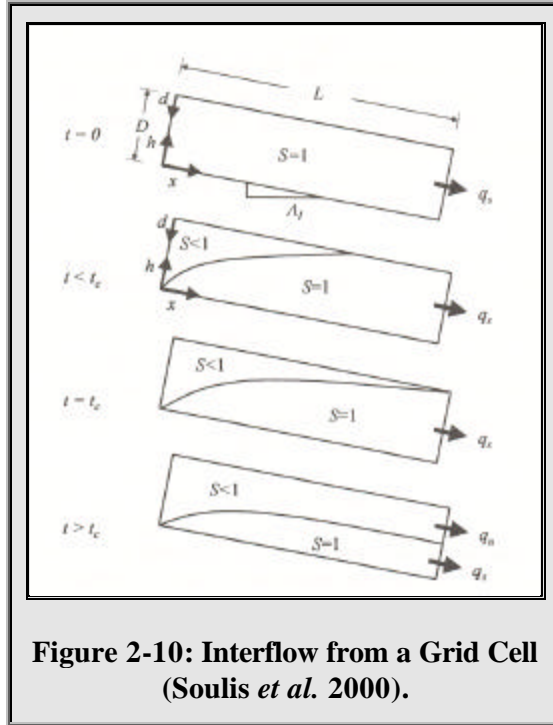
Considering a grid-element of length L and depth D, the interflow, q, in the element is characterized by saturated and unsaturated flow, q_s and q_u, respectively. At time t = 0, the entire element is saturated. The flow at the outlet remains saturated until t_c, the time of

$$q_{INT} = 2D_D K_{S0}(\boldsymbol{q}_S)\left(\frac{\boldsymbol{q}_1 - a\boldsymbol{q}_S}{\boldsymbol{q}_c - a\boldsymbol{q}_S}\right)^f \frac{D}{e+1}\Lambda_I$$

Equation 2-23: Interflow in WATCLASS

concentration, when the outlet flow is a mixture of saturated and unsaturated flow. Soulis *et al.* (2000) developed a power function approximation, q_{INT}, of the interflow (Equation 2-23). D_D is the drainage density, K_{S0} is the horizontal saturated hydraulic conductivity at the surface, $\boldsymbol{q}_1$, $\boldsymbol{q}_c$ and $\boldsymbol{q}_s$ are average soil moisture values for layer 1 at the current time, at maximum interflow, and at complete saturation, respectively, D is the element depth, Λ_I is the internal slope, 'f' is an exponent, 'a' represents the fraction of saturation at which there is no interflow, and 'e' is a horizontal hydraulic conductivity parameter.

In the top 10 to 20 cm of many soils, near surface horizontal hydraulic conductivity often declines by several orders of magnitude and is 10 to 100 times larger than vertical conductivities (Bear 1972). A thorough analysis of interflow under such

$$K_H(\boldsymbol{q}) = K_0(\boldsymbol{q}) \cdot \left(1 - \frac{h}{D}\right)^e$$

Equation 2-24: The Variation in Horizontal Hydraulic Conductivity

circumstances would require a detailed solution to Richard's equation, which would involve substantial data and computational resources. The difficulty associated with such a thorough solution warrants a less-rigorous parameterization, such as the one found in Equation 2-23. Arriving at this equation requires a number of assumptions and simplifications. First, only the relationship between the total outflow at the seepage face, q, and the average moisture stored in the block, u, is needed to provide flow to the grid-square stream element. Secondly, assuming that hill-slopes do not exceed 10% and the horizontal conductivity is 10 to 100 times larger than the vertical conductivity (Bear 1972), horizontal flow can be calculated using a one-dimensional form of Richard's equation. Third, the variation in hydraulic conductivity with depth can be represented by a power law (Soulis *et al.* 2000). The power law is shown in Equation 2-24 where $K_H(\boldsymbol{q})$ is the horizontal hydraulic conductivity at soil moisture value of $\boldsymbol{q}$, K_0 is surface hydraulic conductivity, D is the depth of layer 1 and 'h' is the relative distance below the surface.

2.4.3.2 Snow Mass Balance Model

A number of snow mass processes have been changed from CLASS 2.6 to WATCLASS 2.7. The snow processes that have been changed are precipitation, fresh snow density, maximum snow density and canopy snowfall interception. These processes were researched and implemented into an earlier version of WATCLASS by Fassnacht (2000), and incorporated in WATCLASS 2.7 by the author.

Precipitation

The algorithm for dealing with mixed precipitation is a sixth order polynomial shown in Equation 2-25.

$$F_s(T) = a_1 T^6 + a_2 T^5 + a_3 T^4 + a_4 T^3 + a_5 T^2 + a_6 T + b$$

Equation 2-25: Mixed Precipitation

$F_s(T)$ is the fraction of snow at temperature T and a_n (n = 1 to 6) and 'b' are coefficients. The empirical data collected in a number of studies have been fitted to the polynomial (U.S. Army 1956, Auer 1974, Rohrer 1989), resulting in different values for the coefficients. The studies in this thesis make use of the Auer curve (Auer 1974), with a lower temperature limit of 0.45 degrees Celsius, an upper temperature limit of 5.97 degrees Celsius, and coefficients of a_1 = 0.0202, a_2 = –0.3660, a_3 = 2.0399, a_4 = –1.5089, a_5 = –15.038, a_6 = 4.6664 and b = 100. Below the lower temperature limit of 0.45 degrees Celsius, all precipitation is modelled as snow. Above 5.97 degrees Celsius, all precipitation is modelled as rain. Between the upper and lower temperature limits, the polynomial function determines the percentages of rain and snow.

Fresh Snow Density

Fassnacht (2000) changed the fresh snow density in WATCLASS from a constant value of 100 kg/m^3 to one of the two equations by La Chapelle (1961) or Hedstrom and Pomeroy (1998). These equations were described previously in Equation 2-16 and Equation 2-17, respectively.

The Hedstrom and Pomeroy (1998) equation has been set with an upper limit of 150 kg/m^3 for temperatures greater than +1.22 °C. The lower limit approaches 67.92 kg/m^3 for temperatures below –15 °C. The Alta function, derived by La Chapelle (1961), has been set with an upper limit of 150 kg/m^3 for temperatures above +0.12 °C and a lower limit of 50 kg/m^3 for temperatures less than –15 °C.

Maximum Snow Density

CLASS 2.6 assumes that the magnitude of the density increases from a fresh value of 100 kg/m^3 to a maximum value of 300 kg/m^3. This maximum value was changed to 250 kg/m^3 for forest, as recommended by Gray and Prowse (1993), and 350 kg/m^3 for shallow packs.

Canopy Snowfall Interception

WATCLASS 2.7 treats snowfall canopy interception similarly to rainfall canopy interception, only allowing for a maximum interception of 20% of the Leaf Area Index (LAI). Although the 20% maximum interception value may be valid for rainfall, the maximum value for snow can be 50% or more of the LAI. The increased interception for snowfall is due to the bridging effect that occurs when snow builds up between the leaves and branches of the foliage. The rate of interception is described by Hedstrom and Pomeroy (1998) in Equation 2-14 and Equation 2-15.

Snow Mass Balance Bookkeeping

Figure 2-12 shows how WATCLASS keeps the SCA balanced from time step to time step. Figure Figure 2-12A shows the state of affairs once the SCA has been determined with the SDC. Snow is accumulated or depleted within the sub-areas of canopy over snow, canopy over bare ground, snow on bare ground, and bare ground (Figure 2-12B). The average snow depth is then re-calculated for the entire grid square (Figure 2-12C). This average depth is then passed on to the next time step, where the SDC algorithm calculates the SCA, completing the cycle (Figure 2-12A).
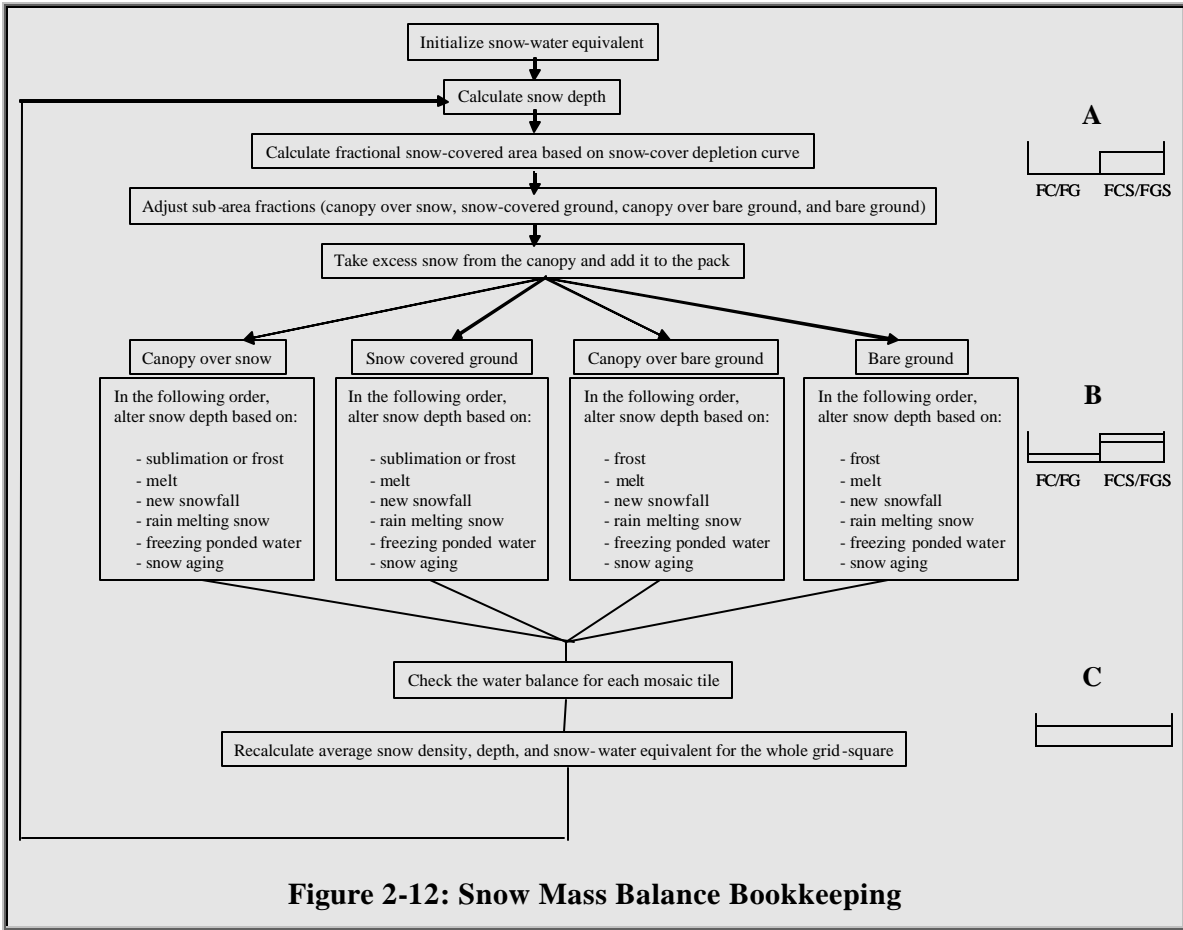
Figure 2-12: Snow Mass Balance Bookkeeping

2.5 Land Surface Heterogeneity

All land-surface and hydrologic models must deal with land-surface heterogeneity. WATFLOOD, CLASS, and WATCLASS are no different in the need to represent sub-grid variability within a grid square. WATFLOOD uses the grouped response unit (GRU) (Kouwen *et al.* 1993). The GRU is an alternative approach to the hydrologic response
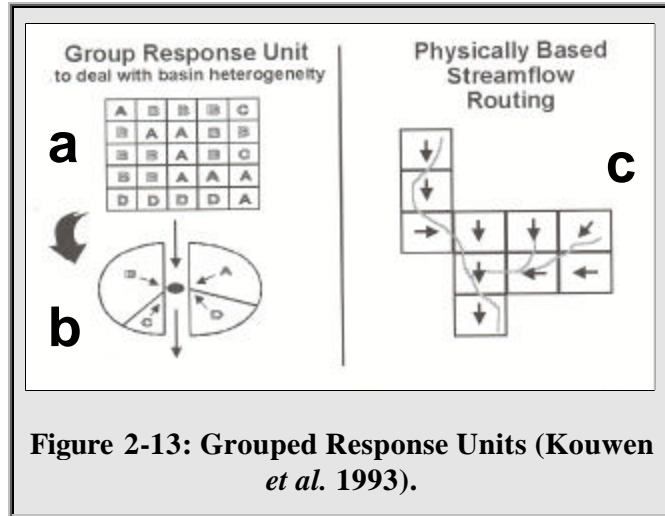
Figure 2-13: Grouped Response Units (Kouwen *et al.* 1993).

unit (HRU) (Leavesley and Stannard 1990) or representative elemental area (REA) (Wood *et al.* 1988). With the HRU and REA approaches, the watershed is categorized into sub-areas of similar hydrologic responses and calculations based on these sub-areas. Areas with uniform hydrologic characteristics would contain few HRU's or REA's while areas with considerable spatial heterogeneity would contain many HRU's or REA's. The GRU approach is similar to the HRU and REA approaches, but fundamentally easier for computational purposes. For the GRU approach, the watershed is carved into evenly spaced grid-squares and the HRU's within each grid-square are grouped together for calculations of the various hydrologic components. Snowcovered and snow free areas are calculated separately within each GRU. Figure 2-13 illustrates the GRU approach. Figure 2-13a is a grid-cell containing twenty-five pixels. The pixels have been classified based on their hydrologic response. The group of pixels with similar hydrologic response is then considered to be a lumped fractional area (Figure 2-13b) of the grid-square and calculations are performed on the grouped response, scaled by the fractional area that they represent in the grid-square. In WATFLOOD, each grid-square is considered to have a stream element, and so the outgoing streamflow for the square is calculated as a function of the overland flow, baseflow, interflow, stream storage and incoming streamflow. The calculations are performed on each grid-square and the streamflow routed to the next grid-element based on the drainage directions as indicated by the arrows on Figure 2-13c.

The GRU approach helps preserve the distributed nature of the watershed while maintaining computational efficiency. The groupings are often based on land class, but can have its foundation in other kinds of categorizations such as soil type, aspect, slope or proximity to other pixel types. It is often assumed that land-class is representative of soil type, which is the characteristic that generally determines the nature of land surface hydrologic responses; the exception being transpiration, which is directly related to vegetation. A recent study by Snelgrove (2002, section 5.3) illustrates that the assumption of land-class being linked with soil-type is not necessarily transferable from watershed to watershed.

CLASS 2.6 incorporates surface hetero-geneity through a combination of sub-area mixtures and vegetation group blends. Each grid-square is dynamically split into the four sub-area categories of canopy over snow (CS), snow over bare ground (GS), canopy over bare ground (C) and bare ground (G). The relative sizes of these sub-areas changes from one time-step to the next and depends on the leaf area index and fractional snowcovered area of the current time-step. Each grid-square also contains a static blend of five vegetation groups: crop, grass, needle leaf and broadleaf tree. If more than half of the grid square is ocean or glacier ice, the whole grid square is considered to be ocean or glacier ice. Otherwise, Figure 2-14 illustrates how the model separates the computational element into a mixture of four sub-areas and a blend of five vegetation groups.

Figure 2-14: CLASS 2.6 Representation of Land-Surface Heterogeneity
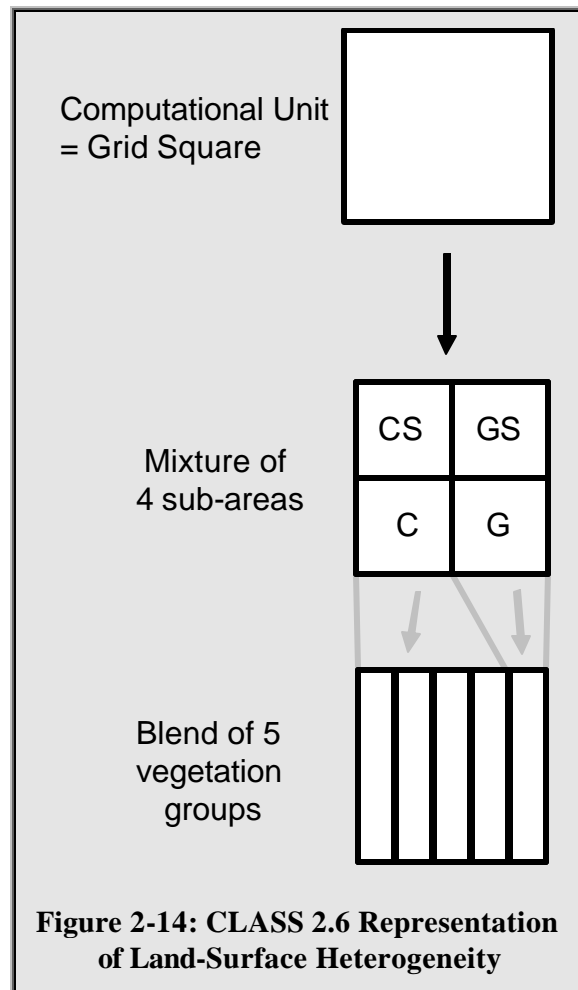
The mixture of sub-areas is dynamic because each sub-area changes from time-step to time-step. The blend of vegetation groups is static because the blend is set at the beginning of the model run. The variables calculated within the vegetation groups (e.g. maximum fractional areal canopy coverage, visible and near-infrared canopy albedoes, roughness length for momentum at vegetation maturity) are different than the variables calculated within the sub-areas (e.g. visible

and near infrared albedoes, outgoing long wave radiation, evaporation). The vertical water and energy balances are calculated based on the mixture of sub-areas.

WATCLASS 2.7 combines the GRU approach of WATFLOOD with the sub-grid heterogeneity methods of CLASS 2.6. This method allows WATCLASS to distribute over a watershed. As Figure 2-15 illustrates, the computational element of the grid square has been replaced with the GRU, providing an additional layer of calculations. In both the WATFLOOD approach and the WATCLASS 2.7 approach, the individual pixels (HRUs) that comprise the GRU are assumed to have similar hydrological responses.

Figure 2-15: WATCLASS 2.7 Representation of Land-Surface Heterogeneity
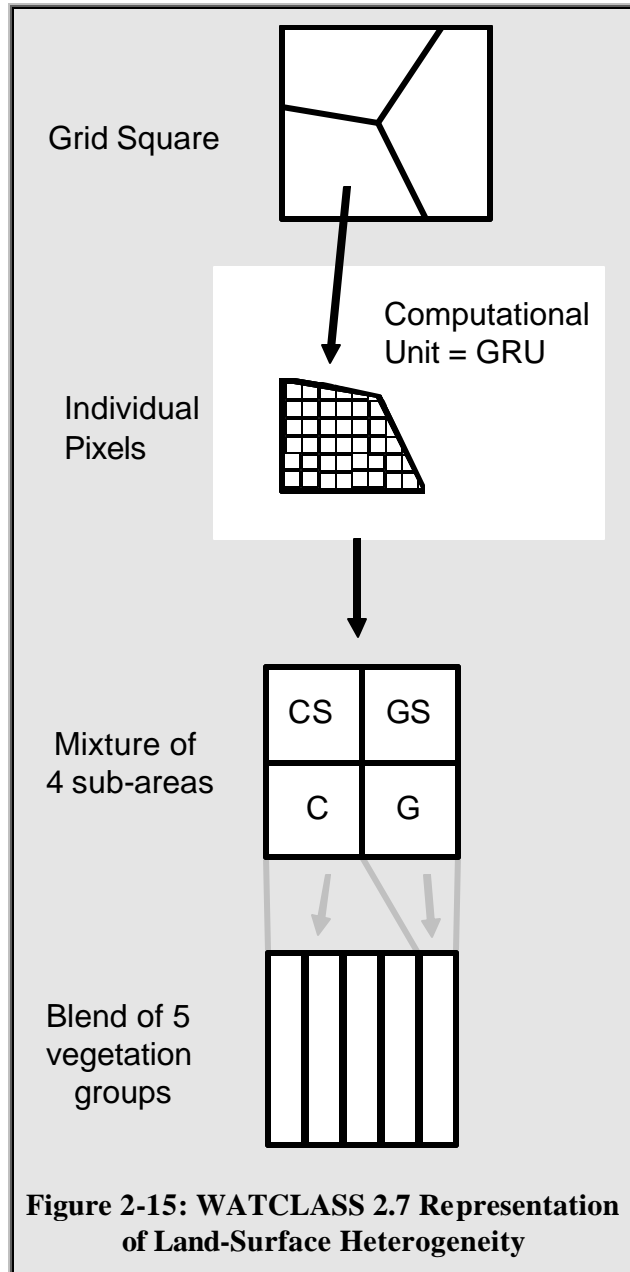
3. Investigating Aspects of Model Structure

This chapter presents an analysis of the modelling investigation performed to meet the first objective. The potential error sources illustrated in Figure 1-4 on page 9 highlight model structure errors as important considerations in modelling studies. In land-surface-hydrologic models, model structure represents physical processes. The previous work of Fassnacht (2000) and Fassnacht and Soulis (2002) identified mixed precipitation, variable fresh snow density, maximum snowpack density and canopy interception as processes that needed improving in the WATCLASS model structure. This chapter shows the results of an additional modelling study to identify the relative importance of these processes in a different basin. Fassnacht and Soulis (2002) performed their study on the 3520 km^2 Upper Grand River watershed in central south-western Ontario. The studies in this thesis are performed on a 397 km^2 watershed in central-northern Manitoba.

It is worth noting that the works of Fassnacht (2000) and Fassnacht and Soulis (2002) are more extensive than the work presented in this chapter. Figure 1-5 on page 10 is useful in making the distinction. Whereas the work of Fassnacht (2000) and Fassnacht and Soulis (2002) is represented by steps 2, 3 and 4 in Figure 1-5, the work presented in this chapter is represented by step 4, with the inclusion of an additional process (fractional SCA-hysteresis). In addition, Fassnacht (2000) and Fassnacht and Soulis (2002) had the benefit of a model that was reasonably calibrated to snow-water equivalent as well as streamflow. The calibration procedure outlined in this chapter produced reasonable results for streamflow, but failed to produce reasonable results for snow-water equivalent during the key snowmelt-period. Under the circumstances of having inaccurate modelled snow-water equivalent and snowcovered area, making conclusions about improvements to model structure based on comparisons to measured sensible and latent heat fluxes, net radiation and soil temperature was deemed inappropriate. As a result, the structural changes to the model are discussed with respect to the difference between the model output before and after implementing the model structure change.

For the remainder of this chapter, the study area is described, the model implementation procedure is explained and the results of the analysis are presented and discussed.

3.1 Study Area and Model Domain

The study area is a 397 km^2 basin near Thompson, Manitoba, near the northern edge of the boreal forest. The boreal forest totally circles the earth and covers just over 20% of the earth's forested area (Whittaker and Likins 1975). Concerns about climate change prompted a large scientific

campaign called the Boreal Ecosystem-Atmosphere Study (BOREAS). The purpose of BOREAS was twofold. The first emphasis was to improve our understanding of the processes governing the exchanges of radiative energy, water, heat, carbon and trace constituents between the boreal forest and the atmosphere, primarily in the form of mathematical process models. The second emphasis was to develop ways of scaling information from the detailed process scale to larger areas that cannot be measured in detail.
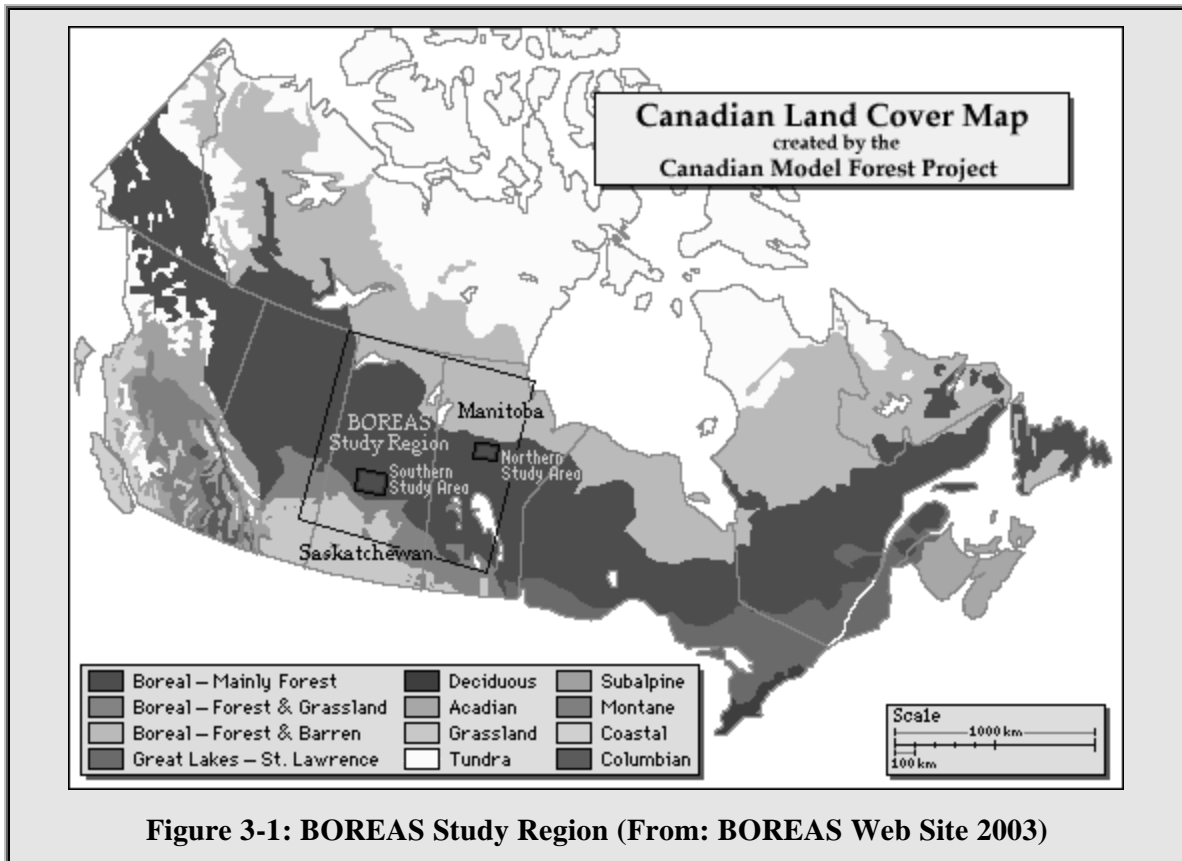
Figure 3-1: BOREAS Study Region (From: BOREAS Web Site 2003)

The BOREAS region encompassed a 1,000,000 km^2 area in central Canada. The study area was chosen to extend just beyond the southern and northern regions of the boreal forest. Figure 3-1 illustrates this region. Within this large area, two study areas were chosen for intensive field campaigns. The Northern Study Area (NSA) was located near Thompson, Manitoba close to the northern edge of the boreal forest. The Southern Study Area (SSA) was located near Prince Albert, Saskatchewan close to the southern edge of the boreal forest. In the SSA, moisture availability is one of the key factors controlling many environmental processes. In the NSA, temperature is more of an environmental control than moisture ([b]Sellers, *et al.* 1997). The NSA is illustrated in Figure 3-2, including the locations of flux towers (OJP, OBS, FEN and YJP) and

stream gauges (NW1, NW2 and NW3). The stream gauges NW1, NW2 and NW3 drain areas of 397 km^2, 28.9 km^2 and 50 km^2, respectively (Snelgrove 2002 – p173).
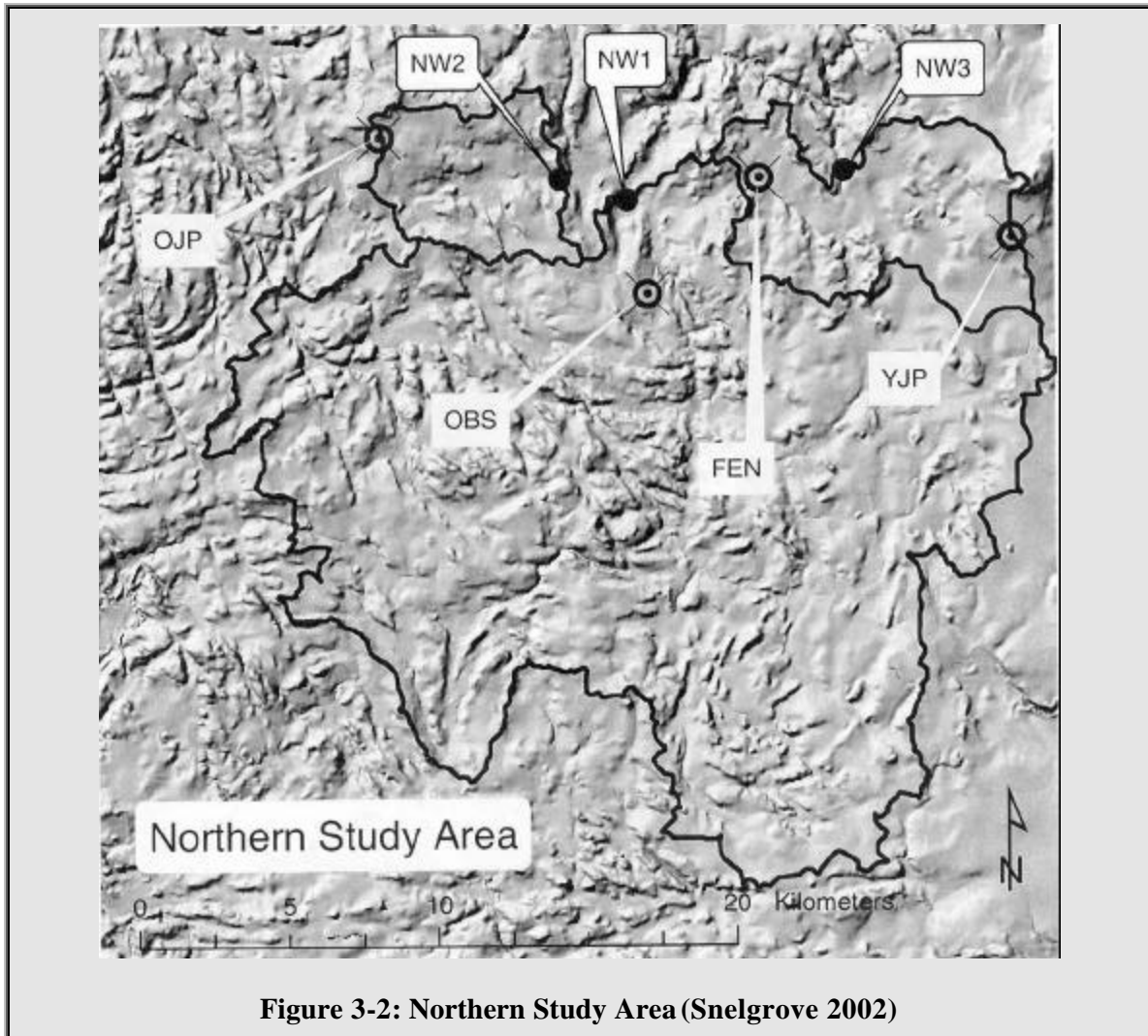
Figure 3-2: Northern Study Area (Snelgrove 2002)

The DEM used to generate the watershed features was derived by Snelgrove (2002) using Canadian National Topographic Database (NTDB) contour data supplemented by 1:50,000 scale river and lake data. A discussion on DEM selection can be found in Snelgrove's PhD Thesis (2002, section 5.2). Figure 3-3 shows the NSA model domain. The various shades of grey in each grid square represent the drainage area fraction for each grid cell. This term represents the area of a cell within the watershed boundary that flows in the indicated drainage direction (Canadian Hydraulics Centre, July 2003. p129). The number can be greater or smaller than 100% depending on the circumstances.

Figure 3-3: NSA Model Domain
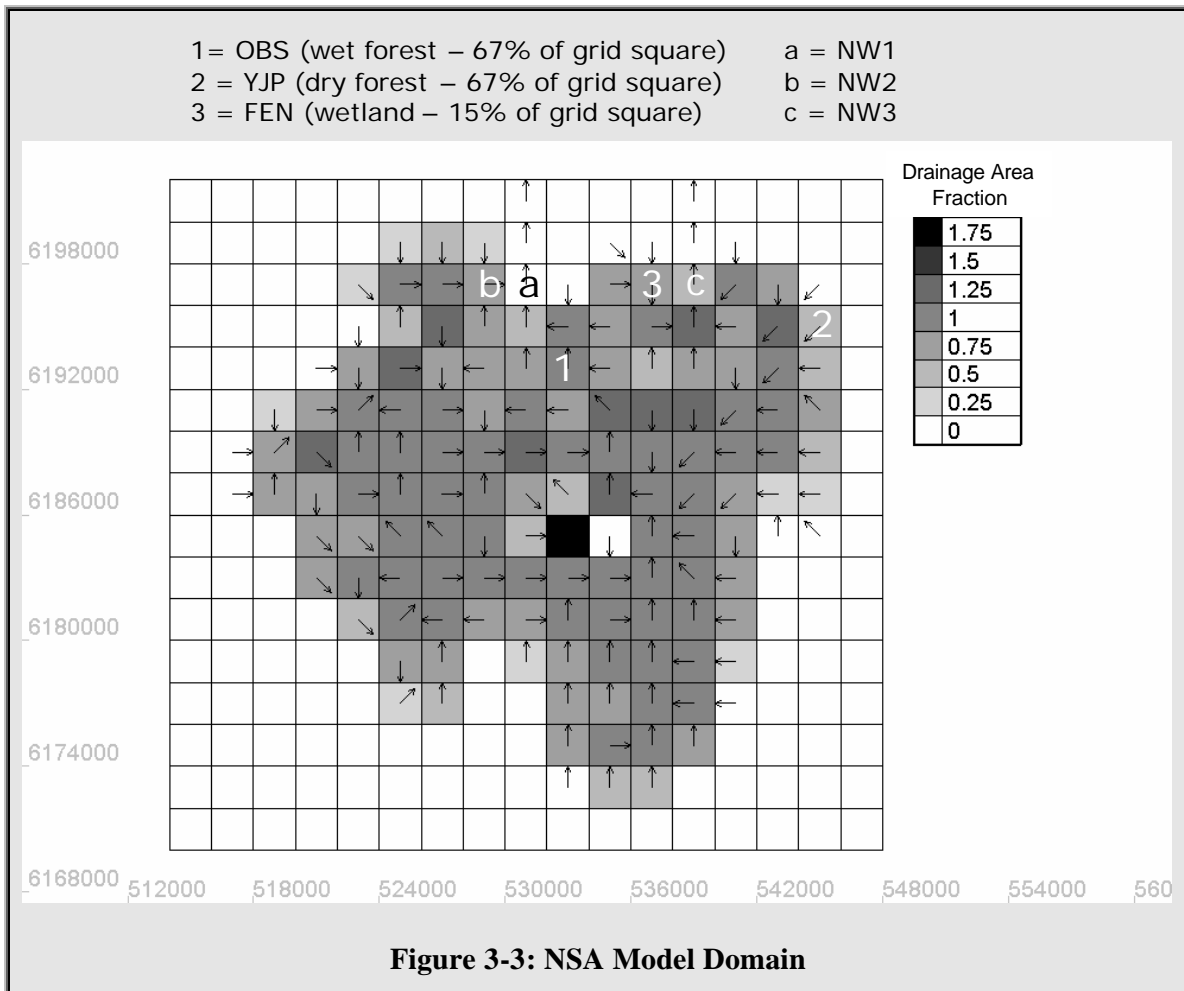
The drainage directions are illustrated with arrows. The fen (FEN), young jack pine (YJP), old jack pine (OJP), and old black spruce (OBS) flux tower sites are shown on the map. The three stream gauge locations, NW1, NW2 and NW3, are also shown. Table 3-1 shows some basic landcover statistics for the NSA, including the area of the watershed, the average internal slope and percentages of each landcover type (Snelgrove 2002, p190).

Table 3-1: Landcover Statistics for the NSA.

Area (km²)	Average Internal Slope (%)	Bare (%)	Dry Forest (%)	Wet Forest (%)	Wetland (%)	Water (%)
397	3.67	3.3	51.8	37.5	6.2	1.2

3.2 Method

The forcing data, parameters and model structure were provided for the study. Observed data were used to determine values and ranges for the initial conditions. The 1996 melt-period, from April 1st to July 31st, was chosen as the time period for the model runs. A manual sensitivity analysis was performed to: a) determine which initial conditions and parameters affect streamflow, and b) determine ranges for the sensitive parameters. A base case run was chosen from a visual inspection of the hydrographs. Objective functions were determined for examining model structure uncertainties and a second sensitivity analysis was performed to analyze the relative importance of these potential error sources.

3.2.1 Forcing Data, Initial Conditions, Parameters and Model Structure

Six of the seven forcing variables used for the run were developed in the BOREAS Follow-On Project (Snelgrove 2002). The precipitation data files were prepared by Whidden (1999). The manual sensitivity analysis was performed over 96 model runs. The sensitive parameters were found to be overland roughness (Manning's 'n' multiplied with effective hillslope length), transmissivity of a 5% slope (cm^2/sec), Clapp and Hornberger b (unitless), Kdepth power (effective depth in m), and river roughness (a combination of Manning's 'n' and channel slope characteristics). The sensitive initial conditions were found to be soil water (fraction of pore-space), soil ice (fraction of pore-space) and SWE (mm). The ranges for these parameters and initial conditions are listed in Table 3-2. The initial condition ranges for SWE are plus or minus 10% of the measured values, and soil water and ice are based on measurements.

Table 3-2: March 31st, 1996 Initial Condition and Parameter Ranges for Sensitive Parameters (units described in the above text).

	Bare	**Dry Forest**	**Wet Forest**	**Wetland**
SWE	119 – 145	110 – 134	119 – 145	107 – 131
Layer 1 ice	0.10 – 0.90	0.10 – 0.90	0.10 – 0.90	0.10 – 0.90
Layer 1 water	0.10 – 0.35	0.10 – 0.35	0.10 – 0.35	0.10 – 0.35
Layer 2 ice	0.06 – 0.90	0.06 – 0.90	0.06 – 0.90	0.06 – 0.90
Layer 2 water	0.04 – 0.10	0.04 – 0.10	0.04 – 0.10	0.04 – 0.10
Layer 3 ice	0.10 – 0.60	0.10 – 0.60	0.10 – 0.60	0.10 – 0.60
Layer 3 water	0.10 – 0.40	0.10 – 0.40	0.10 – 0.40	0.10 – 0.40
Overland Rough.	$5e10^2 - 5e10^6$	$5e10^2 - 5e10^6$	$5e10^2 - 5e10^6$	$5e10^2 - 5e10^6$
5% slope Trans.	$1e10^{-10} - 1e10^{-5}$	$1e10^{-10} - 1e10^{-5}$	$1e10^{-10} - 1e10^{-5}$	$1e10^{-10} - 1e10^{-5}$
Clapp-Horn. b	2 – 8	2 – 8	2 – 8	2 – 8
Kdepth Pwr	0 – 4	0 – 4	0 – 4	0 – 4
River Roughness	0.01 – 2.0 (for all five river-classes)			

The initial conditions were selected based on measurements found in the BOREAS documentation. Soil conditions were assumed to be the same throughout the basin and were based on measurements at the OBS site. In reality, it is likely that soil temperatures, moistures and ice contents would be distributed, but no attempt was made to distribute these values based on location. If the soil water and ice contents were collectively greater than 100%, the ice content was reduced. SWE and snow density were distributed based on landclass, as measured in the field, but would also likely be distributed based on location. The static initial conditions can be found in Table 3-3, followed by a description of the measured data that resulted in initial condition selection.

Table 3-3: Static Initial Conditions for the 1996 Melt Run (April 1 1996).

Initial Condition	Value
Layer 1 Soil Temperature	-5 degrees Celsius
Layer 2 Soil Temperature	-3 degrees Celsius
Layer 3 Soil Temperature	-0.5 degrees Celsius
Canopy Temperature	-10.28 degrees Celsius
Snow Temperature	-10.45 degrees Celsius
Wet Forest Snow Density	189 kg/m^3
Wetland Snow Density	198 kg/m^3
Dry Forest Snow Density	199 kg/m^3

The two soil plots at the OBS site had values of -2.4 and -9.3 degrees Celsius at 5cm, -1.4 and -5.6 degrees at 20cm and -0.1 and -0.9 degrees at 100cm. The chosen initial model temperatures were between these values for each of the three layers. The initial canopy temperature was set to the above canopy air temperature and the initial snow temperature was set to the air temperature at 2m. The SWE and snow density values are taken from standard snow surveys performed on March 30th 1996.

Figure 3-4 shows the measured soil moisture values at the OBS site, starting at 11 PM on July 13th 1995, and running to 3 AM on June 26th 1997. These graphs provided the basis for choosing initial soil water and ice contents.

Figure 3-4: Measured Soil Moisture at the NSA-OBS site (Cuenca, *et al.* **1999)**
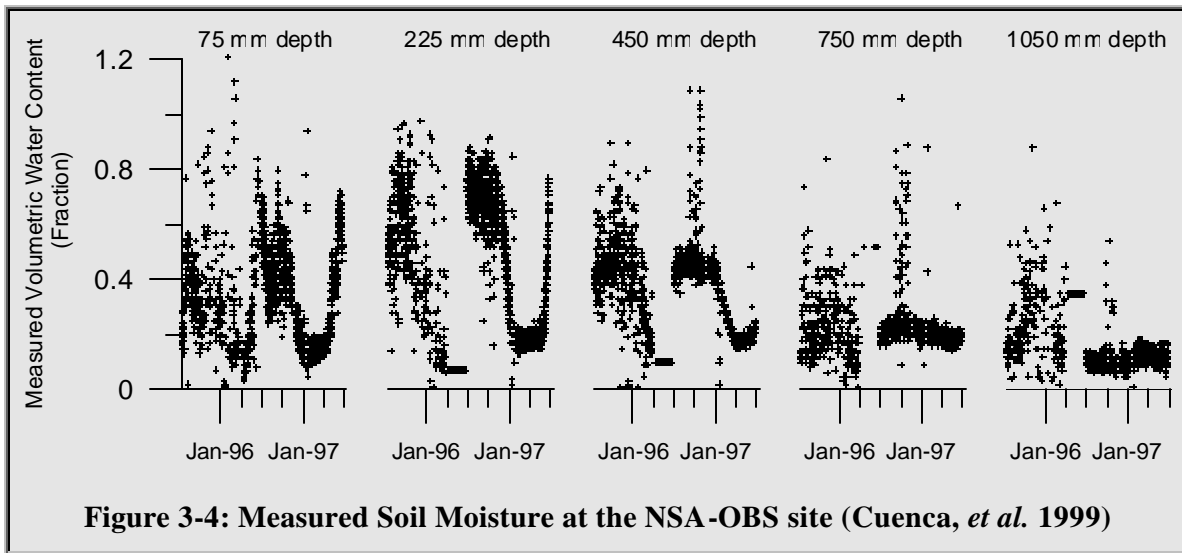
As the data show, the first year of data is extremely variable. This variability is possibly due to the measurement technique used rather than actual moisture variability. The instrument may have been installed in a manner that disturbed the soil considerably. As a result, the measurements would exhibit erratic behavior until the soil has settled back to a more natural structure. The time needed to reach this state of normal soil conditions depends on the soil, but for the northern climate of the NSA, is suspected to be at least one freeze-thaw cycle. The data show that the soil reaches a more stable state in June or July of 1996, one year after installation.

One definite source of error with the measurements is related to the method in which volumetric soil moisture is calculated. The instrument (TDR) estimates water content by passing electrical pulses down a coax or waveguide and measuring the reflected pulses. Due to the high dielectric constant of water, soil containing more water will propagate slower than soil with less water. The dielectric constant of soil is an order of magnitude smaller than that of water. Different soils have different dielectric constants, so some error is introduced if the moisture probe is calibrated to one type of soil and used on a different type of soil. To further complicate matters, the soil at the OBS site has a high organic content, which has a different dielectric constant than mineral soil. As a result, the soil moisture values measured at the site will be offset by an unknown amount.

According to the BOREAS documentation, the drop in soil moisture during the winter months is due to soil water freezing. Consequently, the initial soil ice content for the melt period run can be estimated from the preceding fall's soil water content. Unfortunately, the instrument had not been installed in time to provide stable measurements by the fall of 1995. Initial ice

conditions could be estimated from the stable measurements found in the spring of 1996, but it is unclear how much of the spring soil moisture is due to thawing soil ice and how much is due to infiltrating snowmelt.

The range for soil water in the first soil layer is based on the measured values at 75 mm of depth. On March 25th, 1996 at 8 PM, the measured soil moisture value was 0.31. For the next recorded measurement on April 8th at 8 PM, the value was 0.13. Slightly expanding this range provides some extra confidence that the true integrated value for soil water content from 0 to 100 mm lies within this range. It would be ideal to calculate a 95% confidence interval, but this less-rigorous approach was deemed to be appropriate. The ice content for layer one was estimated to be between the range of 0.10 and 0.90. The lower bound would be closer to the truth if the first 100 mm of soil was very dry before freeze-up the previous fall. The upper bound would be closer to the truth if the soil moisture that appeared in the spring of 1996 was entirely the result of soil ice melting after the snowmelt had already completely runoff.

The range for the soil water in the second layer is based on the measured values at 225 mm. On March 27th, 1996 at 2 PM, the measured soil moisture value was 0.06. For the next recorded measurement on April 8th at 6 AM, the value is 0.07. In an effort to include the errors due to measurement technique and in taking a point measurement to represent an integrated value, the range was set from 0.04 (the minimum water content allowed within WATCLASS) to 0.10. The ice content was set in the same manner as the ice content in layer 1, for dry autumn soil at 0.06 and for wet autumn soil at 0.90.

The range for the soil water in the third layer was based on an analysis of the three sets of measurements at 450 mm, 750 mm and 1050 mm. At the end of March 1996, the soil water contents at 450 mm, 750 mm and 1050 mm were 0.34 (March 25th, 6PM), 0.19 (March 27th, 10AM) and 0.45 (March 27th, 2PM), respectively. The range for the estimate of the true integrated soil water was set between 0.1 and 0.4. The deeper soil water contents at 450 mm, 750 mm and 1050 mm are higher than the soil water contents at 75 mm and 225 mm. It is suspected that the deeper layers contain more water because the freeze-thaw cycle is dampened by the thickness of the soil and vegetation transpiration is likely diminished. The measurements at 450 mm illustrate some freeze-thaw cycle. The measurements at 750 and 1050 mm fail to show such a dramatic freeze-thaw cycle, so the amount of ice in the layer depends on whether or not permafrost is present. The NSA lies in an area of sporadic-discontinuous permafrost ranging from 10% to 50% (Natural Resources Canada, 2003). As the measurements at 750 mm and 1050 mm

suggest in Figure 3-4, it is likely that the amount of ice increases with depth. The presence of permafrost in this region is corroborated with the climate normals for Thompson, Manitoba near the NSA (Environment Canada, 2003). The daily mean temperature for Thompson between 1971 and 2000 was minus 3.2 degrees Celsius. Deep soil temperatures are likely close to the climate normals, which provides additional support that deeper permafrost is present in this region. This evidence indicates that the possible range for ice content in layer three was set between 0.10 and 0.60. Based on the manual sensitivity analysis, the following sensitive parameters and initial conditions were used for the base case run.

Table 3-4: Base Case Run Values for Sensitive Parameters.

GRU	Units	Bare	Dry Forest	Wet Forest	Wetland
SWE	(mm)	132	122	132	119
Layer 1 ice	(Fraction)	0.10	0.40	0.10	0.10
Layer 1 water	(Fraction)	0.10	0.50	0.30	0.04
Layer 2 ice	(Fraction)	0.10	0.44	0.40	0.10
Layer 2 water	(Fraction)	0.06	0.56	0.46	0.04
Layer 3 ice	(Fraction)	0.30	0.30	0.30	0.30
Layer 3 water	(Fraction)	0.30	0.70	0.70	0.30
Overland Rough.*		$2e10^6$	$2e10^3$	$2e10^3$	$2e10^6$
5% slope Trans.(cm^2/sec)		$7.47e10^{-10}$	$1e10^{-7}$	$1e10^{-7}$	$1e10^{-7}$
Clapp-Horn. b	(unitless)	5	2	3	3
Kdepth Pwr	(effective depth)	0	1	1	1
River Roughness**		0.123, 0.918, 0.156, 0.631, 0.191			

* Manning's 'n' multiplied with effective hillslope length.
** A combination of Manning's 'n' and channel slope characteristics.

The resulting hydrographs are illustrated in Figure 3-5.

Figure 3-5: Base Case Run Hydrographs
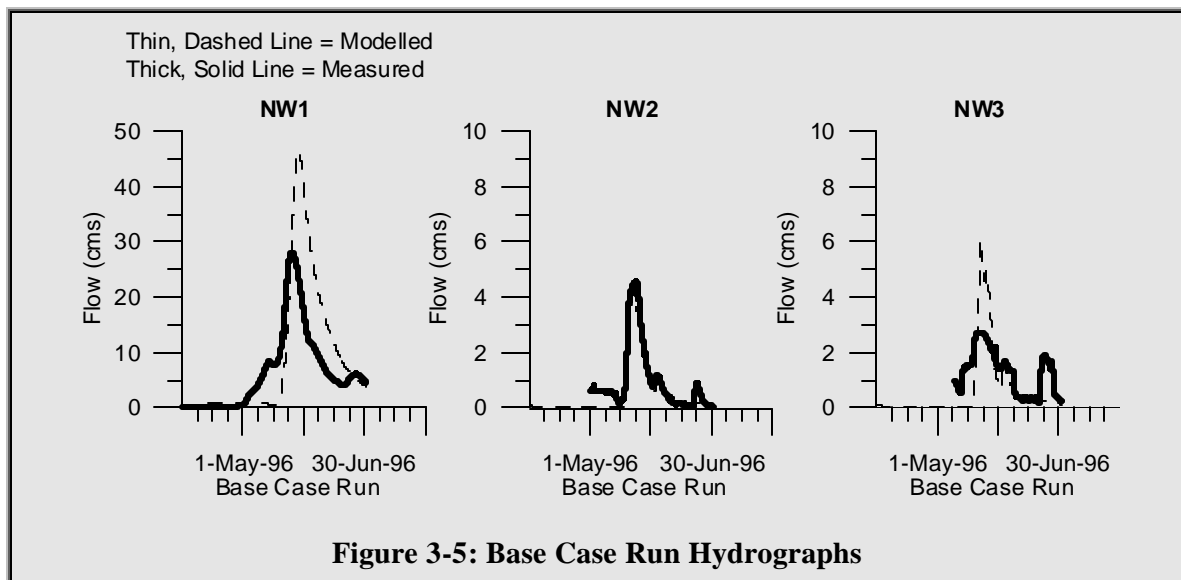
In all hydrographs, the thin, dashed line represents the modelled flow and the thick, solid line represents the measured flow. The timing of NW1 is reasonable, with too little streamflow at the beginning of the melt period and too much volume at the end of the melt period. The modelled hydrograph for NW2 is very close to the measured hydrograph such that the solid line overshadows the dashed line. The timing of NW3 is reasonable, but the volume and peak are too high. It should be noted that the y-axis values are different between the three hydrographs. These hydrographs were considered to be a good starting point for examining model structure components of WATCLASS more closely.

In terms of model structure, Fassnacht (2000) described the effects of implementing a number of new snow process algorithms within WATCLASS. The snow processes that Fassnacht considered in detail were snowfall canopy interception, mixed precipitation, variable fresh snow density and maximum snowpack density. In addition, a fractional SCA-hysteresis algorithm was developed as described in Chapter 4.

3.2.2 Sensitivity Analysis Objective Functions

The current research in objective functions for watershed modelling is being driven by the desire to automatically calibrate watershed models as effectively as an expert hydrologist with considerable calibration experience (Gupta *et al.* 2003 – p 13). Manual calibration by an expert is a very effective method to use, but also a time consuming task to perform and a difficult skill to develop (Gupta *et al.* 2003 – p 13). The highly non-linear nature of a hydrologic model's parameter space makes the selection of effective objective criteria troublesome. Many local maxima compound the problem because different parameter sets result in "reasonable" outcomes. One element of addressing this problem

$$\frac{\sum_{j=1}^{n}\left| y_j^{p_{k-1}} - y_j^{p_k} \right|}{\sum_{j=1}^{n}\left| y_j^{p_{k-1}} \right|}$$

Equation 3-1: Objective Function 1: Normalized Sum of Absolute Differences (NSAD)

$$\frac{\left| \sum_{j=1}^{n} y_j^{p_{k-1}} \right| - \left| \sum_{j=1}^{n} y_j^{p_k} \right|}{\sum_{j=1}^{n}\left| y_j^{p_{k-1}} \right|}$$

Equation 3-2: Objective Function 2: Percent Volume Change (PVC)

involves the move to multi-objective criteria in model calibration and evaluation. For the purposes of this thesis, however, three simple and informal objective functions were selected: the

normalized sum of absolute difference (NSAD), percent volume change (PVC), and maximum absolute difference (MAD).

These objective functions are informal because there are no guidelines about what function values are significant. The purpose of using these objective functions was not to calibrate the model, but to examine the relative importance of a number

$$\text{Max} \left\{ \left| y_j^{p_{k-1}} - y_j^{p_k} \right| \right\}, \, j = 1, 2, 3, \ldots n$$

Equation 3-3: Objective Function 3: Maximum Absolute Difference (MAD)

of model structure uncertainties in the modelled study area, given a set forcing data, initial condition and parameter space. The reader is referred to Duan *et al.* (2003) for a comprehensive discussion on the current state of research in model calibration. Each objective function was applied to streamflow, sensible heat flux and latent heat flux.

The three objective functions are defined by Equation 3-1, Equation 3-2, and Equation 3-3, where y is the streamflow, sensible heat flux or latent heat flux for time-step j; n is the number of time-steps; p_k, k = 1 to 6 are the runs described in Table 3-5. For each of the objective functions, larger numbers represent bigger changes between the model runs. For example, a larger value of the NSAD, PVC, or MAD indicates a larger effect of the model change on the objective function.

Table 3-5: Structural Code Change Runs

k	Description
1	Base Code
2	p_1 + mixed precipitation
3	p_2 + variable fresh snow density
4	p_3 + maximum snow density algorithm
5	p_4 + improved canopy interception
6	p_1 + fractional snowcovered area hysteresis

3.3 Results and Discussion

Table 3-6 shows the results of the sensitivity analysis. The streamflow results are for NW1 while the heat flux results are for the OBS site. The function values presented show the relative importance of the snow processes studied.

Table 3-6: Model Structure Sensitivity Analysis

K	Mixed Precip. 2	Var. Fresh Snow Dens. 3	Max Snow Dens. 4	Canopy Inter. 5	Snow Cov. Area Hyst. 6
NW1 Streamflow					
NSAD[+]	**0.25**	0.01	0.08	0.03	0.00
PVC[+]	**0.02**	0.00	0.00	0.02	0.00
MAD*	**16**	1	4	2	0
OBS Sensible Heat Flux					
NSAD[+]	0.02	0.00	0.01	**0.10**	0.00
PVC[+]	0.02	0.00	0.00	**0.06**	0.00
MAD**	78	75	177	**319**	72
OBS Latent Heat Flux					
NSAD[+]	0.03	0.00	0.02	**0.32**	0.00
PVC[+]	0.01	0.00	0.02	**0.17**	0.00
MAD**	72	71	188	**401**	46

+ Unitless, * Units of $m^3 s^{-1}$, ** Units of $W m^2$

For the NW1 streamflow, the mixed precipitation model run gave relatively high values of NSAD and MAD with low values of PVC, indicating a shift in the timing of streamflow. The other four model structure changes showed little difference in the streamflow results. For the sensible and latent heat fluxes, the canopy interception model run had the most pronounced impact. The mixed precipitation algorithm did not show much sensitivity to the heat fluxes. The fractional SCA-hysteresis algorithm showed no sensitivity to streamflow and minimal sensitivity to the sensible and latent heat fluxes. These results are not surprising because no snow fell on a partial pack for this set of model runs. Chapter 4 shows some results where the model had been adjusted to ensure two snow-falls on a partial pack. The difference between these results and those shown in Chapter 4 illustrate that caution is required when making conclusions. The analysis on model structure components was done on a single point in a very broad multi-dimensional space of forcing data, initial conditions and parameters. The chosen location in the multi-dimensional

space for Chapter 3 was simply unresponsive to fractional SCA-hysteresis. Other locations in this space would produce different results.

3.3.1 Mixed Precipitation

Fassnacht and Soulis (2002) found that the incorporation of mixed precipitation changed the model output at the point/event and watershed/event scales. In both cases, the event was precipitation near freezing air temperatures. For the point process, a mixed precipitation event at the beginning of the fourth week in January resulted in a deeper snowpack for almost a week, increasing the insulation to the soil. For the watershed process, a mixed precipitation event in mid-March resulted in a later contribution to streamflow due to the delay in the ripening of the pack. An increase in solid precipitation affected the energy balance by increasing the amount of snow to be melted while reducing the amount of rain that would apply melt energy to the pack.

Mixed precipitation events were examined for the NSA OBS site by first finding suitable events for the two year and ten month base case run. This approach was taken because it was first assumed that the two year and ten month run would be useable for analysis. The work to find suitable events was completed before the author realized that a melt-period run would be necessary. The resulting determination of potential mixed precipitation events helped to decide which melt-period would be examined. In all cases, the Auer curve (Auer 1974) was used for the analysis. An event was considered to be suitable if a precipitation event had a cumulative volume of greater than 10mm over a ten-hour time period, with an average temperature between -1 and +7 degrees Celsius during the same time frame. If two events occurred within the same twenty-four hour time period, they were considered one event. Using this approach, six such events were found as illustrated in Figure 3-6. It is worth noting that these event selection criteria will miss both short-term and long-term, low-intensity events.
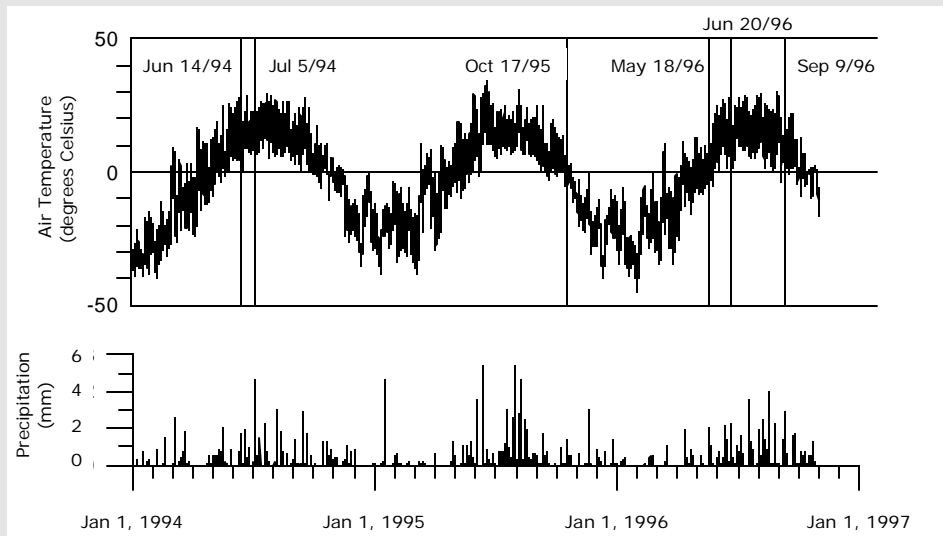
Figure 3-6: Potential Mixed Precipitation Events at the NSA – OBS site.

To determine the nature of the six events, a number of event characteristics were examined. The start time; end time; duration; precipitation volume; and temperature average, standard deviation, minimum and maximum were computed. These event statistics can be found in Table 3-7.

Table 3-7: Potential Mixed Precipitation Event Characteristics

Event	Start Time	End Time	Duration of Event (hours)	Volume (mm)	Avg Temp (°C)	Stdev Temp (°C)	Min Temp (°C)	Max Temp (°C)
1	7:00pm Jun 14/94	11:30am Jun 15/94	16.5	24.7	3.62	2.34	0.3	6.8
2	12:00pm Jul 5/94	5:30pm Jul 5/94	5.5	30.9	4.13	0.65	3.2	5.1
3	0:00am Oct 17/95	8:30am Oct 17/95	8.5	11.5	1.14	1.12	0	3.2
4	4:30pm May 18/96	11:30pm May 18/96	7.0	18.5	2.78	0.72	1.7	3.7
5	4:00am Jun 20/96	3:30pm Jun 20/96	11.5	24.5	7.94	2.72	4.2	10.8
6	6:00pm Sep 9/96	12:30pm Sep 10/96	18.5	58.0	7.07	1.75	4.8	9.8

In contrast to the criteria used to find suitable candidates, Events 5 and 6 had average temperatures above 7 degrees Celsius. This discrepancy occurred because a ten hour window was used to find a suitable event, while the entire event was considered for the analysis. For example, the event selection criteria determined that Event 6 occurred within the window of 1:00

AM and 11:00 AM on September 10th. The average temperature within this ten hour window was 5.9 degrees Celsius. The actual event occurred between the hours of 6:00 PM on September 9th and 12:30 PM on September 10th, a total of eighteen and a half hours with an average temperature of 7.07 degrees Celsius.

Due to the fact that events 4 and 5 fell within the 1996 melt-period, this time frame was chosen for analysis and the melt period sensitivity runs were completed. The impact of the mixed precipitation algorithm was examined by looking at the impact on streamflow; GRU base, overland and interflow; snow and soil mass and energy terms; and the surface energy budget.

3.3.1.1 Spatial Processes – Streamflow

The streamflow analysis illustrated that the mixed precipitation event resulted in a delayed streamflow. In addition, it was found that p_2 produced an increase in streamflow of 2% over the three month run. Figure 3-7 shows the streamflow results.

Figure 3-7: Mixed Precipitation Algorithm Impact on River Flows.
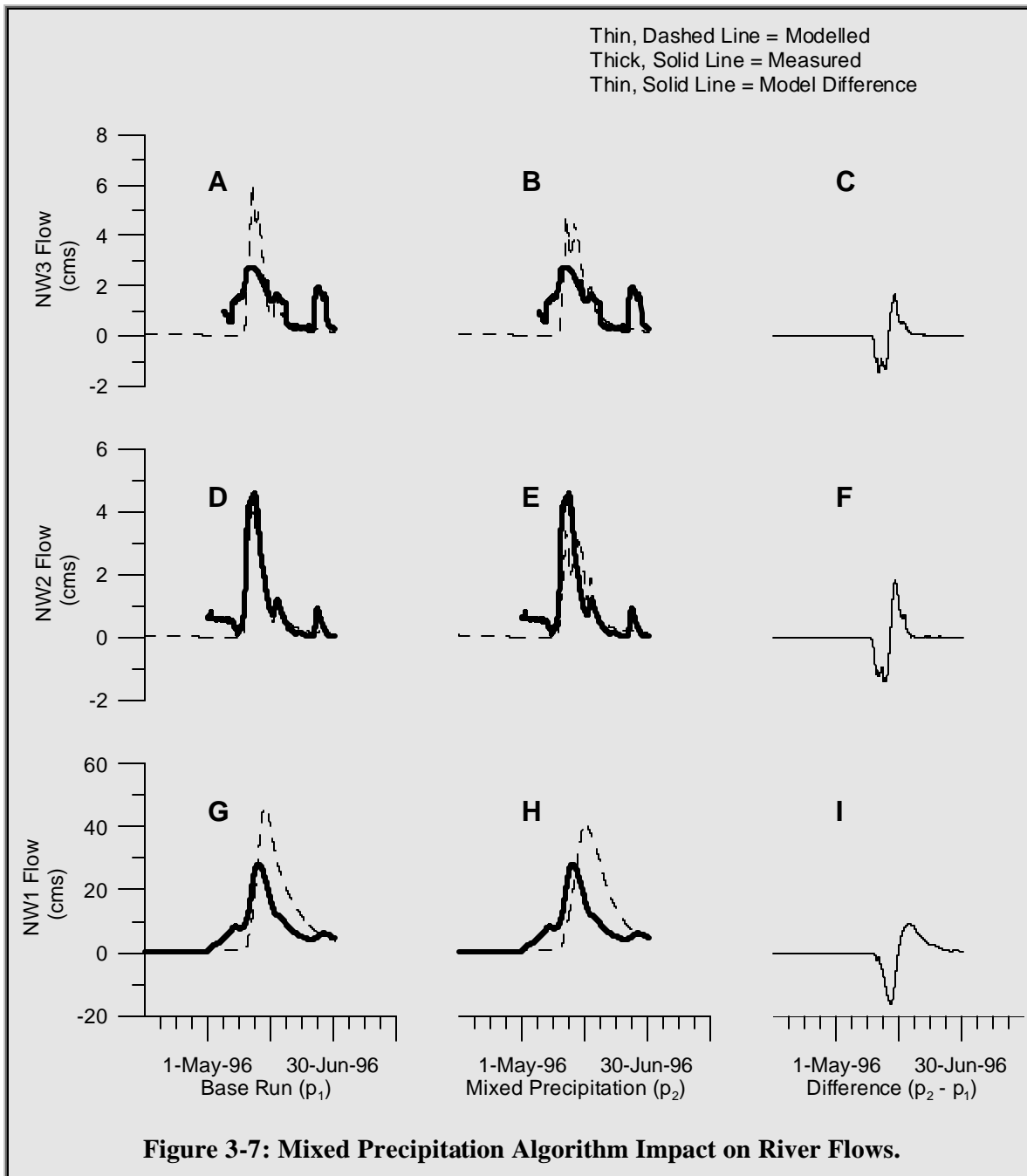
Figure 3-7 A, D and G show the model output without any snow code changes while B, E and H show the output with the mixed precipitation algorithm. Figure 3-7 C, F and I illustrate the differences between model run p_2 and model run p_1. It was clear from these figures that streamflow was delayed. At this point, it was speculated that this result occurred for the same reasons that Fassnacht and Soulis (2002) found in their analysis. An increase in solid precipitation would form a deeper snowpack and delay runoff due to the reduction in energy available for melt

(in addition to the extra snow to be melted). Evaporation would also have to have been reduced to produce more streamflow. A detailed examination of point processes focused on the mass and energy components.

3.4.1.2 Point Processes – Mass Component Analysis

Considering the snow mass terms illustrates the differences between the runs. Figure 3-8 A, B, C, D and E show the modelled values of precipitation, SWE, SCA, snow depth and snow density; and the measured values of SWE, snow depth and snow density. Both model runs failed to match the measured values. The differences between the runs p_1 and p_2 were difficult to discern without the benefit of Figure 3-8 F, G, H and I. (The dashed line is overlaid by the solid line.) These figures show that, after the potential mixed precipitation event, the incorporation of mixed precipitation (p_2) resulted in an increase in SWE, SCA and depth; and a decrease in snow density. The density decreased because the increase in SWE and depth was due to an increase in snowfall that had not yet had time to compact. The hatched box in Figure 3-8 shows the model melt period for the runs, which mainly ranges from May 15th, 1996 to May 31st, 1996. As the density values indicate, some snow remains after May 31st, but it is minimal in SWE.

Figure 3-8: Snow Mass Balance Analysis of the Mixed Precipitation Algorithm.
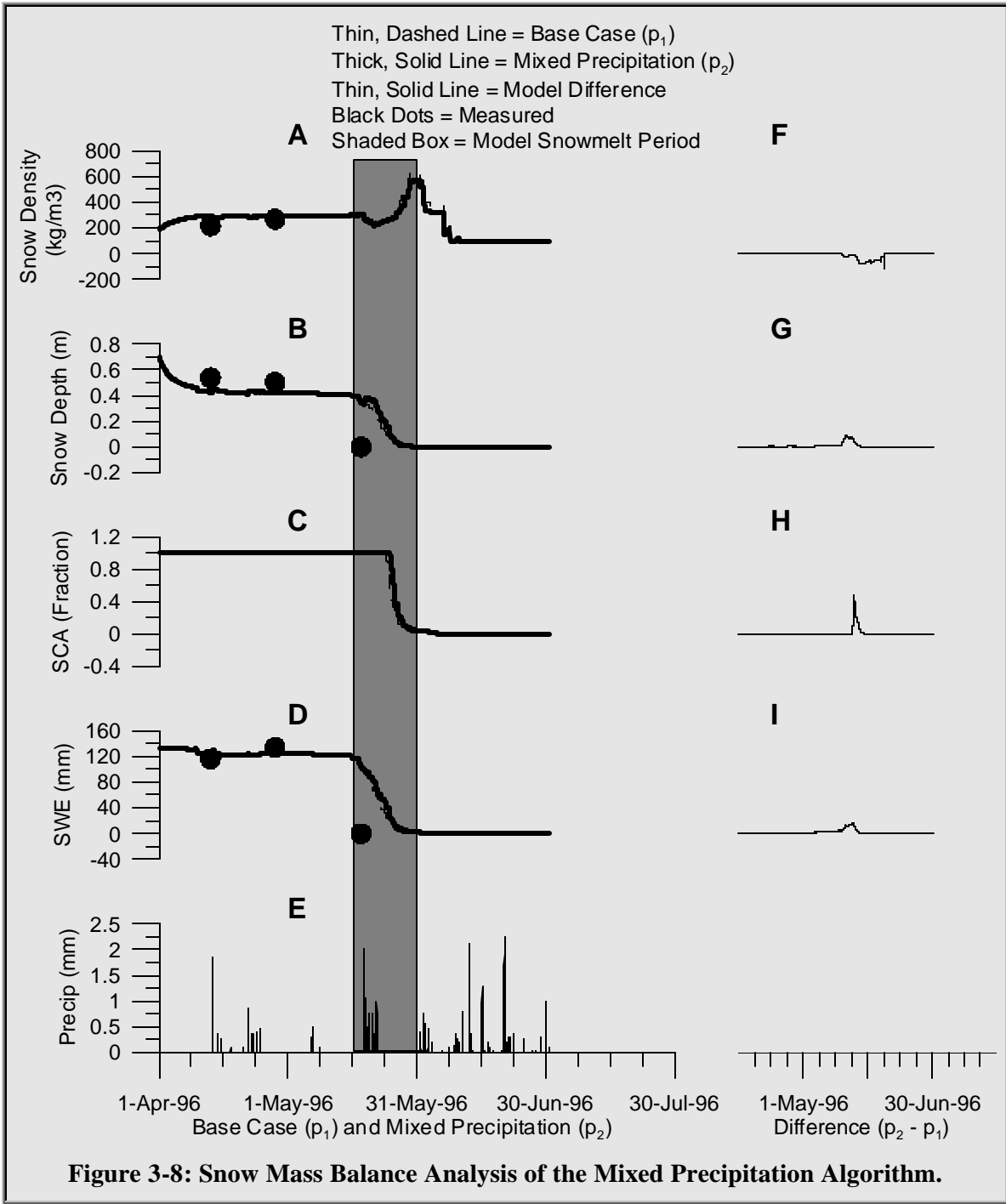
Figure 3-9 shows the impact of the algorithm on the GRU flow components at the OBS site. The difference between the two model runs is not visible in A, B, C or D, but F, G, H and I show that the overland flow was delayed. This corresponds with the streamflow delay shown in Figure 3-7.

Figure 3-9: GRU Flow Balance Analysis of the Mixed Precipitation Algorithm.
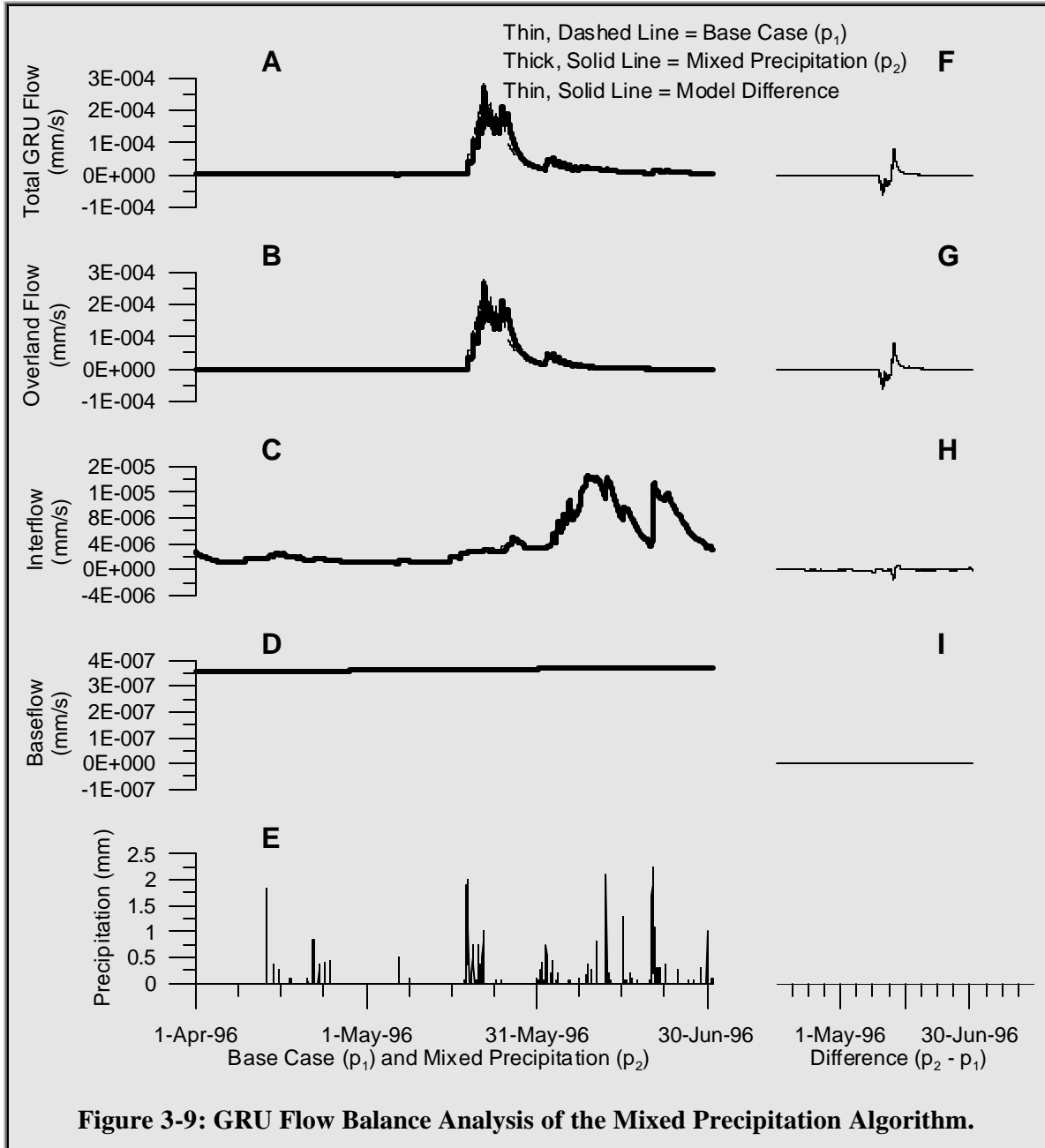
Figure 3-10 shows the results of the algorithm on the modelled soil ice and water contents.

Figure 3-10: Soil Water and Ice Analysis of the Mixed Precipitation Algorithm.
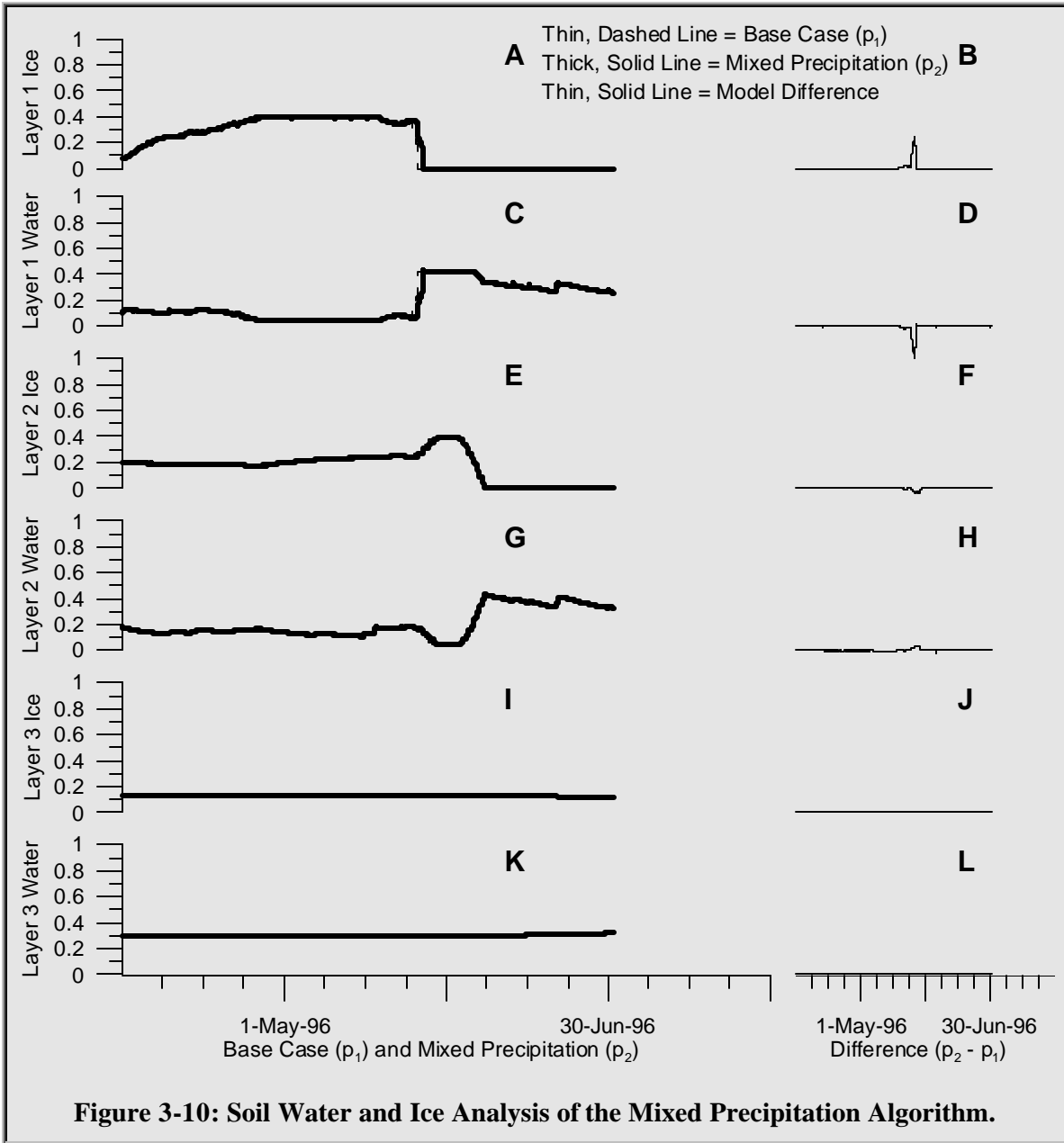
It is clear from Figure 3-10 that there is very little difference between the two runs. The dashed lines are not visible on any of the graphs. The only noticeable impacts, shown in Figure 3-10B and D, are that the algorithm delayed the melting of ice in layer one. This delay in soil-ice melt was an indication that the extra snow in Figure 3-8 insulated the soil from atmospheric energy available later in the melt period.

3.3.1.3 Point Processes – Energy Balance Analysis

The first step in analyzing the energy balance was to consider the soil layer temperatures.
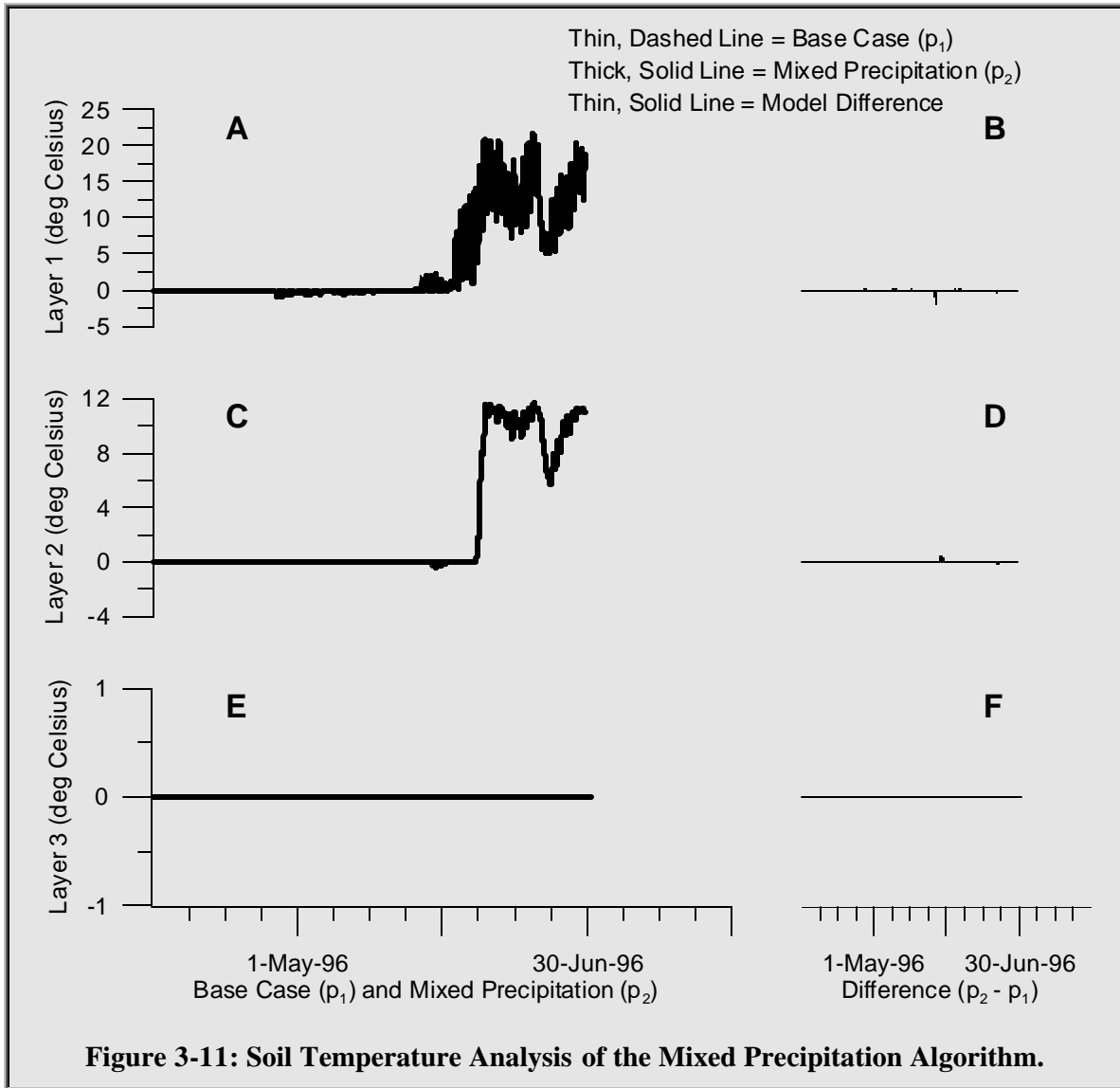
Figure 3-11: Soil Temperature Analysis of the Mixed Precipitation Algorithm.

Figure 3-11B shows a slight decrease in p_2 versus p_1 soil temperature during the period of additional SWE. The extra snow, which provided insulation from the atmospheric energy, needed to melt first. Figure 3-12 shows the energy effects of the mixed precipitation algorithm. Figure 3-12A through G show the time series data for the base case melt-period run (p_1). Figure 3-12H through M show the cumulative differences between p_2 and p_1. Figure 3-12N shows the straight difference between p_2 and p_1 surface temperature. The units for H through M are Watt-hours per

square metre, which is an appropriate unit of measure for a cumulative energy term. (i.e. 1 Watt = 1 Joule per second; 1 Watt-hour = 3600 Joules.)

To determine the significance of the graphs in Figure 3-12, it was worth revisiting the energy balance equation used within WATCLASS. Equation 3-4 is

$$K_\downarrow + K_\uparrow + L_\downarrow + L_\uparrow + Q_H + Q_E + I(z)\frac{dT}{dz}\bigg|_{z=0} = 0$$

Equation 3-4: Surface Energy Balance

an expanded form of Equation 2-21, splitting the net radiation terms into outgoing and incoming components and substituting the ground flux term with the instantaneous change in temperature at the surface.

The outgoing radiation components in Equation 3-4 are preceded by plus signs because their values were plotted as negative, counterbalancing the positive incoming values. Figure 3-12I and K show negative values for the cumulative differences of outgoing shortwave and long-wave radiation. As the values themselves are negative, the cumulative differences indicate that p_2 produced more outgoing shortwave and long-wave radiation than p_1. As a result, less energy reached the surface and, coupled with the increase in SWE, further delayed the melt. The delay in melt insulated the soil for a longer period of time and subsequent input energy was used to release latent heat by melting soil ice instead of contributing to latent flux to the atmosphere by evaporating soil water (Figure 3-12M). As a result, the surface temperature rose (Figure 3-12N), causing a relatively dramatic increase in sensible heat exchange with the atmosphere Figure 3-12L).

The additional snow due to the mixed precipitation algorithm altered the surface energy balance; delaying runoff and layer 1 soil ice melt, reducing evaporation, and increasing sensible heat flux to the atmosphere as a result.

Figure 3-12: Surface Energy Analysis of the Mixed Precipitation Algorithm.
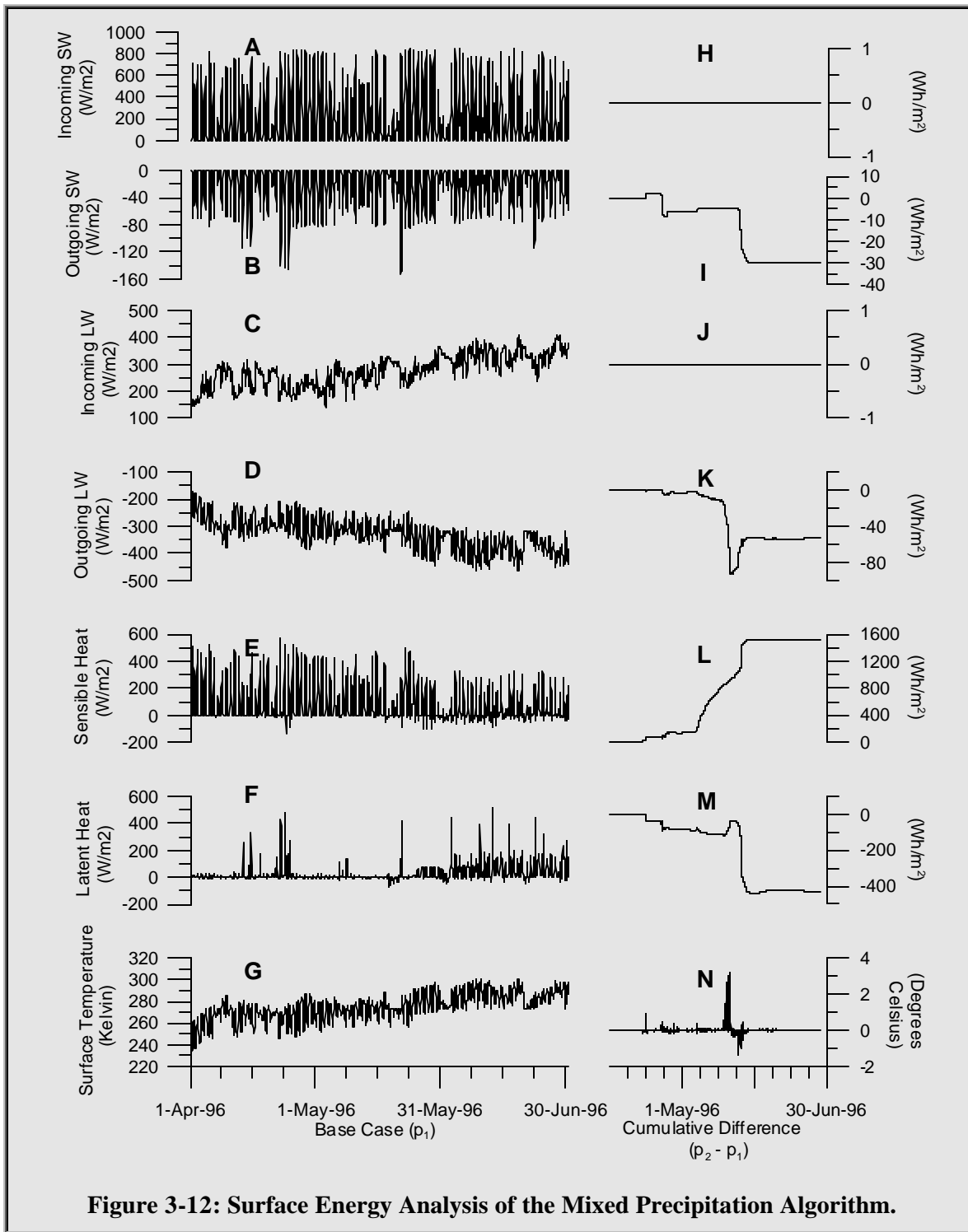
3.3.2 Variable Fresh Snow Density

Fassnacht and Soulis (2002) found that the incorporation of variable fresh snow density changed the model output at the point/event scale. The algorithm had a small impact on the hydrographs which represent the watershed scale. For cold temperatures, the smaller density resulted in a

larger depth. For warmer temperatures, the different density algorithm resulted in a smaller depth, producing a patchy cover to form sooner in the melt phase. This patchy cover then resulted in dramatically different surface heat fluxes while there was a difference between the patchiness.

To examine the impact of variable fresh snow density on the NSA model runs, an analysis was performed in the same manner as with the mixed precipitation algorithm. The Hedstrom and Pomeroy (1998) curve was used in the analysis. The remaining figures only show the differences between the model runs. Figure 3-13 shows the results of the streamflow.

Figure 3-13: Streamflow Impact of the Fresh Snow Density Algorithm.
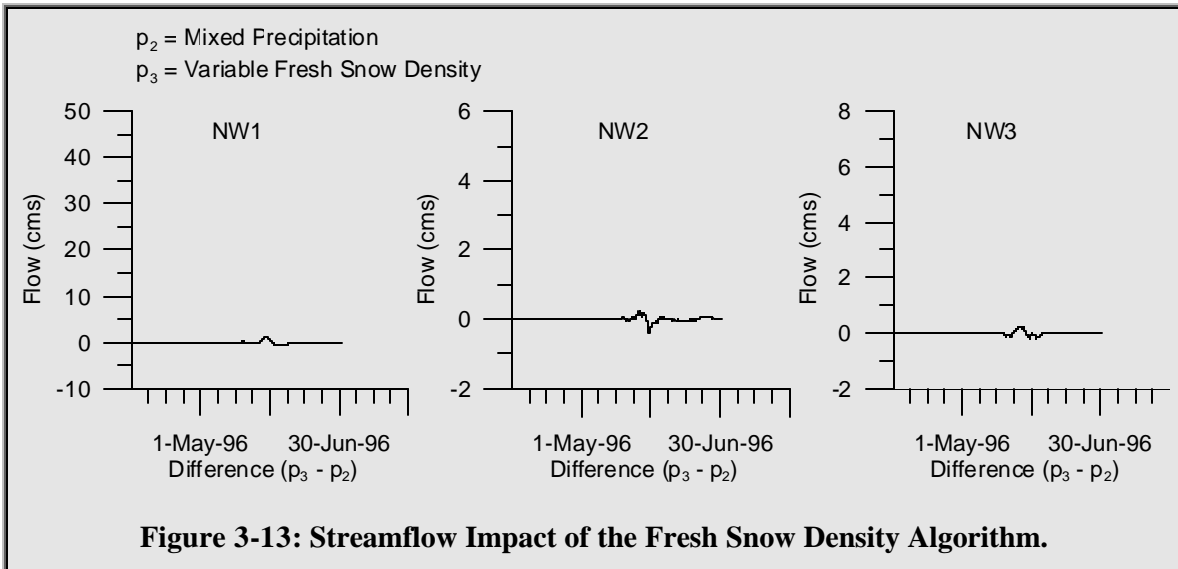
As Figure 3-13 illustrates, the impact on streamflow was minimal. The impact on the GRU flow components (Figure 3-14), soil ice and water contents (Figure 3-15), and soil temperatures (Figure 3-16) was also minimal.

Figure 3-14: GRU Flow Balance Analysis of the Fresh Snow Density Algorithm.

Figure 3-15: Soil Water and Ice Analysis of the Fresh Snow Density Algorithm.

Figure 3-16: Soil Temperature Analysis of the Fresh Snow Density Algorithm
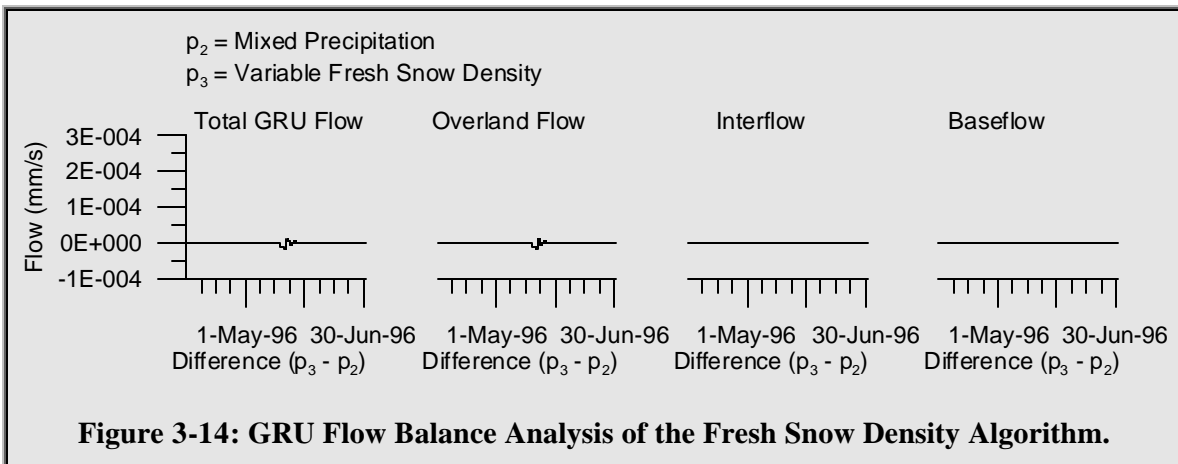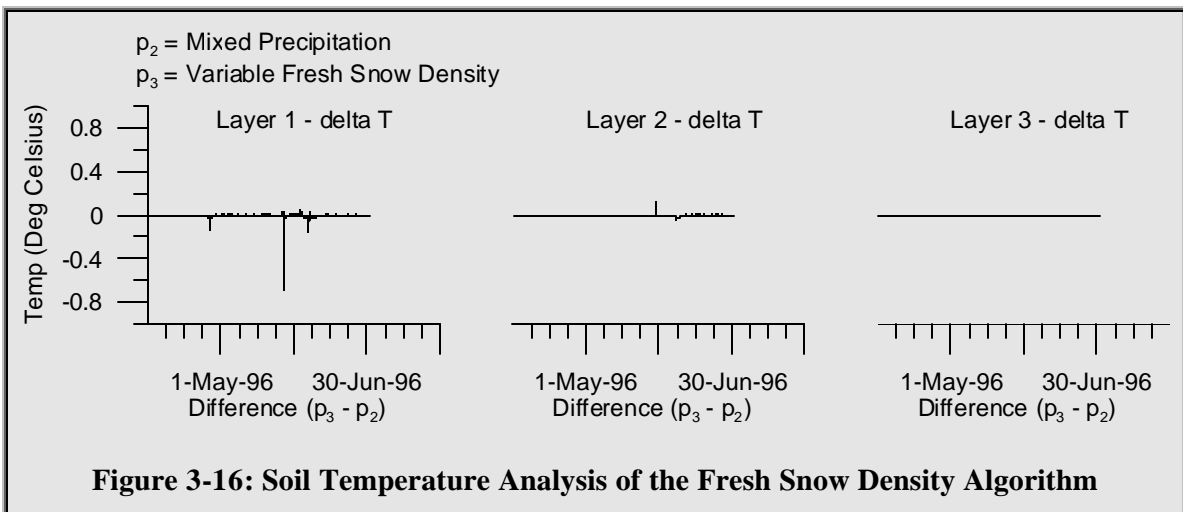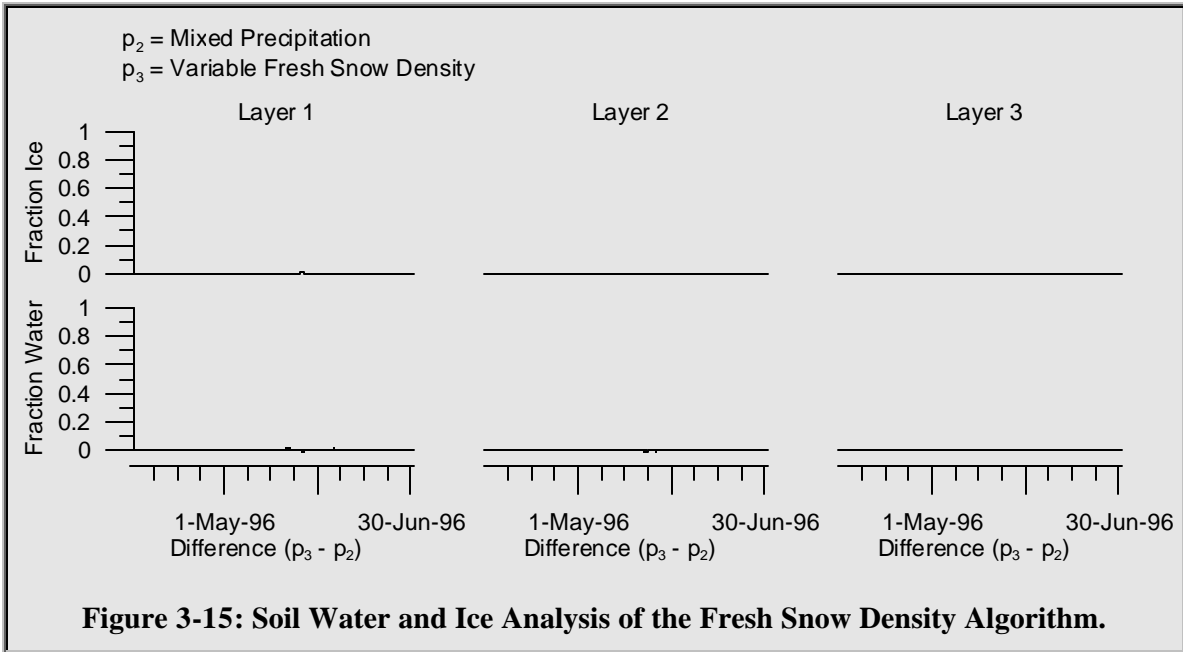
Compared to the differences shown in the mixed precipitation graphs, the impact on the surface energy balance was also minimal, as shown in Figure 3-17. The magnitudes of the y-axes are much smaller than what was shown for mixed precipitation.

Figure 3-17: Surface Energy Impact of the Fresh Snow Density Algorithm.
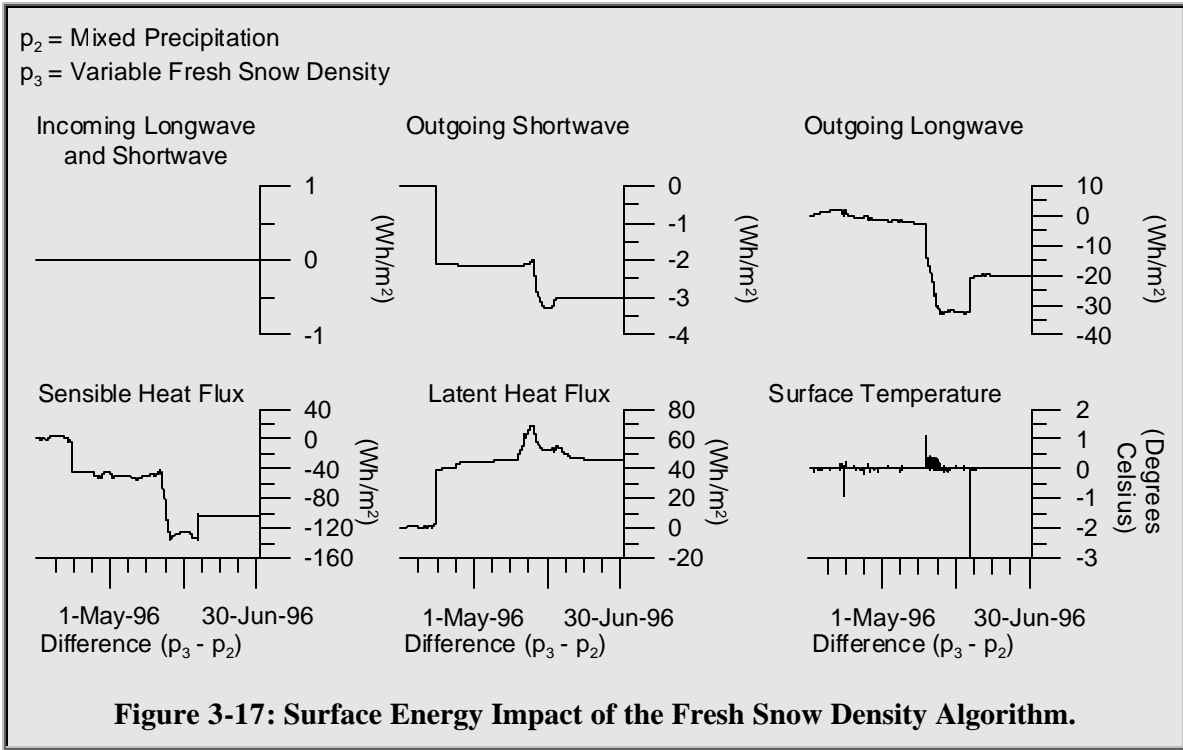
One noteworthy result was the impact on snow density. Figure 3-18A shows that the late-season snowpack became exceptionally dense. This was likely due to the freezing of ponded water, which was lumped into the snowpack. Whether or not this freezing actually occurred is unknown.

Figure 3-18: Snow Mass Impact of the Fresh Snow Density Algorithm.
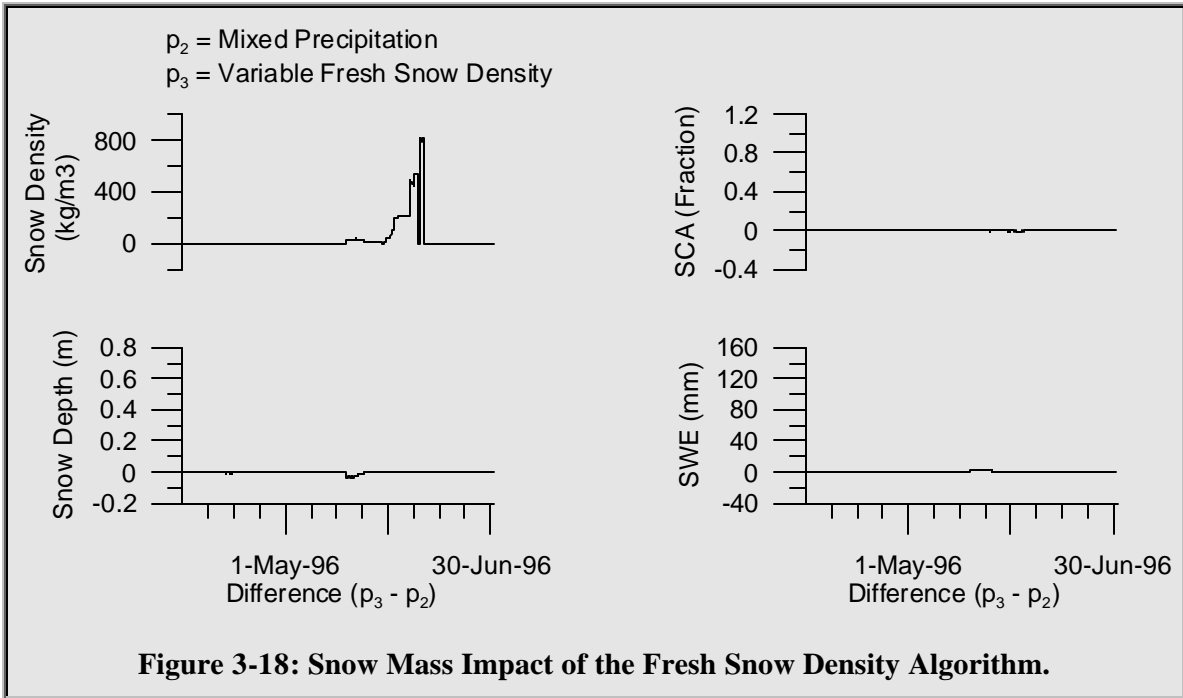
3.3.3 Maximum Snowpack Density

Fassnacht and Soulis (2002) found that the changes to maximum snow density changed the model output at the point/event and point/season scales. Maximum density was increased for open areas (300 to 350 kg/m^2) and decreased for forested areas (300 to 250 kg/m^2). As a result, open packs could attain smaller depths while forest packs could attain larger depths. For the shallow and denser pack, the soil got colder. At warmer temperatures, more heat was therefore transferred to the soil and not used for melt. The deeper and less dense pack had more snowmelt at warmer temperatures. The more dense pack therefore retained more SWE than the less dense pack. The impact on SWE, however, was not significant until the end of the season, when soil temperatures, which had been colder throughout the season, finally converge at zero degrees Celsius, altering the amount of energy available for the melt event.

Where appropriate, the results for the mixed precipitation analysis are shown for both the FEN (open) and OBS (forest) sites. Figure 3-19 illustrates the results of the algorithm change on the NSA hydrographs.

Figure 3-19: Streamflow Impact of the Maximum Snowpack Density Algorithm.
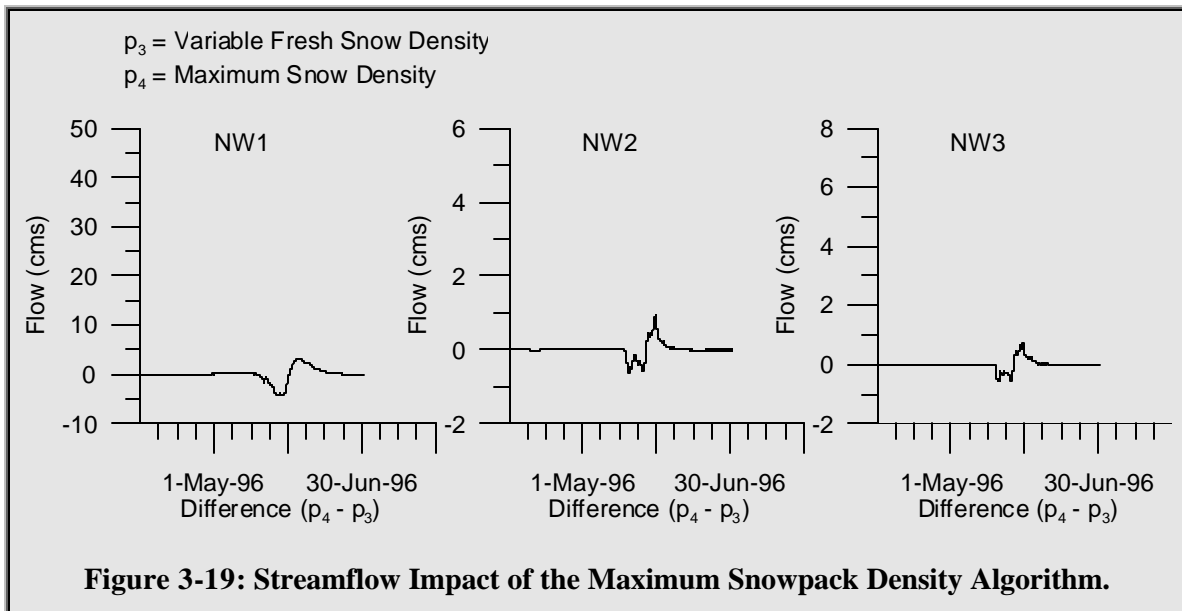
Figure 3-20 illustrates the results on the snow mass components for the forest GRU, while Figure 3-21 shows the results for the open GRU. With the algorithm, the forested GRU experiences a reduced density, increased depth and increased SWE throughout the life of the pack. The SCA was increased as bare patches began to appear. The open GRU experienced an increased density and decreased depth throughout the life of the pack. The SWE and SCA was decreased as bare patches of ground appeared.

Figure 3-20: Forest GRU: Snow Mass Analysis of the Maximum Snowpack Density Algorithm.

Figure 3-21: Open GRU: Snow Mass Analysis of the Maximum Snowpack Density Algorithm.
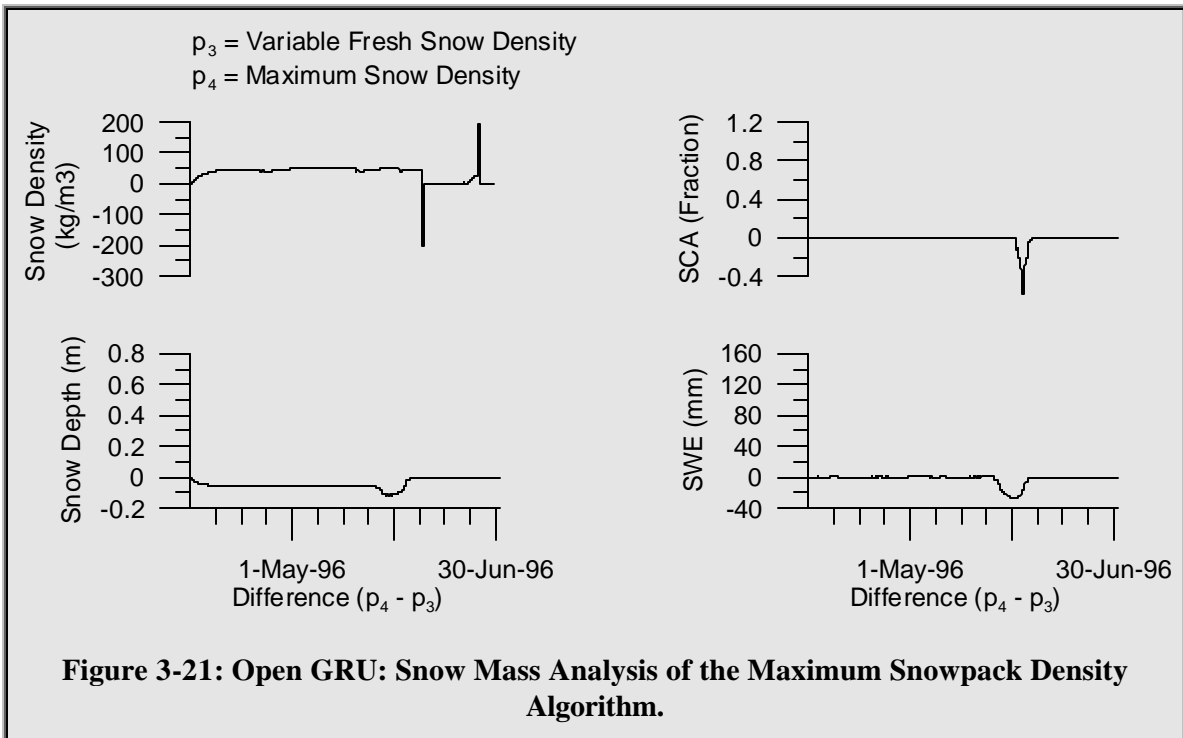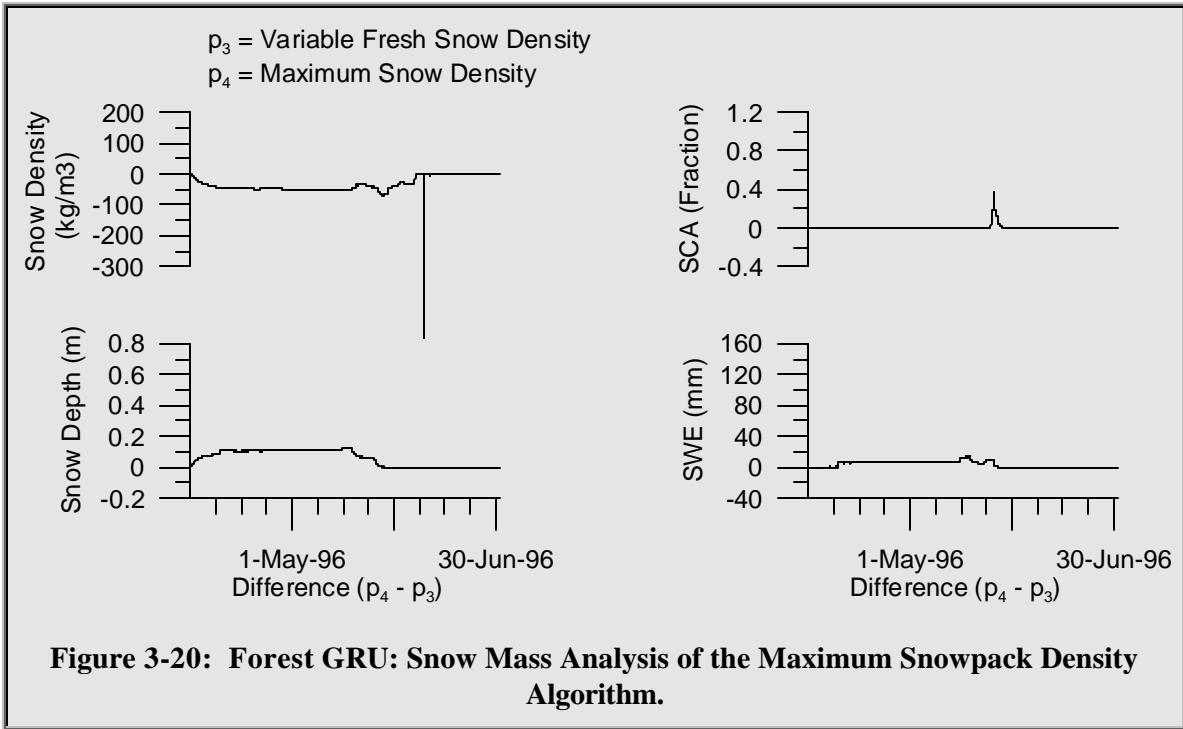
Figure 3-22 illustrates the results on the forest GRU flow components, while Figure 3-23 shows the results for the open GRU flow components. The forest GRU flow shows a delayed response while the open GRU shows a minimal impact on the flow.

Figure 3-22: Forest GRU Flow Analysis of the Maximum Snowpack Density Algorithm.

Figure 3-23: Open GRU Flow Analysis of the Maximum Snowpack Density Algorithm.
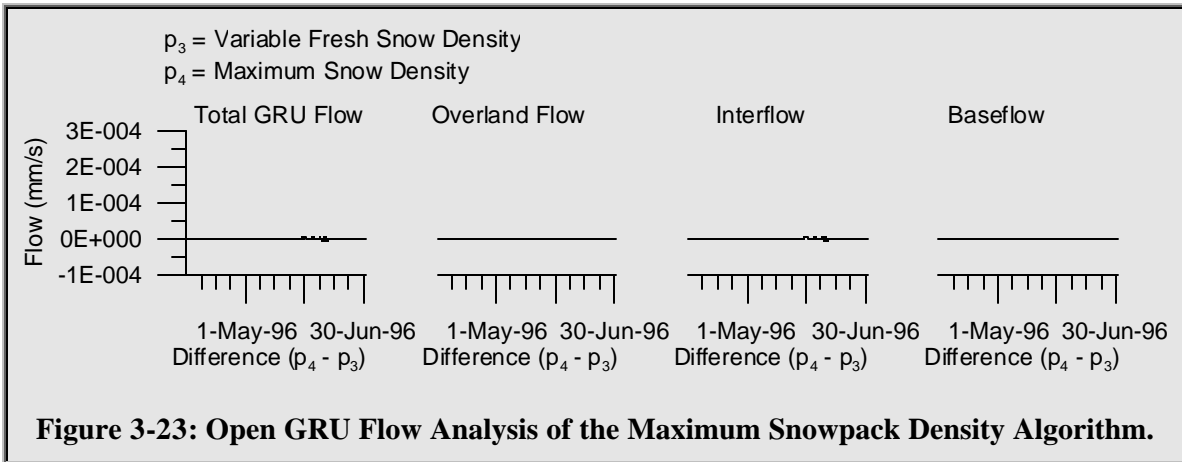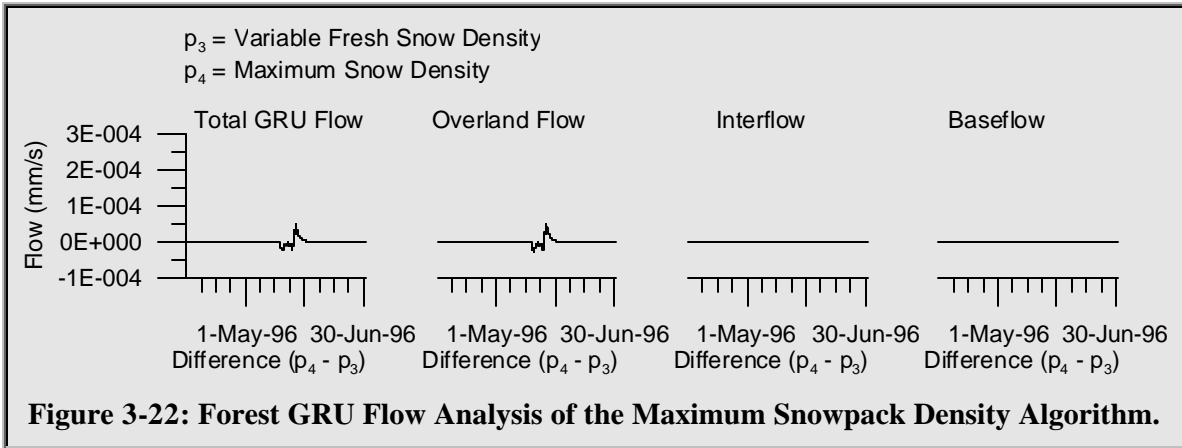
Figure 3-24 illustrates the results on the soil water and ice components for the forest GRU, while Figure 3-25 shows the results for the open GRU. The forest GRU shows that more water and less ice was present in the first two soil layers prior to the onset of melt. The open GRU shows a minimal impact on the ice content of the soil, but an increased variability of the water content during the melting of the pack.

Figure 3-24: Forest GRU: Soil Water/Ice Analysis of the Maximum Snowpack Density Algorithm

Figure 3-25: Open GRU: Soil Water/Ice Analysis of the Maximum Snowpack Density Algorithm
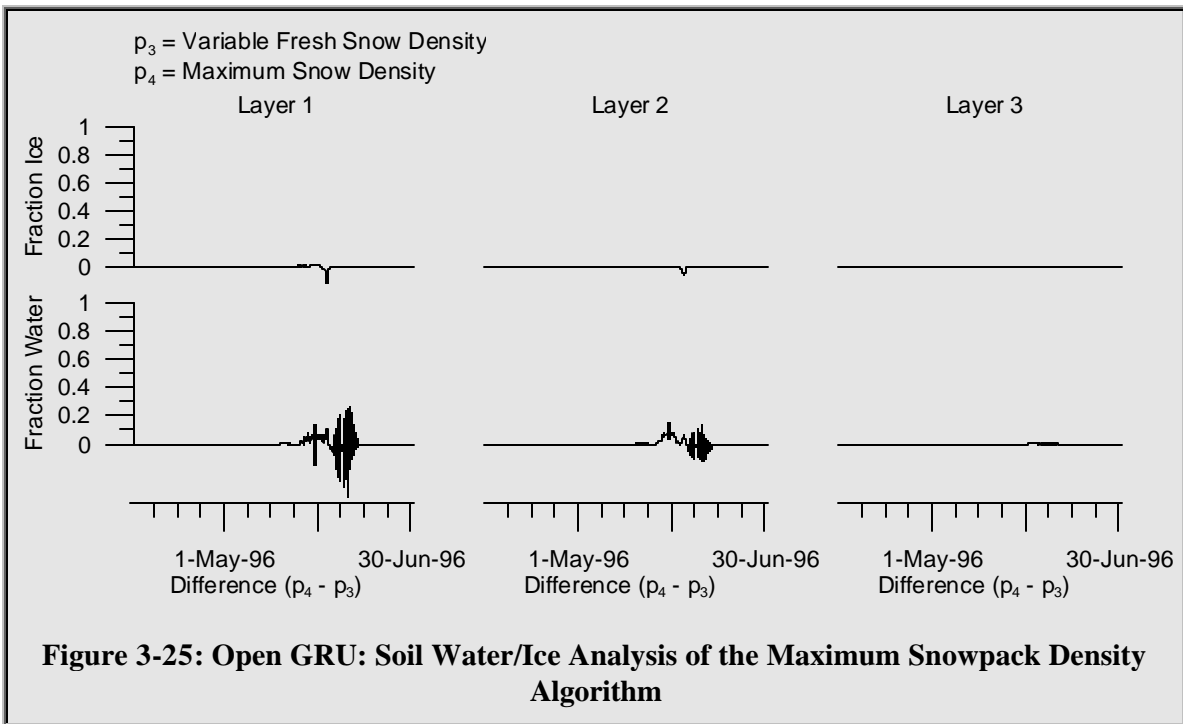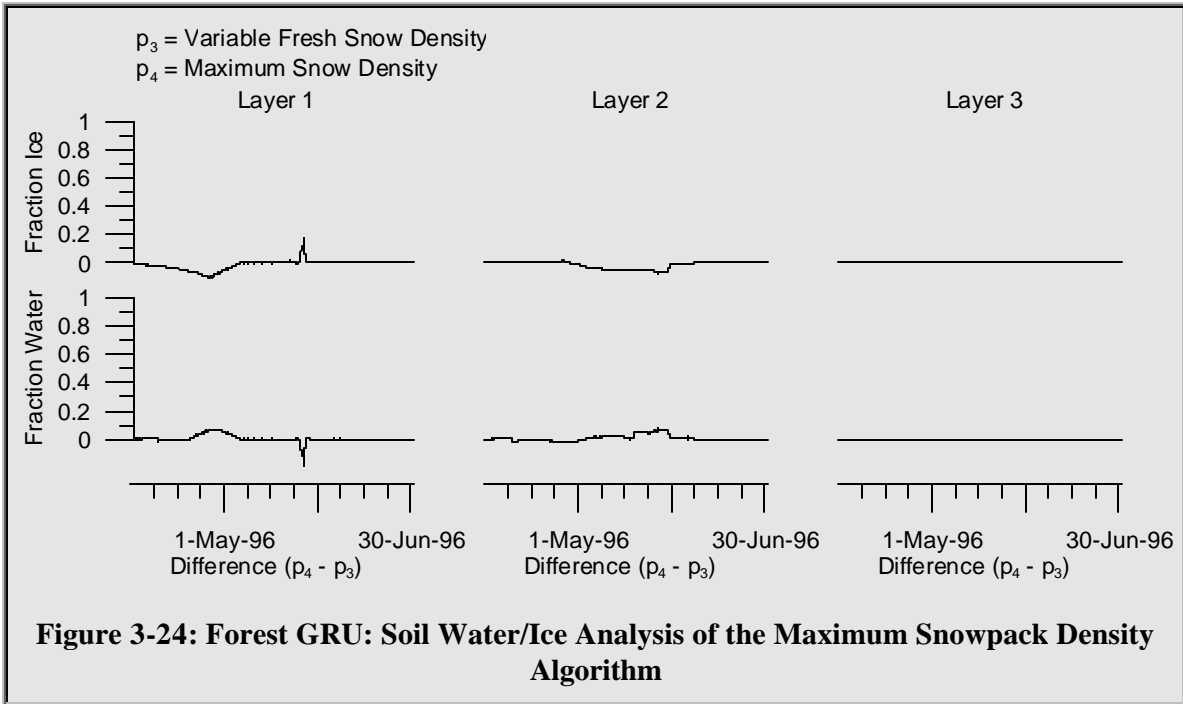
Figure 3-26 illustrates the results on the soil layer temperatures for the forest GRU, while Figure 3-27 shows the results for the open GRU. The forest GRU shows a slight increase in the layer 1 soil temperature prior to melt, while the open GRU shows a slight decrease in the layer 1

and 2 soil temperatures prior to melt. The open GRU also shows an increase in layer 1 and 2 soil temperature after the melt period. As with Figure 3-8 on page 62, the shaded boxes show the model snowmelt period.

Figure 3-26: Forest GRU: Soil Temperature Analysis of the Maximum Snowpack Density Algorithm.

Figure 3-27: Open GRU: Soil Temperature Analysis of the Maximum Snowpack Density Algorithm.
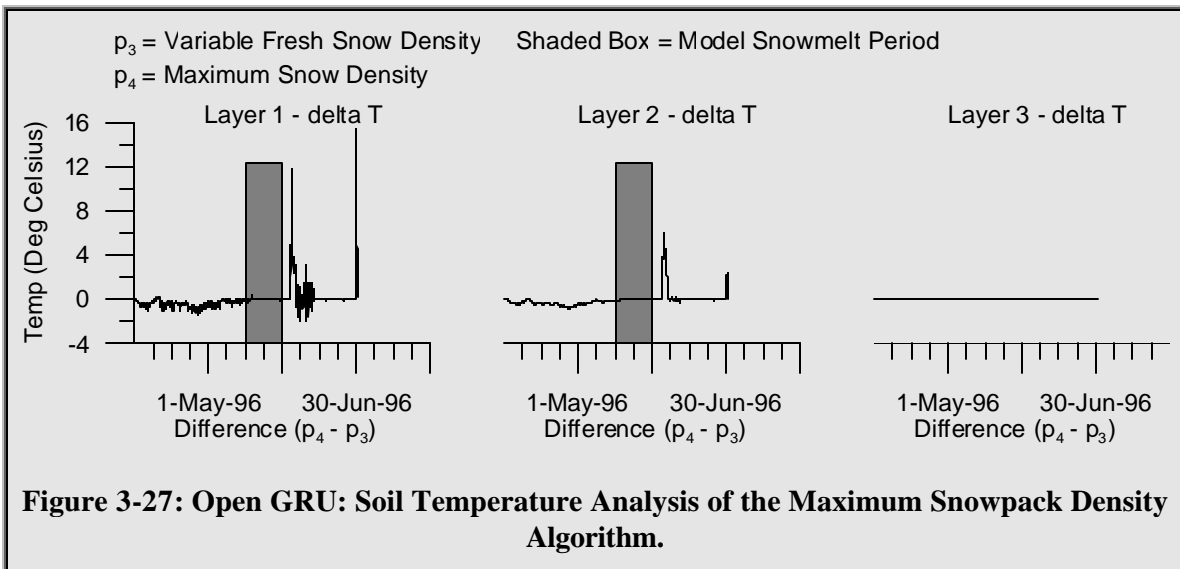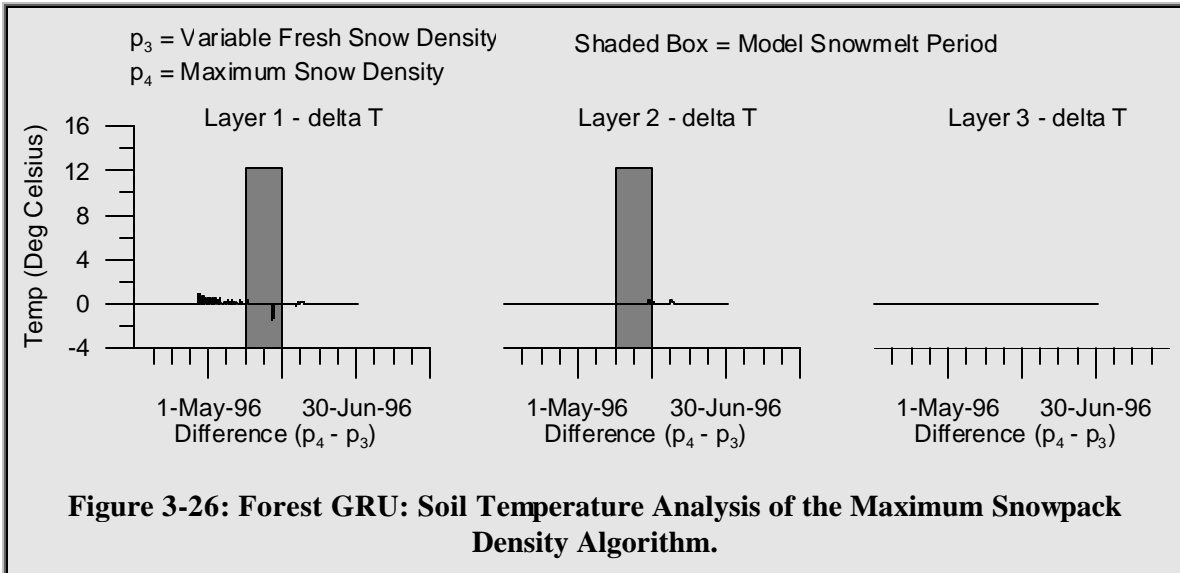
Figure 3-28 illustrates the results on the surface energy balance for the forest GRU, while Figure 3-29 shows the results for the open GRU. For the forest GRU, the outgoing long-wave radiation is decreased, the latent exchange to the atmosphere is decreased, the sensible heat to the atmosphere is increased, and the surface temperatures are colder while snow is present. For the open GRU, the outgoing shortwave radiation is decreased, the outgoing long-wave radiation is

increased, the sensible and latent heat fluxes to the atmosphere are increased and the surface temperature is generally warmer.

Figure 3-28: Forest GRU: Surface Energy Analysis of the Maximum Snowpack Density Algorithm.

Figure 3-29: Open GRU: Surface Energy Analysis of the Maximum Snowpack Density Algorithm.
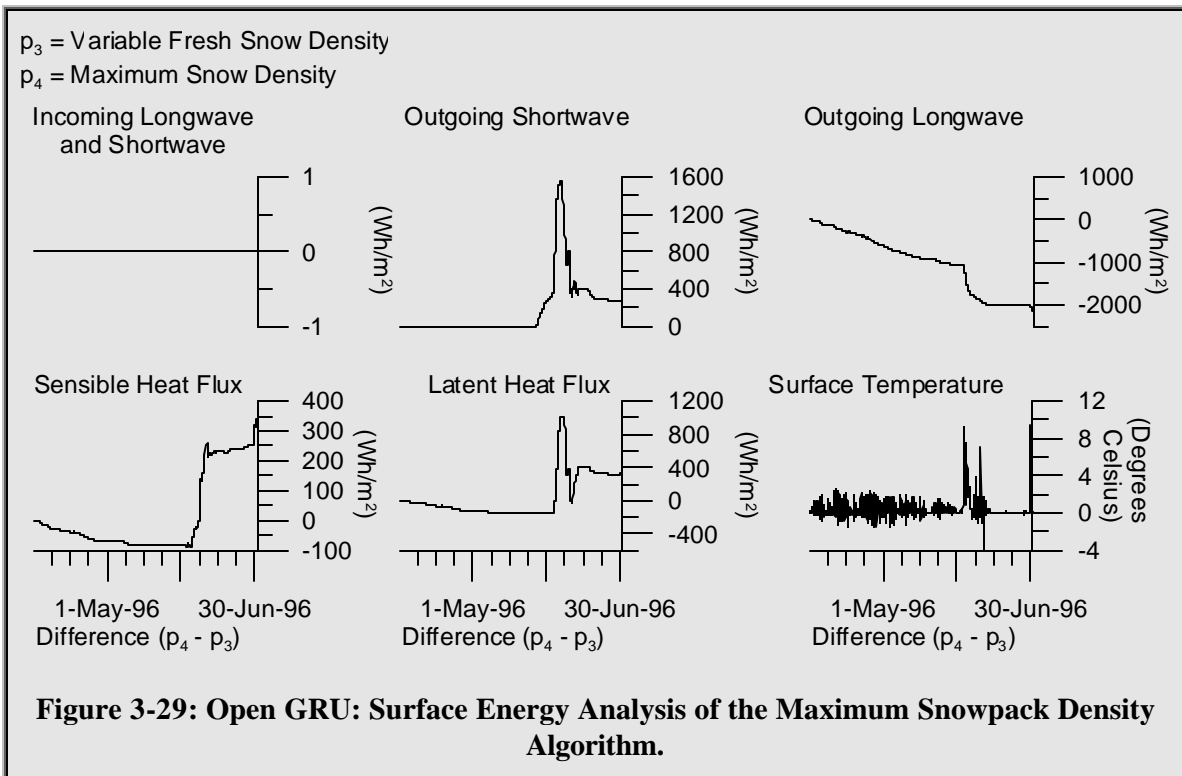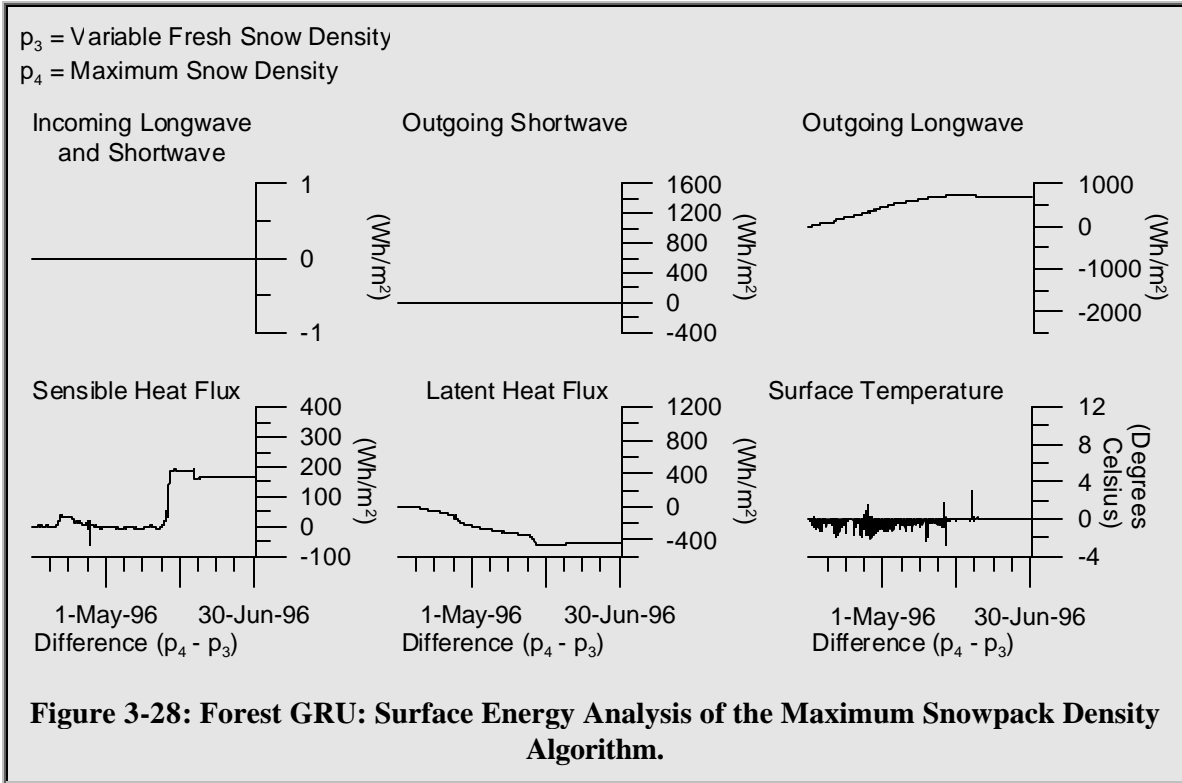
Table 3-1 shows that 89.3% of the NSA is forested, which means that the dominant maximum snowpack density process comes from the forested GRUs. Forested GRUs had a decrease in maximum snow density from 300 kg/m^3 to 250 kg/m^3. The decreased maximum density of the forest class would have a much stronger affect than the increased maximum density of the open classes. Figure 3-20 shows that the density of the snow in the forest was smaller in the pre-melt phase of the pack. The depth was subsequently higher during the same time period. The delay in the GRU flow illustrated in Figure 3-22 dominated the basin and produced the later streamflow shown in Figure 3-19. The energy balance in Figure 3-28 indicates an increase in available energy, which was used to heat the soil. Accordingly, Figure 3-24 shows that more water and less ice was present in the first two soil layers prior to the onset of melt. Perhaps because the model run was dominated by overland flow, the results were in contrast to those presented by Fassnacht and Soulis (2002), who found that a decrease in density produced an earlier melt. Another significant difference between the two basins was the amount of forest and open areas. The Upper Grand River contained only 14% forest while the NSA contained 89.3% forest.

3.3.4 Canopy Snow Interception

Fassnacht and Soulis (2002) found that the increase in canopy snow interception changed the model output at the point/event and point/season scales. The algorithm had a minimal impact on the hydrographs which represent the watershed scale. Increasing snowfall canopy interception reduced the ground SWE for each event, affecting the seasonal value of maximum ground SWE. For forested sites, increased canopy interception resulted in decreased snowpack SWE. There was an important distinction between coniferous and deciduous forest types. LAI for conifers generally varies from a maximum of 2.0 to a minimum of 1.6. For deciduous forests, the LAI can vary from 6.0 to 0.5. A 100% deciduous forest resulted in a 1% decrease in maximum SWE. 65% deciduous and 35% coniferous resulted in a 3% decrease in maximum SWE. 100% coniferous forest resulted in a 10% decrease in maximum SWE.

As Figure 3-30 illustrates, the impact of the algorithm on the NSA streams was also minimal.

Figure 3-30: Streamflow Analysis of the Canopy Snow Interception Algorithm.
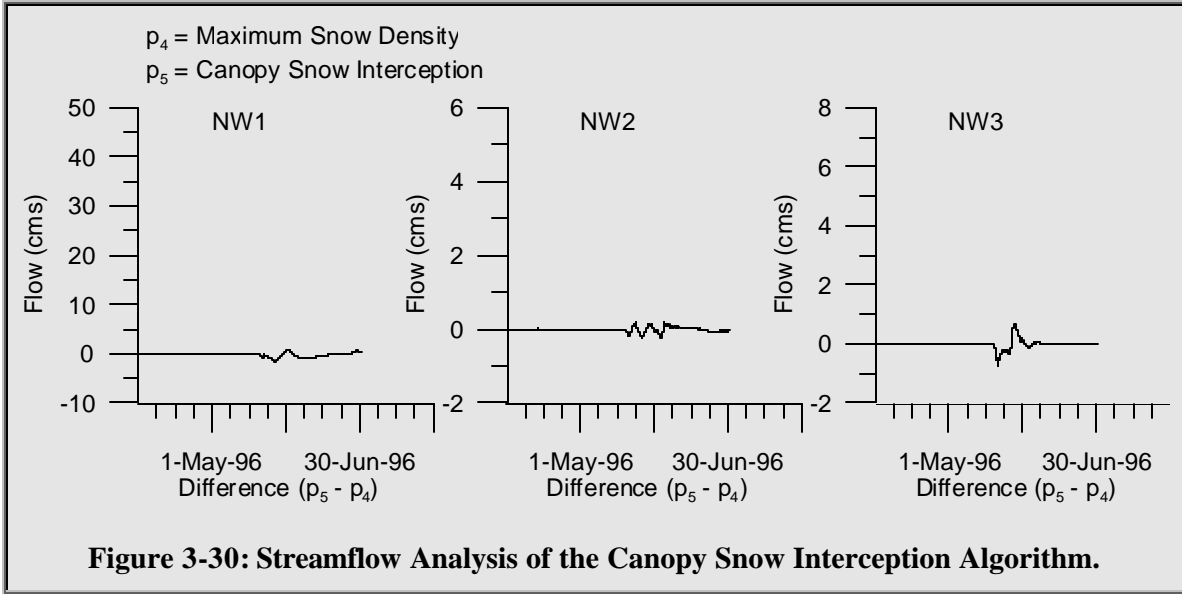
The snow mass analysis in Figure 3-31 shows a generally insignificant impact on the snowpack, except for an extended period of ice formation on the surface.

Figure 3-31: Snow Mass Analysis of the Canopy Snow Interception Algorithm
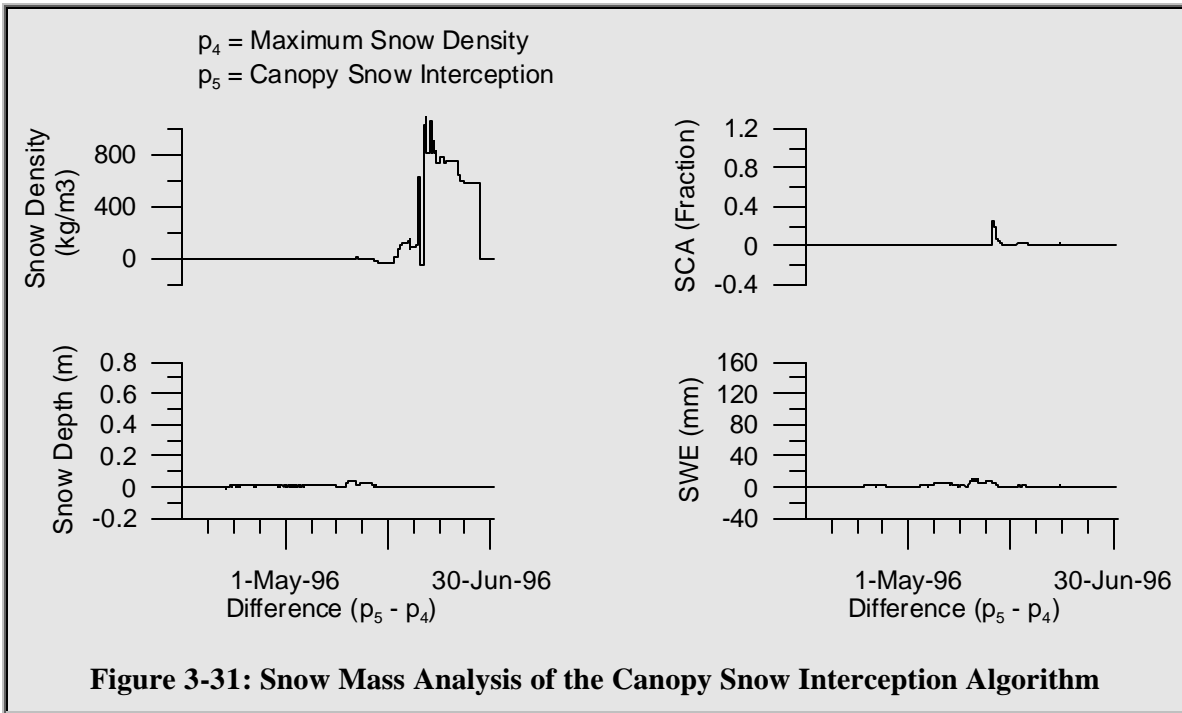
This extended period of ice on the surface had an impact on the GRU interflow and surface energy balance, as illustrated in Figure 3-32 and Figure 3-33.

Figure 3-32: GRU Flow Impact of the Canopy Snow Interception Algorithm

Figure 3-33: Surface Energy Impact of the Canopy Snow Interception Algorithm
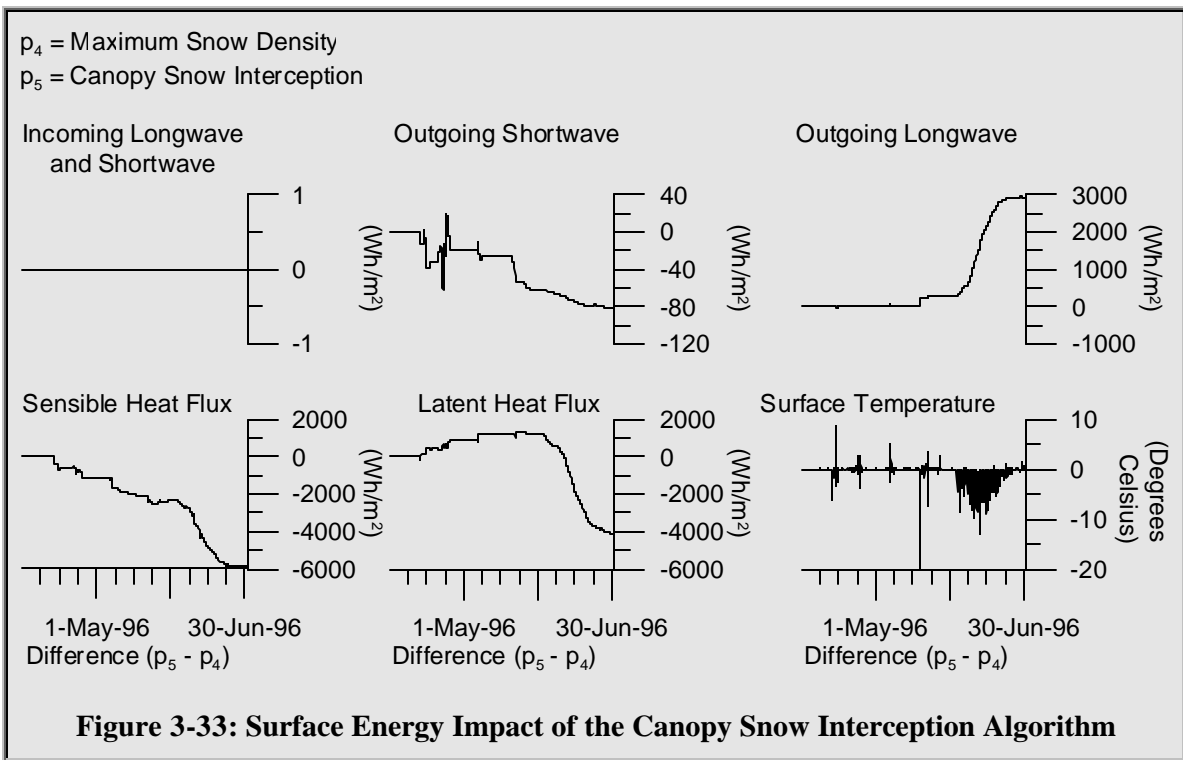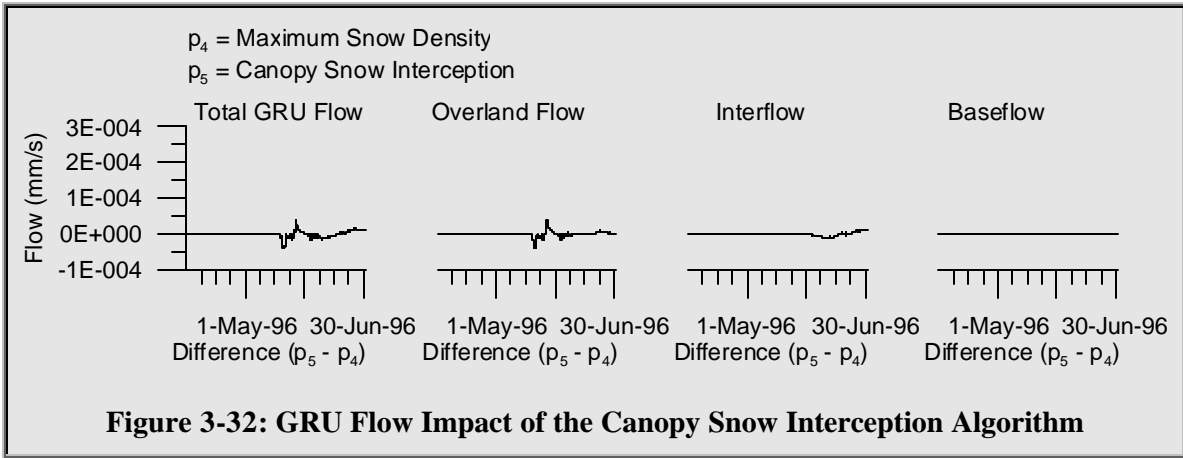
Figure 3-33 shows a decrease in outgoing long-wave radiation, and sensible and latent heat fluxes to the atmosphere in addition to a colder surface temperature. The energy balance terms indicate that canopy snow interception is an important process in the model.

3.3.5 Known problems with the model structure

Notwithstanding the improvements described in the previous section, a number of gaps remain with snow modelling in WATCLASS. With respect to the energy balance, the most obvious gap is the lack of horizontal advection in the model. The energy balance equations described by Marsh (Equation 2-10) and Male (Equation 2-11 and Equation 2-12) are clearly limited in their applicability for situations where horizontal advection is a significant factor in the energy balance of a snowpack. Patchy snowcover or open water could enhance melt in a way that the current energy balance models fail to capture. Another potential problem with the energy balance of WATCLASS snow is the isothermal nature of the pack.

With respect to the mass balance, a number of gaps are also apparent. Blowing snow is not incorporated at all, although much work has been done to understand this phenomenon. Fassnacht (2000. p 85-87.) has tested a simple wind distribution algorithm, moving snow from open areas to forested areas. Fassnacht (2000. p 86) suggested a more complex method for including blowing snow into WATCLASS, but it has yet to be tested. Neither blowing snow model is implemented in an official version of the software. Another gap in the WATCLASS snow model is the lack of water storage in the pack. Melt or rain water that enters the pack will freeze if the snow temperature is below zero degrees, releasing latent heat and increasing the snow temperature until the pack reaches zero degrees Celsius. After reaching zero degrees, any additional melt or rain on snow is simply applied as rainfall at the top of the first soil layer. In reality, some of this water would be retained in the pack and released when the capillary action of the snow particles is no longer able to hold the water (Colbeck 1978). A third gap in the mass balance of snow in WATCLASS has to do with the sub-grid variability of snow-covered area within a GRU. The relationship between average snow depth and snowcovered area has been adequately described for a depleting pack (Donald 1992; Donald *et al.* 1995), but this relationship is suspect for fresh snowfalls. The sub-grid variability of snow-covered area within a GRU is essentially a question of albedo. The fractional snow-covered area will impact the net GRU albedo. The simplistic nature of albedo decay within WATCLASS also brings into question the accuracy of the snow portion of albedo. Gray and Landine (1987) present an alternative approach to simulating the decrease of albedo for a melting prairie snowcover.

4. Developing and Analyzing a Fresh Snow Accumulation Algorithm

This chapter presents an analysis of the modelling study performed to meet the second objective, which is to develop and analyze a fresh snow accumulation algorithm. The true relationship between SCA and mean depth depends on the accumulation and depletion history of the pack, which is currently unaccounted for within the model. The theory behind the algorithm is described and the algorithm itself is explained. Results of the study are presented and discussed.

4.1 Theoretical Development

The SCA can be expressed mathematically as a function of the mean depth (D_m) by the expression shown in Equation 4-1, where $f(D)$ is the depth distribution function (Donald 1992 p45). The current version of WATCLASS first calculates the mean depth and then the SCA based on the depth distribution

$$SCA(D_m) = \int_{D_m}^{\infty} f(D)\, dD$$

Equation 4-1: SCA expression

function as characterized by the SDC. The depth distribution function is assumed to be the same throughout the lifecycle of the snowpack. Donald (1992, p33) illustrated that the variability about the mean depth remains constant as the pack melts, indicating that $f(D)$ remains constant throughout the melt period. Within WATCLASS, the idea of a constant depth distribution function is extrapolated beyond just the melt period and $f(D)$ is assumed to be constant throughout the life cycle of the snowpack.

The assumption for the second thesis objective is that $f(D)$ changes throughout the complete life cycle of a pack. For a fresh snowmelt, $f(D)$ is still assumed to be log-normally distributed, but with a smaller standard deviation. The function $f(D)$ for fresh snow would be affected by the wind speed and the natural variability of the falling snow. The natural variability of the snow would be stochastic in nature, but would be due to the variability in temperature, humidity and wind speed within the clouds as the snow crystals form as well as during their descent. Once on the ground, $f(D)$ would be affected by metamorphic and redistribution processes, which are determined by topography, vegetation and meteorological conditions.

Figure 4-1 parallels the snow depth verses SCA SDC theory development in the background section. A fresh snowmelt covers the landscape at a much smaller depth, corresponding to point A in Figure 4-1a. As the average depth increases, the assumed log-normal distribution shifts to the right (Figure 4-1b). The subsequent areal accumulation curve and snow accumulation curve (SAC) are illustrated in Figure 4-1c and d, respectively. The melt cycle has already been described and is illustrated in Figure 4-1e-h for comparison purposes. Assuming

Figure 4-1: Variable Depth Distribution Hypothesis
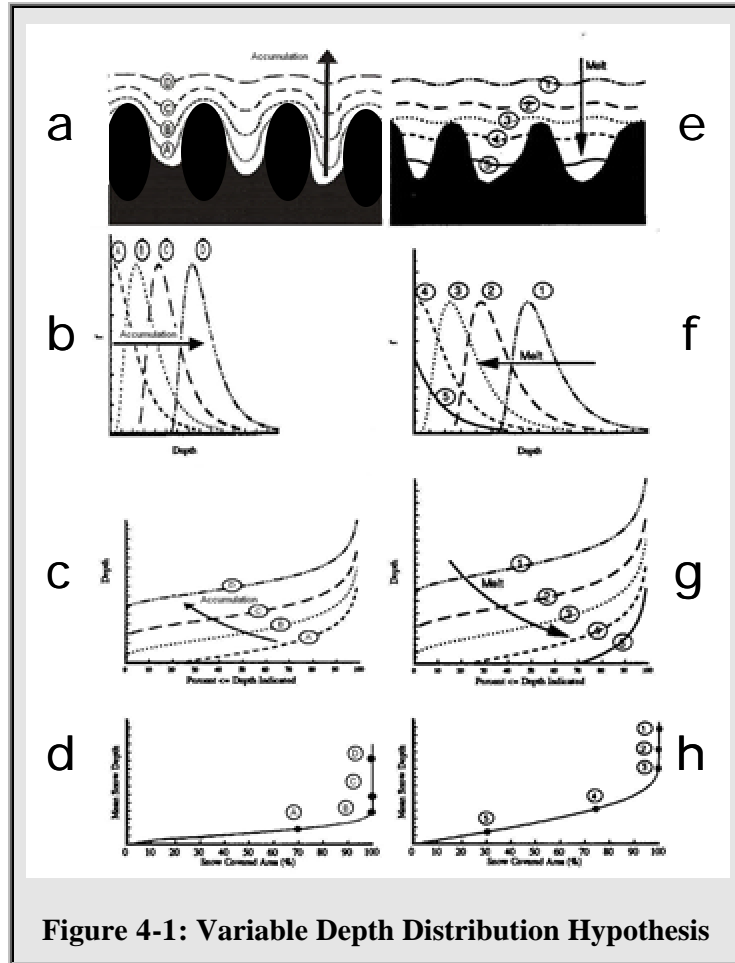
that Figure 4-1b accurately describes fresh snow depth distribution, the metamorphic and distribution processes alter the pack distribution from Figure 4-1b to f.

Figure 4-1d and h combine to produce in the SAC-SDC framework. The "a" line in Figure 4-2 illustrates the linear approximations of the mature pack SDC while the "b" line illustrates the linear approximation of the fresh snowmelt SAC. The D100 value for snow-accumulation (D100A) is lower than the D100 value for snow-depletion (D100D). This distinction between accumulation and depletion creates a fractional SCA-hysteresis zone. At any time, a measurement of snow depth verses fractional snowcovered area could fall anywhere within

Figure 4-2: SAC-SDC
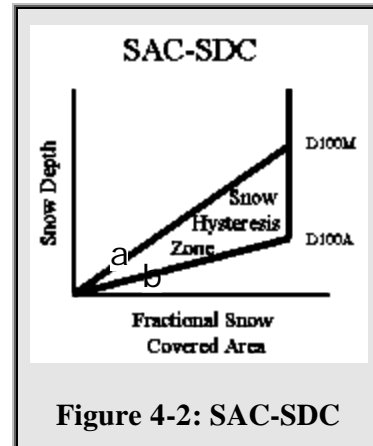
the hysteresis zone or on the lines bounding this zone, depending on the history of the pack. Within this zone, the average snow depth cannot be determined from the fractional snowcovered area and the fractional snowcovered area cannot be determined from the average snow depth.

4.2 Method

4.2.1 Algorithm Development

The first step in developing the algorithm was to identify the scenarios that would be encountered in the model, including identifying the key variables for each scenario. The second step was to develop a flow chart and write the computer code to follow the paths laid out in the chart. The third step was to test each of the identified scenarios. The fourth step was to test the new algorithm on the NSA.

To begin scenario identification, snow events were categorized as new snow, snow-on-snow, and snow depletion. Within each of the three scenarios, a further breakdown was developed based on specific "zones" within the SAC-SDC framework. As illustrated in Figure 4-3, zone 1 is considered to be the area within the SAC-SDC which is below the D100A, zone 2 is the area between the D100A and the D100D, and zone 3 is the vertical line above the D100D. Within the context of new snow, snow-on-snow, snow depletion and the three zones, a series of scenarios could be developed
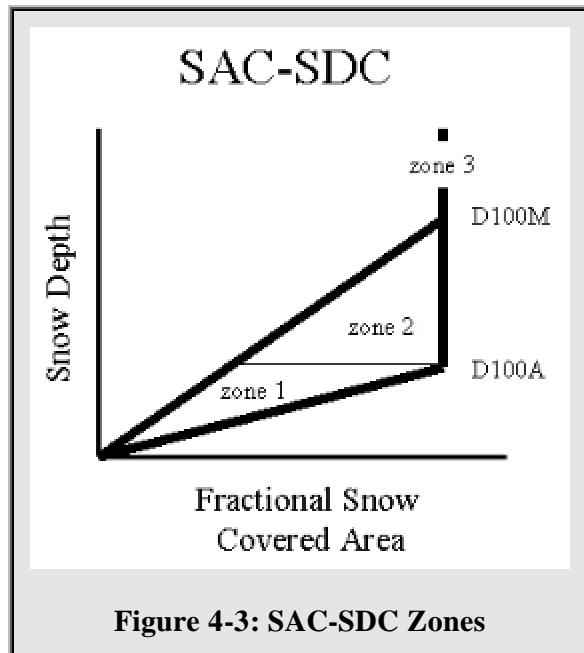
Figure 4-3: SAC-SDC Zones

that encompassed a number of different snow-pack situations encountered within the life of a snowpack. Seventeen such snow scenarios were developed by this method; three for the new snow case, five for the snow depletion case, and nine for the snow-on-snow case.

Figure 4-4 provides an overview of the resulting algorithm. The first branch in the algorithm takes the path of snow or no snow, depending on the presence of SWE in the model domain. The second level of branches take the paths of new snow, snow-on-snow, or snow depletion depending on the relationship between the current and previous snow depths. The third level of branches takes the path of zones 1, 2 or 3 depending on the depth of the pack in relation to the values of D100A and D100D.

Initialization

FSNOW(I) = 0.0
ZSNOW(I) = 0.0
FSPREV(I) = 0.0
ZSPREV(I) = 0.0
D100(I) = D100A
meltpath(I) = 0

No snow
SNO(I) < 0.0001

Snow: SNO(I) >= 0.0001
ZSNOW(I) = SNO(I)/RHOSNO(I)

New Snow
ZSPREV(I) = 0

ZSNOW(I) < D100A
ZSNOW(I) < D100D
ZSNOW(I) >= D100D

zone 1   zone 2   zone 3

Snow on snow
ZSNOW(I) >= ZSPREV(I)

ZSNOW(I) < D100A
ZSNOW(I) < D100D
ZSNOW(I) >= D100D

zone 1   zone 2   zone 3

Smaller snow depth (snow melt or aging)
ZSNOW(I) < ZSPREV(I)

ZSNOW(I) < D100A
ZSNOW(I) < D100D
ZSNOW(I) >= D100D

zone 1   zone 2   zone 3

Figure 4-4: SAC-SDC Algorithm Overview

84

New Snow

The three "new snow" scenarios are new snowfalls that fail to reach the D100A depth ending in zone one of the SAC-SDC, new snowfalls that reach a depth between the D100A and D100D range ending in zone two, and a significant snowfall above the D100D level ending in zone three. These scenarios are illustrated on the SAC-SDC's in Figure 4-5a to c.
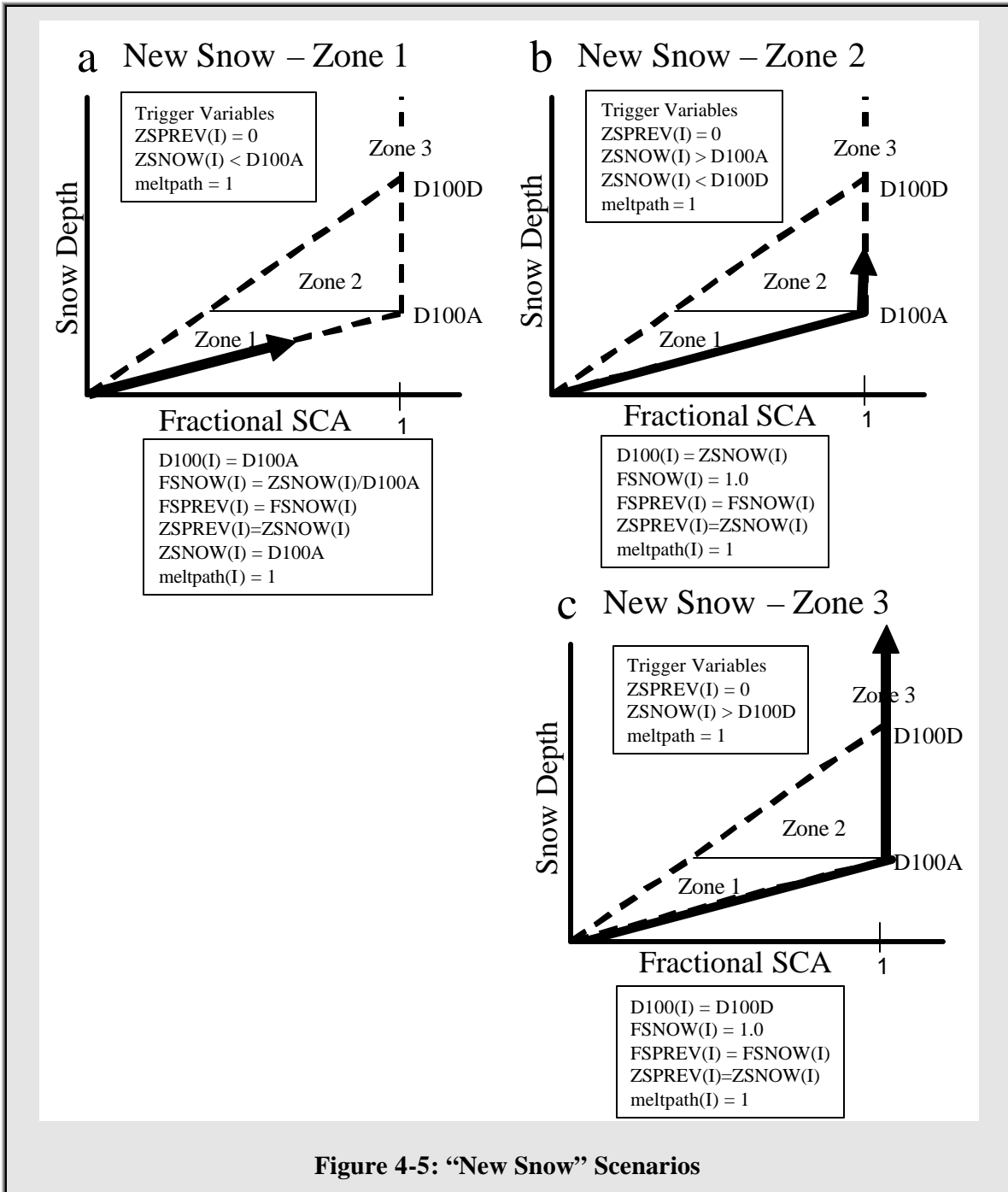
Figure 4-5: "New Snow" Scenarios

The variables of interest fit into two categories: trigger variables and response variables. The trigger variables represent the necessary conditions for the scenario to be identified while the response variables represent the necessary conditions after the scenario has been selected.

In all "new snow" cases, the previous snow depth is zero. If the snow depth (ZSNOW) is less than the value for D100A, then the model is in zone 1 following a path along the bottom line of the SAC-SDC (Figure 4-5a). In this case, the D100 value for that particular GRU and time-step is D100A, the fractional SCA (FSNOW) is calculated using similar triangles on the SAC-SDC. The SCA and snow depth values (FSPREV and ZSPREV, respectively) are saved for the next time-step and the snow depth is set to D100A for future calculations within the model. The variable meltpath, which determines whether or not the snowfall is a departure snowfall, is set to unity. If the snow depth is between D100A and D100D, then the model is in zone 2 (Figure 4-5b). The D100 value is set to the snow depth and the SCA is set to 100%. The snow depth and SCA values are saved for the next time-step and the meltpath is set to one. If the new snow goes above D100D (Figure 4-5c), the model is in zone 3. In this case, the D100 value is set to D100D; the SCA and meltpath are set to one, and the snow depth and SCA are saved for the next time-step. Figure 4-6 illustrates the "new snow" portion of the algorithm chart shown in Figure 4-4.

Figure 4-6: "New Snow" Portion of the Chart
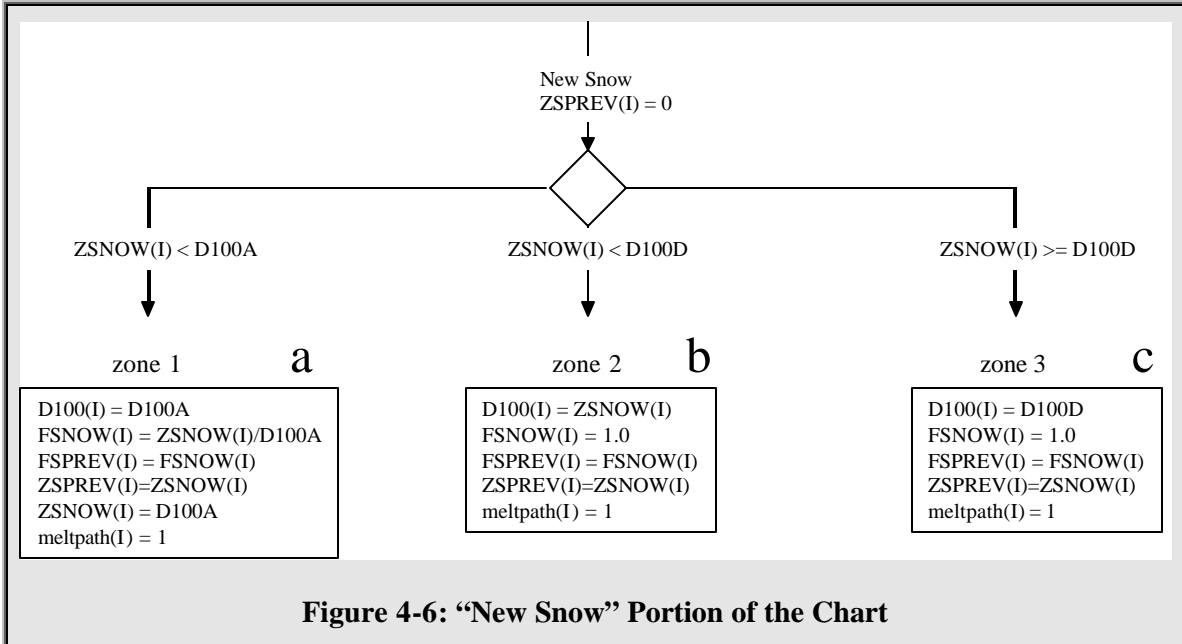
Snow Depletion

Figure 4-7 illustrates the paths taken for the "Snow Depletion" portion of the algorithm chart. In all cases, the snow depth for the current time-step is less than the depth for the previous time-step.
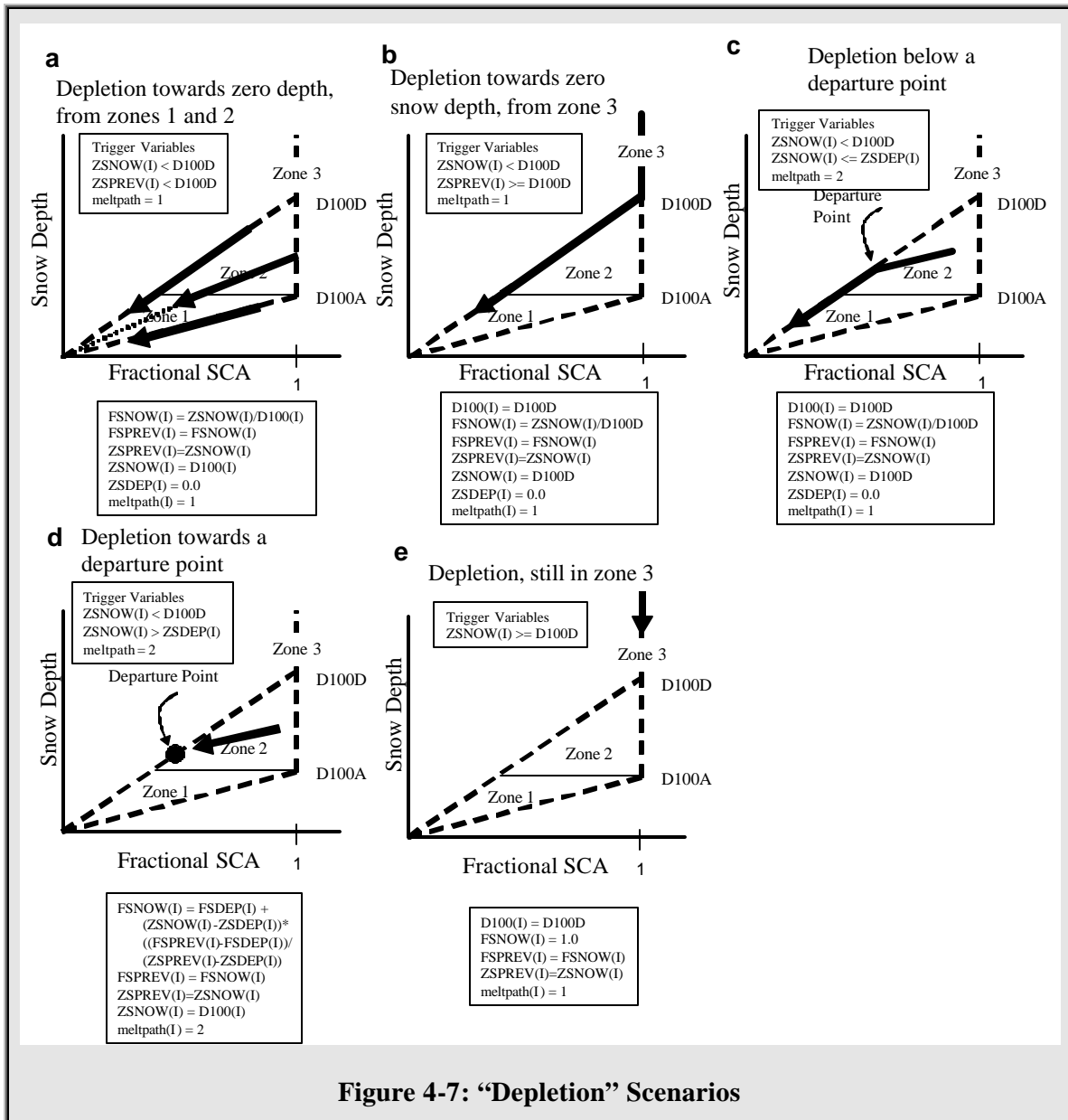
Figure 4-7: "Depletion" Scenarios

Figure 4-7 a, b and e represent snow depletion for situations where a departure point is not a concern. Figure 4-7c and d, on the other hand, represent depletion scenarios where a departure snowfall has taken place. Departure snowmelts are defined as fresh snowfalls on partially depleted packs. To be considered a departure snowfall, the pack must be in the melt phase when it experiences a fresh snowmelt.

If the snow depth is not decreasing towards a departure point, and if both the current and previous snow depths are below D100D, then the model is depleting the pack directly towards zero depth from zones 1 and 2 (Figure 4-7a). In this case, the SCA is calculated using similar triangles, the SCA and depth are saved for the next time-step, the depth is set to the current D100 value, the departure point is set to zero and the melt path is set to one. If the current snow depth is less than D100D and the previous snow depth is above D100D, then the snow is depleting into zones 1 or 2 from zone 3 (Figure 4-7b). In this situation, the D100 value is set to D100D, SCA is calculated using similar triangles, the SCA and snow depth are saved for the next time-step, the snow depth is set to D100D, the departure point is set to zero and the meltpath is set to one. If the current snow depth is less than D100D and the departure point (ZSDEP), and if the meltpath is two, then the snow depth is depleting below a departure point (Figure 4-7c). In this case, the D100 value is set to D100D, the fractional SCA is calculated using similar triangles, the SCA and snow depth are saved for the next time-step, the snow depth is set to D100D, the departure point is reset to zero, and the meltpath is reset to one. If the current snow depth is less than D100D and greater than the departure depth, and if the meltpath is two, then the snow is depleting towards a departure point (Figure 4-7d). In this case, the SCA is calculated using similar triangles, the SCA and snow depth are saved for the next time-step, the snow depth is set to the current D100 value for that GRU and time-step, and the meltpath remains at two. If the snow depth is greater than D100D (Figure 4-7e), then the depleting pack is still in zone 3. In this case, the D100 value is set to D100D, SCA is set to one, the snow depth and SCA are saved for the next time-step, and the meltpath is set to one. Figure 4-8 illustrates the "snow depletion" portion of the algorithm chart shown in Figure 4-4.

Smaller snow depth (snow melt or aging)
ZSNOW(I) < ZSPREV(I)

ZSNOW(I) < D100A   ZSNOW(I) < D100D   ZSNOW(I) >= D100D

zone 1   zone 2   zone 3

e
D100(I) = D100D
FSNOW(I) = 1.0
FSPREV(I) = FSNOW(I)
ZSPREV(I)=ZSNOW(I)
meltpath(I) = 1

meltpath = 1   meltpath = 2

ZSPREV(I) < D100D   ZSPREV(I) >= D100D

a   b

FSNOW(I) = ZSNOW(I)/D100(I)
FSPREV(I) = FSNOW(I)
ZSPREV(I)=ZSNOW(I)
ZSNOW(I) = D100(I)
ZSDEP(I) = 0.0
meltpath(I) = 1

D100(I) = D100D
FSNOW(I) = ZSNOW(I)/D100D
FSPREV(I) = FSNOW(I)
ZSPREV(I)=ZSNOW(I)
ZSNOW(I) = D100D
ZSDEP(I) = 0.0
meltpath(I) = 1

ZSNOW(I) <= ZSDEP(I)   ZSNOW(I) > ZSDEP(I)

c   d

D100(I) = D100D
FSNOW(I) = ZSNOW(I)/D100D
FSPREV(I) = FSNOW(I)
ZSPREV(I)=ZSNOW(I)
ZSNOW(I) = D100D
ZSDEP(I) = 0.0
meltpath(I) = 1

FSNOW(I) = FSDEP(I) +
   (ZSNOW(I)-ZSDEP(I))*
   ((FSPREV(I)-FSDEP(I))/
   (ZSPREV(I)-ZSDEP(I)))
FSPREV(I) = FSNOW(I)
ZSPREV(I)=ZSNOW(I)
ZSNOW(I) = D100(I)
meltpath(I) = 2

Figure 4-8: "Snow Depletion" Portion of the Chart

Snow-on-snow

Figure 4-9 illustrates the paths taken for the 'Snow-on-snow" scenarios. In all cases, the snow depth for the current time-step is greater than the depth for the previous time-step.

a Extremely small snowfall, Zones 1 and 2 (no overshoot)

Trigger Variables
ZSNOW(I) – ZSPREV(I) < small number

D100(I) = MIN(D100(I),D100D)
D100(I) = MAX(D100(I),D100A)
FSNOW(I) = ZSNOW(I)/D100(I)
FSPREV(I) = FSNOW(I)
ZSPREV(I)=ZSNOW(I)
ZSNOW(I) = D100(I)

b Departure Snowfall – Zone 1

Trigger Variables
ZSNOW(I) <= D100A
D100(I) = D100D

Departure Point

D100(I) = D100A
FSNOW(I) = ZSNOW(I)/D100A
FSPREV(I) = FSNOW(I)
FSDEP(I) = FSNOW(I)
ZSPREV(I) = ZSNOW(I)
ZSDEP(I) = ZSNOW(I)
ZSNOW(I) = D100A
meltpath(I) = 2

c Snowfall – Zone 1

Trigger Variables
ZSNOW(I) <= D100A

D100(I) = D100A
FSNOW(I) = ZSNOW(I)/D100A
FSPREV(I) = FSNOW(I)
ZSPREV(I)=ZSNOW(I)
ZSNOW(I) = D100A

d Snowfall – Zone 2 Already full cover

Trigger Variables
D100A < ZSNOW(I) < D100D
FSNOW(I) = 1.0

FSNOW(I) = 1.0
D100(I) = ZSNOW(I)
ZSPREV(I) = ZSNOW(I)
FSPREV(I) = FSNOW(I)

e Departure Snowfall – Zone 2

Trigger Variables
D100A < ZSNOW(I) < D100D
D100(I) = D100D

Departure Point

D100(I) = ZSNOW(I)
FSDEP(I) = FSNOW(I)
FSNOW(I) = 1.0
FSPREV(I) = FSNOW(I)
ZSPREV(I)=ZSNOW(I)
ZSDEP(I) = ZSNOW(I)
meltpath(I) = 2

f Snowfall – Zone 2

Trigger Variables
D100A < ZSNOW(I) < D100D

D100(I) = ZSNOW(I)
FSNOW(I) = 1.0
FSPREV(I) = FSNOW(I)
ZSPREV(I)=ZSNOW(I)

g SCA overshoot

Trigger Variables
FSNOW(I) > 1.0

D100(I) = ZSNOW(I)
FSNOW(I) = 1.0
FSPREV(I) = FSNOW(I)
ZSPREV(I)=ZSNOW(I)

h Snowfall – Zone 3

Trigger Variables
ZSNOW(I) >= D100D

D100(I) = D100D
FSNOW(I) = 1.0
FSPREV(I) = FSNOW(I)
ZSPREV(I)=ZSNOW(I)
ZSDEP(I) = 0.0
meltpath(I) = 1

Figure 4-9: "Snow-on-snow" Scenarios

If the snowfall is very small, it was likely due to frost or freezing ponded water (Figure 4-9a). In this case, the D100 value is not changed, but constraints are included to ensure that its value is between D100A and D100D. The fractional SCA is calculated using similar triangles, the SCA and depth are saved for the next time-step, and the snow depth is set to D100. If the snow depth is less than D100A and the D100 value for the current GRU and time-step is equal to D100D, then the model predicts a departure snowfall from zone 1 (Figure 4-9b). In this case, the D100 value is reset to D100A and the fractional SCA is calculated using similar triangles. The SCA and depth are saved for the next time-step and departure SCA and depth values are saved for future reference. The snow depth is set to D100A and the meltpath is set to two.

If the snow depth is less than D100A and it is not a departure snowfall, then the snowfall is in zone 1 Figure 4-9c). In this case, the D100 value is set to D100A and the fractional SCA is calculated using similar triangles. The fractional SCA and snow depth are saved for the next time step and the depth is reset to D100A. If the SCA is already 100% and the snow depth is below D100D, then the snowfall is in zone 2 with an already full cover Figure 4-9d). In this case, the SCA remains at 100%, the D100 value is changed to the new snow depth, and the depth and SCA are saved for the next time-step. If the D100 is equal to D100D and the depth is between D100A and D100D, then the snowfall is a departure snowfall in zone 2 (Figure 4-9e). In this case, the D100 value is reset to the new depth, the departure point values are saved for future reference, and the SCA is set to full coverage. The depth and SCA are saved for the next time step and the meltpath is set to two.

If the snow depth is between Dl00A and D100D and is not equal to D100D, then the snowfall is in zone 2 (Figure 4-9f). In this case, the D100 is reset to the snow depth, the depth and SCA are saved for the next time step, and the SCA is set to one. In the rare case where a small snowfall overshoots 100% snowcoverage, the model detects a SCA overshoot (Figure 4-9g). In this case, the D100 value is set to the depth, SCA is reset to 100%, and the depth and SCA are saved for the next time step.

If the depth is greater than D100D, then the snowfall is in zone 3 (Figure 4-9h). In this case, the D100 value is set to D100D, the SCA is set to one and the departure point is set to zero. The depth and SCA are saved for the next time-step and the meltpath is set to one. The above

scenarios are considered to be nine in number because the small snowfalls in zones 1 and 2 are considered to be different in the chart, illustrated in Figure 4-10.
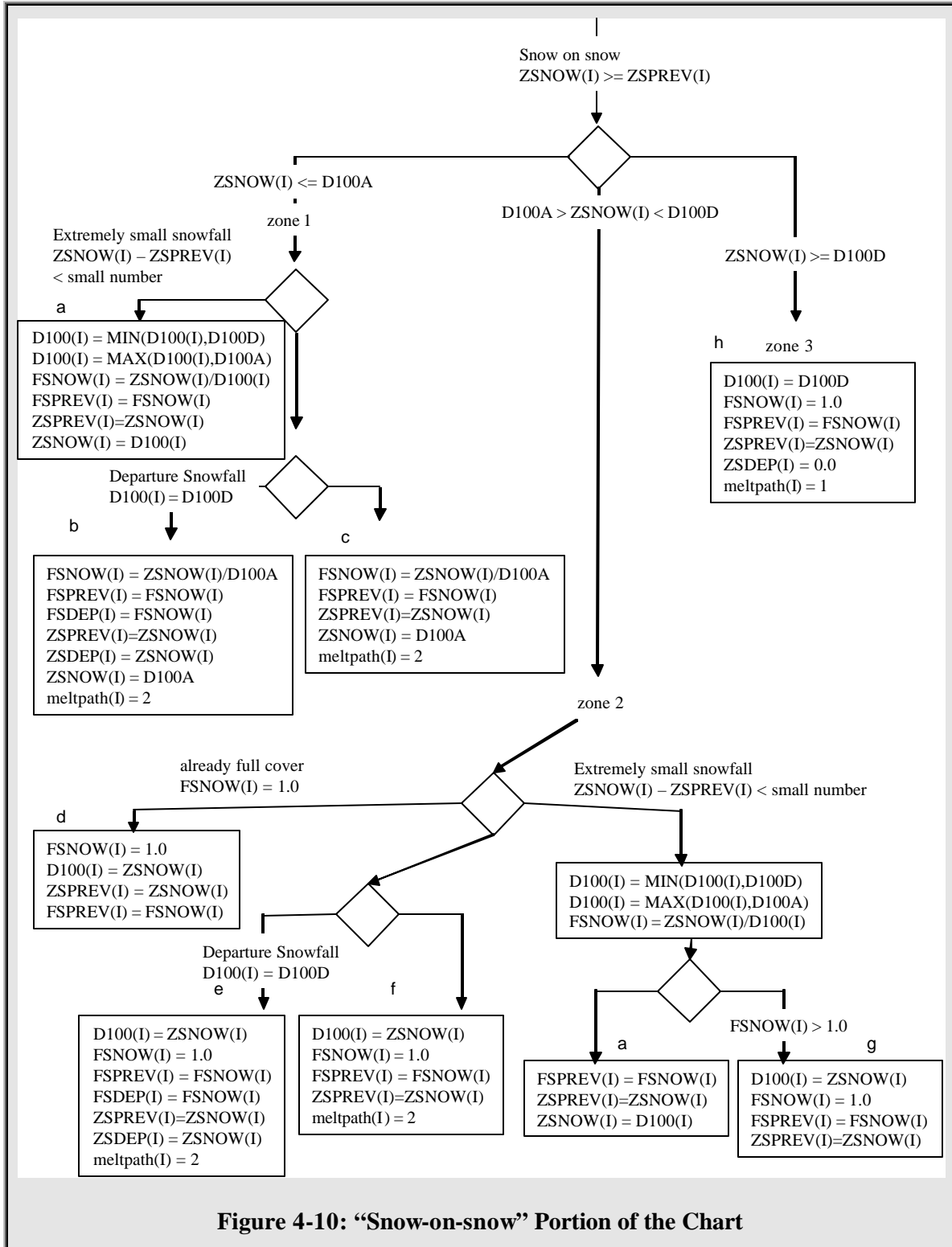
Figure 4-10: "Snow-on-snow" Portion of the Chart

The code for the SAC-SDC algorithm can be found in Appendix B.

4.2.2 Algorithm Testing

The test grid is a three-by-three theoretical basin designed specifically for the purpose of quickly testing model scenarios. For this thesis, the scenarios tested were related to the development of the fresh snow accumulation algorithm. Figure 4-11 illustrates the test grid. The shaded cells are not part of the test basin, leaving two grid squares for model

Figure 4-11: Test Grid.

calculations. A minimum of two cells are needed for WATCLASS to run. The test grid was created with one land cover type. The forcing variables for short model runs were created using spreadsheet macros.
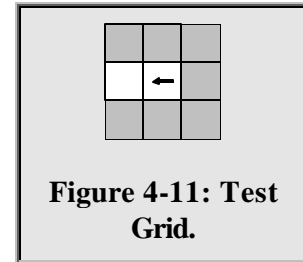
With the scenarios identified and initially coded, each one had to be tested to make sure that it worked as designed. Forcing input files were then created to produce the desired scenarios of no snow, new snow, snow-on-snow, and snow depletion. The testing of each scenario with the simple test grid and forcing input files revealed some errors in the initial coding of the algorithm, which were subsequently corrected. The final test of the algorithm was to set the D100D and the D100A to the same value as the old D100. The results were the same, showing that the algorithm worked under this circumstance. The results of the tests can be found in Appendix C.

4.3 Results and Discussion

4.3.1 SAC-SDC Runs

Three 2 year and 10 month model runs were completed on the basin. The runs had two snowfall events on partial packs, ensuring sensitivity to the algorithm. The differences between the three runs were the values used for D100A and D100D, as displayed in Table 4-1. The study site of interest was the FEN site because it was open and would not be affected by canopy processes.

Table 4-1: Model Comparison Runs

Model Run	D100A	D100D
Base Run	10cm	10cm
Comparison 1	5cm	10cm
Comparison 2	10cm	15cm

The new algorithm had an impact on the calculated sensible and latent heat fluxes during periods of change in the SCA. Figure 4-12 shows the effects of the comparison runs on the sensible and

latent heat fluxes from the 18th to the 26th of May 1996, during which there were two snowfalls on partial snowcovers.

Figure 4-12: SAC-SDC comparison, May 18th to May 26th, 1996
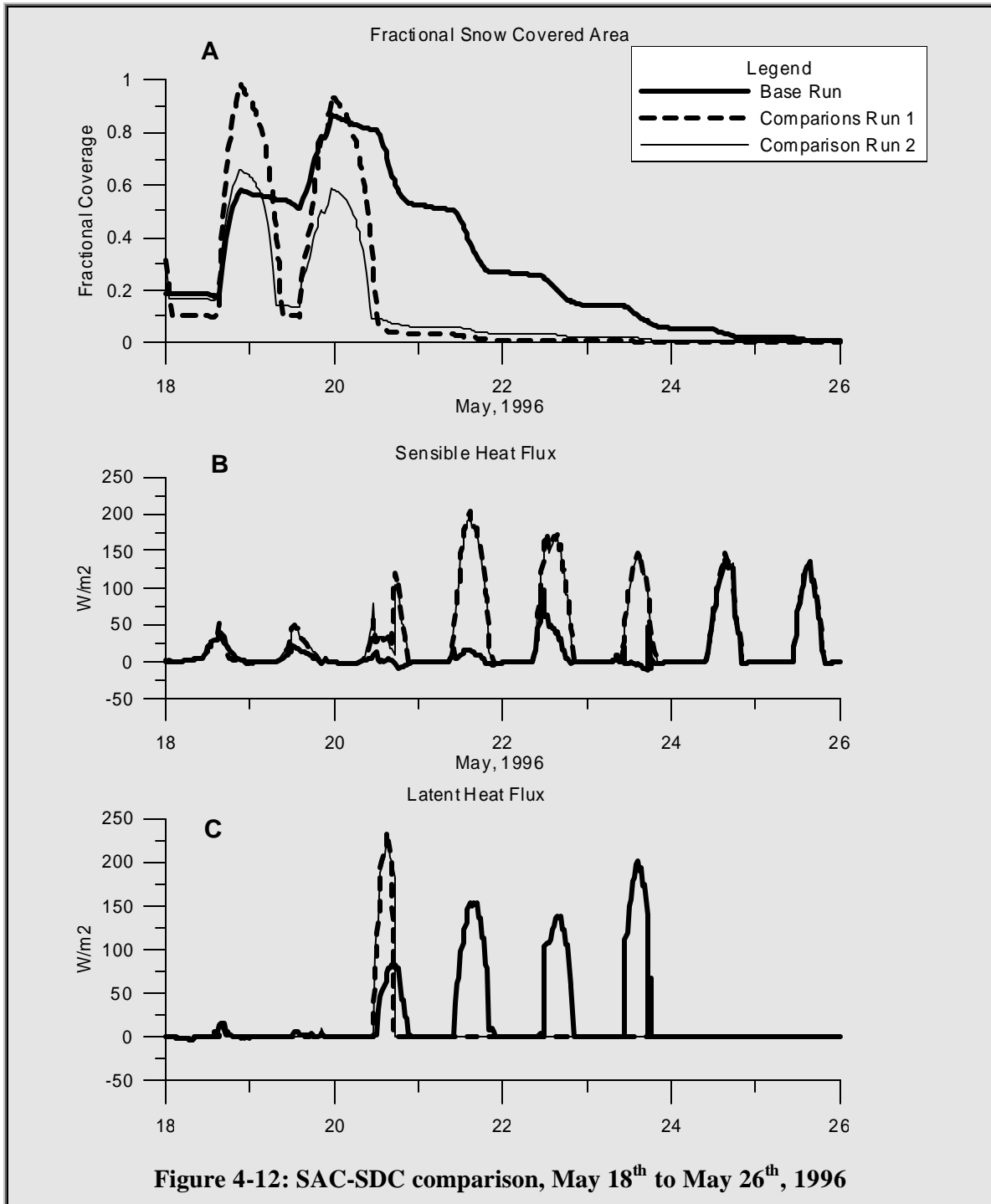
For this time-period, the SCA increased and decreased much more quickly for both comparison runs. The most significant change was the disappearance of the snowpack four days

earlier in the comparison runs, with the consequence that the sensible heat fluxes increased four days earlier than for the base-case run. During this period of higher sensible heat-fluxes, the latent heat fluxes had been reduced to zero. The impact on the sensible and latent heat fluxes to the atmosphere for comparison run 1 in 1994 is summarized in Table 4-2.

Table 4-2: Depletion (Jan 1 - Jun 30) and Accumulation (Jul 1 - Dec 31) statistics for 1994

	Sensible Heat Flux (W/m2)		Latent Heat Flux (W/m2)	
	Depletion	Accumulation	Depletion	Accumulation
Maximum positive (negative) differences	154 (-171)	44 (-60)	44 (-167)	105 (-87)
Average Difference above 15 W/m^2 (below -15 W/m^2)	41 (-74)	18 (-52)	82 (-41)	42 (-61)
Number of hours with more than 15 W/m^2 (less than -15 W/m^2) difference	12.5 (29)	10 (1.5)	45 (47)	6 (1)

Both the maximum increase and decrease in sensible heat flux occurred during the depletion phase. The maximum increase was 154 W/m^2 and the maximum decrease was -171 W/m^2. The maximum increase in latent heat flux (105 W/m^2) occurred during the accumulation phase while the maximum decrease (-167 W/m^2) occurred during the depletion phase. A threshold of 15 W/m^2 was chosen for calculating the amount of time that the fluxes were significantly different. This threshold was necessary because the fractional SCA hysteresis algorithm had minimal impact for the majority of the simulation. To quantify the impact, the average difference above and below the threshold was calculated along with the number of hours during which the threshold was exceeded. For the 12.5 hours during the depletion phase when the sensible heat flux was increased by more than 15 W/m^2, it experienced an average increase of 41 W/m^2. For the 29 hours during the depletion phase when it was decreased by less than -15 W/m^2, it was decreased on average by -74 W/m^2. In comparison to the accumulation phase, the difference in the sensible heat flux was more pronounced during the depletion phase as tabulated in Table 4-2. For the 45 hours during the depletion phase when the latent heat flux was increased by more than 15 W/m^2, the average difference was 82 W/m^2. For the 47 hours during the depletion phase when the latent heat flux was below -15 W/m^2, the average difference was -41 W/m^2. The average difference below -15 W/m^2 during the depletion phase was greater (-61 W/m^2), but the duration was only 1 hour.

The impact on the SCA is found in Table 4-3, which shows the period of time for the model grid-square to go from 100% to 5% cover for the 1994, 1995 and 1996 depletion periods.

Table 4-3: 100% Snowcovered Area to 5% Snowcovered Area in the FEN

	1994 100% SCA – 5% SCA	1995 100% SCA – 5% SCA	1996 100% SCA – 5% SCA
Base Case	20:30 Apr 21–22:30 May 6	22:00 Apr 29–21:00 May 7	17:30 May 11–11:30 May 25
Comparison 1	21:00 Apr 21–17:30 May 1	20:00 Apr 29–20:30 May 7	17:30 May 11–14:30 May 21
Comparison 2	19:00 Apr 19–21:00 May 4	17:30 Apr 24–18:30 May 7	19:30 May 10–12:30 May 22

The results in Table 4-3 show that one major impact is the timing of the opening of the pack and completion of ablation, which changes the sensible and latent heat fluxes. The base case and comparison run 1 start dates were almost identical. The comparison run 2 start dates were earlier as the pack opened up sooner with the higher D100D value. In 1994 and 1996, the comparison runs reached 5% SCA sooner than the base-case run. This was due to snowfalls on partial packs in the depletion phase. In 1995, no fresh snow fell on the partial pack and the pack depleted to 5% SCA at the same time regardless of the run.

For this study, the impact was greater during the depletion phase than during the accumulation phase. The reason is because of the fresh snowmelts on the partial packs during the depletion phase. The findings would likely be reversed if more fresh snowmelts occurred on partial packs during the accumulation phase.

4.3.2 Implications of the New Algorithm

Two of the biggest challenges with large-domain hydrologic land-surface modelling are the representation of soil moisture and the representation of snow processes. These models currently simulate physical soil and snow processes in a somewhat crude manner. The development of fractional SCA-hysteresis represents one component of addressing the representation of snow and soil in the models. Under certain circumstances, such as fresh snow accumulation on partially melted snowcovers, the fractional SCA-hysteresis algorithm has an impact on the model output. Important influences include the impacts on the sensible and latent heat fluxes and the timing of the opening of the pack. In the study presented in this thesis, the new algorithm changed the sensible and latent heat fluxes by as much as 170 W/m^2 and the opened the pack up to 5 days earlier. Full depletion of the pack was also up to 5 days earlier, which would likely complete even earlier with the incorporation of horizontal advection.

Assuming that the theory is justified, the implications for the land-surface modelling community are clear. The current relationship between fractional snow-covered area and average snow depth is limited and will present a bias in the model output. Although the existing relationship may be adequate for melt periods, the calculation of sensible and latent heat fluxes will likely be miscalculated during fresh snowmelts on bare ground or partial snowpacks. This situation may occur more frequently in areas which experience more ephemeral snowpacks.

4.3.3 Needed Studies

The theory of fractional SCA-hysteresis has been described and an algorithm has been shown to fit the theory. Field work is needed to verify the theory. Some results have illustrated the impact of the algorithm. Further studies are needed to validate and parameterize the model as well as to refine the algorithm.

The first step is to verify the theory. The SCA-hysteresis framework is based on the assumption that a fresh snow depth distribution has a different mean and standard deviation than a pre-melt snow depth distribution. Field data are needed to verify this assumption. An additional result to this assumption is that the distribution alters throughout the life cycle of the pack, moving from a fresh snow distribution to a pre-melt distribution. Studies should be conducted to determine the nature of this change in distribution. The mechanisms of change are certainly related to a pack's metamorphic and redistribution processes, which have been studied extensively within the snow hydrology community. Work is needed, however, to relate these processes to snow depth distribution in a way that will be useful for the large watershed modelling community. Specifically, more work is needed to consider the "actual" SCA-depth relationship in different scenarios, at different scales, and with different land-classes or meteorological conditions. How would a pack "really" develop according to the "SCA-snow depth" relationship? What are the driving forces behind the development along this plot? Meteorological conditions, land-class, energy, blowing snow, metamorphism and topography all likely play a role. One method of effectively studying these findings is to study snow processes in areas where fresh snowmelts on partial packs are common. These studies could help to validate and parameterize the model.

The second step would be to further refine the algorithm. Refining the algorithm has two parts. The first part is to develop a more generic framework for the algorithm and the second part is to simplify the algorithm based on the geometric features of the generic framework. The following discussion examines the first part of developing a more general framework. For this

discussion, the "system" is defined as the relationship between average snow depth and fractional SCA for a unit of land.

The SDC is one-dimensional with a discontinuous derivative. At any point in time, the system in question could be at any location on the two lines comprising the SDC. This location depends on the previous state of the system as well as the most recent inputs, resulting in an infinite number of possibilities for potential scenarios. For comparison with the SAC-SDC, Figure 4-13 illustrates four zones on the SDC. Zone 1 is the terminus of the SDC, zone 2 is the line joining the terminus and the D100 at 100% SCA, zone 3 is the

Figure 4-13: SDC zones
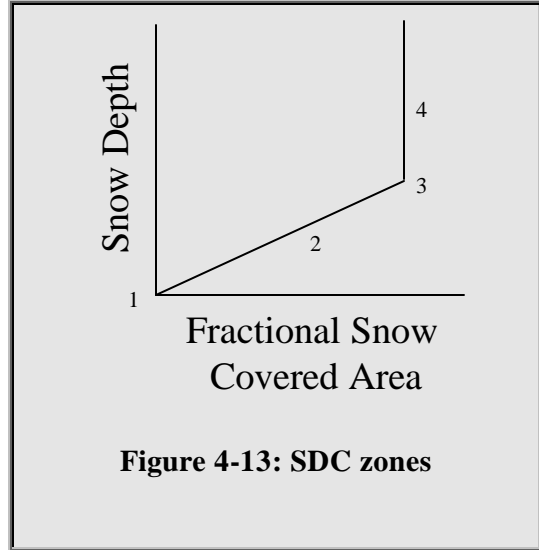
D100 at 100% SCA, and zone 4 is the vertical line beginning at the D100 at 100% SCA. Due to the one-dimensional nature of the SDC, however, a simple algorithm is sufficient to account for all of these scenarios. The previous history of the pack can be ignored and the state of the system can be calculated based on the current snow depth and one physical property (D100). If there is no snow, the system is in zone 1. If there is snow, the depth is compared to the D100 property of the system and it lies on zone 2, 3 or 4. If the depth is less than the D100 value, it is in zone 2. If the depth is equal to the D100 value, it is in zone 3. If the depth is greater than the D100 value, it is in zone 4. In all of these situations, the calculation of SCA is trivial.

The SAC-SDC requires a more complicated approach. As with the SDC, an infinite number of possibilities exist for the location of the system on the snow-depth/SCA plane. To categorize these possibilities, Figure 4-14 shows nine zones on the SAC-SDC. These zones are points, lines or areas on the SAC-SDC. Zones 1, 2 and 3 have already been discussed in detail. Zones 4, 5 and 6 are points. Zone 4 is the terminus of the SAC and SDC, zone 5 is the D100A at 100% SCA, and zone 6 is the D100D at 100% SCA. Zones 7, 8 and 9 are

Figure 4-14: More SAC-SDC zones

lines. Zone 7 is the SAC line joining the SAC-SDC terminus and the D100A at 100% SCA, zone 8
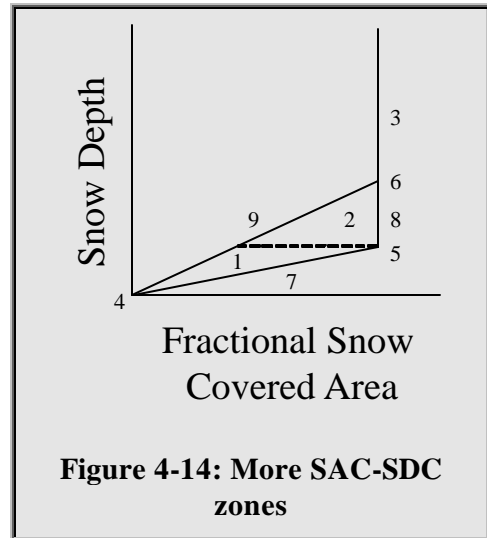
is the vertical line joining the D100A and D100D at 100% SCA, and zone 9 is the SDC line joining the SAC-SDC terminus and the D100D at 100% SCA. Due to the two-dimensional nature of the SAC-SDC, the history of the pack cannot be ignored and must be incorporated into the algorithm.

Given the framework of the nine zones, a method of categorizing the infinite number of scenarios can be developed. If the physical realities of the system are ignored and only the geometry of the SAC-SDC is considered, eighty-one categories can be identified. From one time-step to the next, the system can stay in its current zone or jump to any of the other eight zones, resulting in a total of 9 x 9 = 81 categories of scenarios. Many of these categories are physically impossible and the number of categories can be reduced. Table 4-4 shows the eighty-one scenario categories and associated algorithm identification numbers. The scenario categories marked with an 'x' were deemed to be physically impossible. The algorithm identification numbers show which parts of the SAC-SDC algorithm are used to handle the scenario category. Future iterations of algorithm development may find more appropriate sub-algorithms to handle the possible scenarios.

Table 4-4: SAC-SDC Scenario Categories

		Start Zone								
		1	2	3	4	5	6	7	8	9
End Zone	1	5,8,10	5,8	x	x	8	x	x	8	x
	2	10,15	5,8,10	x	x	x	x	x	8	x
	3	17	17	9,17	4	17	17	17	17	17
	4	6	5	5	1	5	5	5	5	5
	5	12	x	x	3	10	x	12	x	11
	6	17	17	9	4	17	9,17	17	17	17
	7	x	x	x	2	5	x	5,12	x	x
	8	15	15	x	3	15	x	15	13	14
	9	7	7	6	x	7	6	x	7	5,10

Scenario 16 is not included in the chart. This scenario category is necessary as an error checking mechanism. Future algorithm development should also consider possible error sources.

5. Conclusions and Recommendations

The NSA is a 397 km^2 basin and most of the information and basin set-up had already been completed prior to the initiation of this work. The process issues under consideration had already been identified and further work was needed to examine their impacts on a different basin. The two contributions in identifying process issues are with respect to: a) the identification of the relative importance of five snow processes in one modelling scenario, and b) the relationship between SCA and average snow depth.

Conclusions

With respect to the study investigating various snow processes in the WATCLASS model structure (Chapter 3), the mixed precipitation algorithm had the maximum effect on the streamflow while the canopy interception algorithm had the greatest impact on the sensible and latent heat fluxes. The variable fresh snow density, maximum snow density and depth-SCA hysteresis algorithms had a comparatively small effect. The key results are shown in Table 5-1.

Table 5-1: Key Model Structure Sensitivity Results

	Mixed Precipitation	Canopy Interception	
	NW1 Streamflow	OBS Sensible Heat Flux	OBS Latent Heat Flux
NSAD	0.25	0.10	0.32
PVC	0.02	0.06	0.17
MAD	16 m^3 s^{-1}	319 W m^{-2}	401 W m^{-2}

For the mixed precipitation algorithm the large change in the normalized sum of absolute differences (NSAD) and the small difference in the percent volume change (PVC) indicates a shift in streamflow, verified by an inspection of the hydrographs (Figure 3-7). The delay in streamflow was caused by additional snow. The extra snow resulted directly from precipitation occurring at temperatures just above zero degrees Celsius, which the new algorithm considered as a mixture of rain and snow rather than just rain. The increased albedo and energy requirements to melt the extra snow delayed runoff and layer 1 soil ice melt, reducing evaporation and increasing sensible heat flux to the atmosphere as a result.

For the canopy interception algorithm, all three objective functions show an important change in the latent heat fluxes, with a maximum absolute difference (MAD) of 401 W/m^2. The

sensible heat flux shows a MAD of 319 W/m^2 with a smaller effect on the NSAD and PVC. Relative to the other snow processes under consideration, however, the effect on all three objective functions is larger. All of these results indicate that canopy processes are important in partitioning energy fluxes to the atmosphere.

In a different model study (Chapter 4), the incorporation of snow-depth-SCA hysteresis had an impact on the sensible and latent heat fluxes without noticeably altering the streamflow. The maximum absolute difference for sensible and latent heat fluxes were 171 W/m^2 and 167 W/m^2, respectively. These values are smaller than for the canopy interception algorithm, but sizable nonetheless. The absolute difference in sensible heat flux was above 15 W/m^2 for 41.5 hours for the depletion period (from Jan 1st to Jun 30th, 1994) and 11.5 hours for the accumulation period (from Jul 1st to Dec 31st, 1994). Similarly, the absolute difference in latent heat flux above 15 W/m^2 was 92 hours for the depletion period and 7 hours for the accumulation period. The disparity between the accumulation and depletion periods suggests that the snow-depth-SCA hysteresis relationship is more important during the depletion phase of the pack in the BOREAS NSA. In addition, the algorithm resulted in an opening of the pack as much as five days earlier than with the SDC alone. Full depletion also occurred up to five days earlier. With local horizontal advection yet to be incorporated into the model, the full magnitude of how the snow-depth-SCA hysteresis algorithm would affect the opening and depletion of the pack remains to be determined. The interaction between the two processes is certainly non-linear.

The studies also show that different initializations and model time-periods can result in different snow processes being important. This is a caution that should be made when drawing conclusions about modelling studies. Without examining a larger parameter, initial condition, and forcing data space, making general conclusions is questionable. This underlines the need to consider calibration as an important procedure that requires more emphasis in future studies. As noted by Gupta *et al.* (2003), manual calibration is a difficult task to master and advances to the science of modelling would be facilitated by improved calibration techniques.

Recommendations

Mixed precipitation and canopy interception are processes that clearly have a relatively important impact under certain circumstances. If models are run in areas that experience mixed precipitation events or contain canopies, the models should be examined to see if they incorporate the most up-to-date component models of these processes. In the case of mixed precipitation, field work would

be needed to determine the empirical relationship local to the area. On the other hand, the output of the atmospheric models could be altered to provide the solid-liquid mixture of the precipitation to the land-surface scheme.

Field measurements should be taken to validate and parameterized the fresh snow accumulation algorithm. As a first step, the field work should include a survey of snow-depths with a high temporal resolution. The standard bi-weekly snow surveys have a temporal resolution that is too sparse. Daily measurements would provide a starting point for determining the needed temporal resolution. Care should be taken to ensure that the snow surveys are of an appropriate length. Shook (1995) contains a discussion of appropriate snow survey lengths.

A number of process issues were identified in the "known problems with model structure" sub-section at the end of Chapter 3. Although these were not examined in detail, it does represent a culmination of snow process issues that need to be explored within WATCLASS. A standardized procedure could be developed to determine the relative importance of these other snow processes to the model output. This procedure would likely be very similar to, or intricately tied with, better methods of calibration. Future modelling studies could explore a larger parameter, initial condition, and forcing data space in the calibration procedure. Using methods that explore uncertainty in the modelling exercise will improve the generality of the conclusions. Multi-criteria objective functions could be used in conjunction with extensive search or global optimization methods.

Appendix A.   CLASS 2.6 Snow Energy Balance Model

The energy balance for snow in CLASS is handled as if it were a variable-depth soil layer. There is no horizontal heat flow. The one dimensional heat conservation equation is applied to each layer to calculate the temperature changes in the three soil layers and snow layer.

$$\overline{T_i}(t+1) = \overline{T_i}(t) + [G(z_{i-1},t) - G(z_i,t)]\frac{\Delta t}{C_i \Delta z_i} \pm S_i$$

Equation A-1: One-Dimensional Heat Conservation Equation for CLASS

where $\overline{T_i}(t)$ and $\overline{T_i}(t+1)$ are the soil layer temperatures at the beginning and end of the time step, Δt, $G(z_{i-1},t)$ and $G(z_i,t)$ are the downward heat fluxes at the top and bottom of the layer, C_i is the volumetric heat capacity of the soil, Δz_i is the layer depth, and S_i is a correction term applied in the case of freezing or thawing, or the percolation of ground water. G and z are both considered to be positive downward.

If the surface temperature is known, the soil layer heat fluxes can be calculated by

$$G(z) = -\lambda(z)\frac{dT}{dz}\bigg|_z$$

Equation A-2: Soil Layer Heat Flux

where λ is the thermal conductivity.

Assuming that dT/dz is zero at the bottom of the lowest soil layer, 4.1 m below the surface, results in three linear equations in the three unknown G's and an unknown surface temperature. If the surface temperature can be found, the fluxes can be computed.

When there is no snow, the surface temperature is calculated by iteratively solving a non-linear representation of the surface energy balance.

$$K_* + L_* + Q_H + Q_E = G(0)$$

Equation A-3: Surface Energy Balance

where K_* is the net shortwave radiation, L_* is the net longwave radiation, Q_H is the sensible heat flux, Q_E is the latent heat flux, and G(0) is the surface heat flux. Each of the terms in Equation A-3 can be represented as a function of the surface temperature T(0), except for net shortwave radiation which is calculated as a function of albedo and the incoming shortwave radiation. The result is an equation that can be solved to find T(0), which can then be substituted

back into the original equations to calculate the energy balance, heat flux, and layer temperature terms for the next time step. Equation A-3 is the implementation of the energy balance, similar to the energy balance models described earlier, only for a surface without snow.

When snow is present, the same approach is used, with one more heat conservation equation (Equation A-1) and one more unknown flux between the soil and snow. The inclusion of melting snow brings Equation A-3 into line with Equation 2-10 and Equation 2-12 as described by Marsh and Male. To gain a more in-depth understanding of how WATCLASS handles the snow energy balance, each of the components of the balance will be considered individually. Equation A-3 will be used as the comparison equation, splitting the net all-wave radiation into shortwave and long-wave components.

Net Shortwave Radiation

The net shortwave radiation depends on the incoming shortwave radiation and the snow surface albedo according to

$$K_* = (1 - a_s)K^{\downarrow}$$

Equation A-4: Net Shortwave Radiation

where a_s is the snow albedo and $K^{\downarrow}$ is the incoming shortwave radiation.

The incoming shortwave radiation is one of the forcing variables for WATCLASS, and its quality is dependent on the nature of the creation of the data. The albedo is calculated based on a series of empirical formulas. For bare ground, fresh snow is assumed to have a value 0.84, decreasing exponentially to a value of 0.70 if no melt occurs and 0.50 if melt occurs. The empirical equations that determine the snow albedo are:

$$a_s(t+1) = [a_s(t) - 0.70]e^{\left[\frac{-0.01\Delta t}{3600}\right]} + 0.70$$

Equation A-5: Non-melting Snow Albedo

and

$$a_s(t+1) = [a_s(t) - 0.50]e^{\left[\frac{-0.01\Delta t}{3600}\right]} + 0.50$$

Equation A-6: Melting Snow Albedo

Equation A-5 and Equation A-6 are based on work by Aguado (1985), Robinson and Kukla (1984) and Dirmhirn and Eaton (1975).

If the area under consideration has a canopy, two new situations need to be considered. The first is the alteration of the albedo and incoming shortwave radiation at the snow-surface. The second is the albedo and incoming shortwave radiation on the canopy. Canopies absorb more photosynthetic active radiation than near-infrared radiation. To find the net shortwave radiation for the canopy and underlying ground or snow surface, the visible and near-infrared canopy albedos and transmissivities are calculated, as described thoroughly by Verseghy (1993). The resulting equations for net shortwave radiation are:

$$K_{*,g/s} = \overline{t}_{c,vis} K_{\downarrow,VIS}\left[1 - a_{g/s,VIS}\right] + t_{c,NIR} K_{\downarrow,NIR}\left[1 - a_{g/s,NIR}\right]$$

Equation A-7: Ground and Snow Net Shortwave Radiation under a Canopy

and

$$K_{*,c} = K_{\downarrow,VIS}\left[1 - \hat{a}_{c,VIS}\right] + K_{\downarrow,NIR}\left[1 - a_{c,NIR}\right] - K_{*,g/s}$$

Equation A-8: Above Canopy Net Shortwave Radiation

where the subscripts g, s and c stand for ground, snow and canopy, respectively, and t stands for transmissivity, which is calculated differently for clear or cloudy skies. The albedos are calculated as with Equation A-5 and Equation A-6, but with visible albedos of 0.95, 0.84 and 0.61 and near-infrared albedos of 0.72, 0.56 and 0.38 for the boundary values of fresh snow, old dry snow and old melting snow, respectively. If snow is on the canopy, the canopy does not take on the albedo values of snow, but reaches a maximum value of 0.20, as measured in the field (Leonard and Eschner 1968).

Shortwave radiation also penetrates the pack and a certain amount is absorbed by the underlying soil.

Net Long-wave radiation

The net long-wave radiation absorbed by the snow is equal to the difference between the incoming long-wave radiation and the outgoing long-wave radiation emitted from the snow.

$$L_* = L^{\downarrow} - s T(0)^4$$

Equation A-9: Net Longwave Radiation

where $L^{\downarrow}$ is the incoming long-wave radiation, s is the Stefan-Boltzmann constant and T(0) is the absolute surface temperature. Comparing Equation A-9 and Equation 2-4 clearly shows that the emissivity of the surface, whether it is snow or soil, is assumed to be 1.

If there is a canopy, the net long-wave radiation is recalculated based on a 'sky view' factor, ?, representing how much energy can penetrate the canopy. In addition, the canopy radiates long-wave radiation to the snow. The equation governing this relationship in CLASS is

$$L_{*,s} = \left(1 - \hat{\boldsymbol{c}}\right)\boldsymbol{s}\overline{T}_c^4 + \hat{\boldsymbol{c}}L_{\downarrow} - \boldsymbol{s}T(0)^4$$

Equation A-10: Canopy Longwave Radiation to the Snow

where $\hat{\boldsymbol{c}}$ is the sky view factor averaged over crop, grass, needleleaf trees and broadleaf trees, and $\overline{T}_c$ is the effective canopy temperature.

Sensible Heat Flux

The sensible heat flux is calculated based on Equation 3-31.

$$Q_H = \boldsymbol{r}_a c_p V_a c_D \left[T_a - T(0)\right]$$

Equation A-11: Sensible Heat Flux

where $?_a$, c_p and T_a represent the density, specific heat, and temperature of the air, respectively. V_a is the wind speed and c_D is a drag coefficient depending on the surface roughness, wind speed and atmospheric stability (McFarlane and Laprise 1985).

Canopies alter the calculation of sensible heat flux of the underlying ground or snowpack. Under stable conditions, the sensible heat under the canopy is assumed to be zero. Under unstable conditions, the following equation for free convection is used, derived from Townsend (1964) by Deardorff (1972).

$$Q_{H,g/s} = 1.9x10^{-3}\,\boldsymbol{r}_a c_P \left[T_{a,c} - T(0)\right]\left[T^{'}(0) - T^{'}_{a,c}\right]^{1/3}$$

Equation A-12: Below Canopy Sensible Heat Flux in Unstable Conditions

where T(0) and Ta,c are the actual and T'(0) and T'a,c are the virtual temperatures of the ground surface under the canopy and of the air within the canopy respectively. The virtual temperatures are calculated as

$$T'(0) = T(0)\left[1.0 + 0.61q(0)\right]$$

Equation A-13: Virtual Skin Temperature

and

$$T'_{a,c} = T_{a,c}\left[1.0 + 0.61q_{a,c}\right]$$

Equation A-14: Virtual Air within the Canopy Temperature

for a snow surface, the specific humidity q(0) is equal to the saturation specific humidity at T(0). The temperature of the air within the canopy is set to the average canopy temperature and the specific humidity is set equal to the specific humidity of the air above the canopy.

Latent Heat Flux

The latent heat flux is calculated based on Equation A-15.

$$Q_E = L_v r_a V_a c_D \left[q_a - q(0)\right]$$

Equation A-15: Latent Heat Flux

where L_v, q_a and q(0) are the latent heat of vaporization/sublimation, specific humidity and surface humidity, respectively.

Canopies also alter the calculation of latent heat flux. As with sensible heat flux, stable conditions result in zero flux while unstable conditions result in a modelled flux of

$$Q_{E,g/s} = 1.9x10^{-3} L_v c_P \left[q_{a,c} - q(0)\right]\left[T'(0) - T'_{a,c}\right]^{1/3}$$

Equation A-16: Below Canopy Latent Heat Flux in Unstable Conditions

where Lv is the latent heat of vaporization.

Latent heat is also increased if melt-water or rain freezes in the pack.

Rain on Snow

Rain falling on snow is re-frozen, releasing latent heat from the pack until the temperature of the pack is zero degrees. At this point, any additional rain is applied directly to the first soil layer.

Ground Heat Flux

The ground heat flux has already been described as it represents the underpinning series of equations for heat conservation. Assuming proper initialization, the heat flux between the ground and the snow-pack should be reasonable. Properly initializing soil temperatures is probably very important as it would likely take a number of years to "spin-up" the modelled layer 3 temperature

that affects the long-term heat fluxes. Underestimating the layer-three soil temperature would likely suppress snowmelt while overestimating it would likely accelerate melt.

Melt Energy

Snowmelt occurs in two ways. The first is if the surface energy balance produces a skin temperature greater than zero degrees Celsius. In this case, the excess energy is used to melt snow, the skin temperature is reset to zero and the appropriate flux terms, L_*, Q_H, Q_E and $G(0)$, are recalculated. If the pack temperature is below zero, the melt water re-freezes in the pack, releasing latent heat. If the pack is at zero degrees, the melt water infiltrates or ponds. The second method of melting snow is if the ground heat flux brings the temperature of the pack above zero degrees Celsius. In this case, the pack temperature is reset to zero degrees and the excess energy is used to melt snow and treat it as rainfall at the soil surface.

Due to the lack of melt-water storage in the pack, it is quite likely that water is released from the pack too early, resulting in hydrographs that start early. Coupling this with the lack of horizontal advection for patchy snowcovers would probably decrease the "flashiness" of the hydrograph, resulting in a smaller peak and a wider base.

Appendix B.   SAC-SDC Fortran Code

The following code comes from classa.f

```
C        *  New parameters for the snow accumulation algorithm
         REAL*8 ZSPREV(ILG), FSPREV(ILG), ZSDEP(ILG), FSDEP(ILG),
     1      D100(ILG)
         integer meltpath(ILG)
      integer snow_switch

      DATA ALVSI,ALIRI/0.90,0.70/
cbjd  for the snow accumulation algorithm
      DATA D100A,D100D/0.02,0.05/
      ACCLMT=3.0*DELT/3.1536E7

      IF(IC.NE.4)              CALL XIT('CLASSA',-1)
C----------------------------------------------------------------
C   * CALCULATION OF SNOW DEPTH ZSNOW AND FRACTIONAL SNOW COVER
C   * FSNOW; ESTIMATION OF FRACTIONAL CLOUD COVER FCLOUD.
C   * INITIALIZATION OF COMPUTATIONAL ARRAYS.
C
      snow_switch = 0

      DO 100 I=IL1,IL2
c    choose to use the SDC or the SAC-SDC
      if(snow_switch.eq.1) then ! use SDC only
        IF(SNO(I).GT.0.0) THEN
           ZSNOW(I)=SNO(I)/RHOSNO(I)
           IF(ZSNOW(I).GT.D100D) THEN
              FSNOW(I)=1.0
           ELSE
              FSNOW(I)=ZSNOW(I)/D100D
              ZSNOW(I)=D100D
           ENDIF
        ELSE
           ZSNOW(I)=0.0
           FSNOW(I)=0.0
        ENDIF
      else ! use SAC-SDC
        IF(SNO(I).EQ.0.0) then ! NO SNOW
          FSNOW(I)  = 0.0
          ZSNOW(I)  = 0.0
          FSPREV(I) = 0.0
          ZSPREV(I) = 0.0
          D100(I) = D100A
          meltpath(I) = 0
        ELSE
          ZSNOW(I) = SNO(I)/RHOSNO(I)
          IF(ZSPREV(I).EQ.0.0) THEN        ! NEW SNOW
            IF(ZSNOW(I).LT.D100A) THEN     ! new snow: zone 1
               D100(I) = D100A
               FSNOW(I) = ZSNOW(I)/D100A
               FSPREV(I) = FSNOW(I)
```

109

```
              ZSPREV(I)=ZSNOW(I)
              ZSNOW(I) = D100A
              meltpath(I) = 1
            ELSE IF(ZSNOW(I).LT.D100D) THEN ! new snow: zone 2
              D100(I) = ZSNOW(I)
              FSNOW(I) = 1.0
              FSPREV(I) = FSNOW(I)
              ZSPREV(I)=ZSNOW(I)
              meltpath(I) = 1
            ELSE                 ! new snow: zone 3
              D100(I) = D100D
              FSNOW(I) = 1.0
              FSPREV(I) = FSNOW(I)
              ZSPREV(I)=ZSNOW(I)
              meltpath(I) = 1
            ENDIF
          ELSE IF(ZSNOW(I).LT.ZSPREV(I)) THEN ! LESS SNOW (smaller depth)
            IF(ZSNOW(I).LE.D100D) THEN       ! less snow: zones 1 and 2
              IF(meltpath(I).EQ.1) THEN      ! melt towards zsnow = 0
                IF(ZSPREV(I).LT.D100D) THEN ! from zone 1 or 2
                  FSNOW(I)=ZSNOW(I)/D100(I)
                  FSPREV(I) = FSNOW(I)
                  ZSPREV(I)=ZSNOW(I)
                  ZSNOW(I) = D100(I)
                  ZSDEP(I) = 0.0
c                 meltpath(I) = 1
                ELSE                 ! from zone 3
                  D100(I) = D100D
                  FSNOW(I) = ZSNOW(I)/D100D
                  FSPREV(I) = FSNOW(I)
                  ZSPREV(I)=ZSNOW(I)
                  ZSNOW(I) = D100D
                  ZSDEP(I) = 0.0
c                 meltpath(I) = 1
                ENDIF
              ELSE IF(meltpath(I).EQ.2)THEN ! melt towards a departure point
                IF(ZSNOW(I).LE.ZSDEP(I)) THEN ! melt below departure point
                  D100(I) = D100D
                  FSNOW(I) = ZSNOW(I)/D100D
                  FSPREV(I) = FSNOW(I)
                  ZSPREV(I)=ZSNOW(I)
                  ZSNOW(I) = D100D
                  ZSDEP(I) = 0.0
                  FSDEP(I) = 0.0
                  meltpath(I) = 1
                ELSE               ! melt doesn't reach departure point
                  FSNOW(I) = FSDEP(I) +
     +                (ZSNOW(I)-ZSDEP(I))*
     +                (FSPREV(I)-FSDEP(I))/
     +                (ZSPREV(I)-ZSDEP(I))
                  FSPREV(I) = FSNOW(I)
                  ZSPREV(I)=ZSNOW(I)
                  ZSNOW(I) = D100(I)
c                 meltpath(I) = 2
```

```fortran
            ENDIF
          ELSE ! we have a problem with setting meltpath
            print*, 'problem setting meltpath in classa.f'
            STOP
          ENDIF
        ELSE IF(ZSNOW(I).GT.D100D) THEN  ! less snow: zone 3
          D100(I) = D100D
          FSNOW(I) = 1.0
          FSPREV(I) = FSNOW(I)
          ZSPREV(I)=ZSNOW(I)
c         meltpath(I) = 1
        ENDIF
      ELSE IF(ZSNOW(I).GE.ZSPREV(I)) THEN ! SNOW ON SNOW
        IF(ZSNOW(I).LT.D100A) THEN        ! more snow: zone 1
          IF(ZSNOW(I)-ZSPREV(I).LT.0.001) THEN ! extremely small snowfall
            D100(I) = MIN(D100(I),D100D)
            D100(I) = MAX(D100(I),D100A)
            FSNOW(I) = ZSNOW(I)/D100(I)
            FSPREV(I) = FSNOW(I)
            ZSPREV(I)=ZSNOW(I)
            ZSNOW(I) = D100(I)
          ELSE                    ! significant snowmelt
            IF(D100(I).EQ.D100D) THEN       ! departure snowfall
              D100(I) = D100A
              FSDEP(I) = FSNOW(I)
              ZSDEP(I) = ZSPREV(I)
              FSNOW(I) = ZSNOW(I)/D100A
              FSPREV(I) = FSNOW(I)
              ZSPREV(I)=ZSNOW(I)
              ZSNOW(I) = D100A
              meltpath(I) = 2
            ELSE                   ! already in hysterisis zone
              D100(I) = D100A
              FSNOW(I) = ZSNOW(I)/D100A
              FSPREV(I) = FSNOW(I)
              ZSPREV(I)=ZSNOW(I)
              ZSNOW(I) = D100A
c             meltpath(I) = 2
            ENDIF
          ENDIF
        ELSE IF(ZSNOW(I).LT.D100D) THEN ! more snow: zone 2
          IF(FSNOW(I).EQ.1.0) THEN
            FSNOW(I) = 1.0
            D100(I) = ZSNOW(I)
            ZSPREV(I) = ZSNOW(I)
            FSPREV(I) = FSNOW(I)
          ELSE IF(ZSNOW(I)-ZSPREV(I).LT.0.001) THEN ! extremely small snowfall
            D100(I) = MIN(D100(I),D100D)
            D100(I) = MAX(D100(I),D100A)
            FSNOW(I) = ZSNOW(I)/D100(I)
            IF(FSNOW(I).GT.1.0) THEN ! overshoot of FSNOW = 1.0
              D100(I) = ZSNOW(I)
              FSNOW(I) = 1.0
              FSPREV(I) = FSNOW(I)
```

111

```fortran
                ZSPREV(I)=ZSNOW(I)
              ELSE               ! still below FSNOW = 1.0
                FSPREV(I) = FSNOW(I)
                ZSPREV(I)=ZSNOW(I)
                ZSNOW(I) = D100(I)
              ENDIF
            ELSE                        ! significant snowmelt
              IF(D100(I).EQ.D100D) THEN    ! departure snowfall
                D100(I) = ZSNOW(I)
                FSDEP(I) = FSNOW(I)
                ZSDEP(I) = ZSPREV(I)
                FSNOW(I) = 1.0
                FSPREV(I) = FSNOW(I)
                ZSPREV(I)=ZSNOW(I)
                meltpath(I) = 2
              ELSE               ! already in hysterisis zone
                D100(I) = ZSNOW(I)
                FSNOW(I) = 1.0
                FSPREV(I) = FSNOW(I)
                ZSPREV(I)=ZSNOW(I)
c               meltpath(I) = 2
              ENDIF
            ENDIF
          ELSE                  ! more snow: zone 3
            D100(I) = D100D
            FSNOW(I) = 1.0
            FSPREV(I) = FSNOW(I)
            ZSPREV(I)=ZSNOW(I)
            ZSDEP(I) = 0.0
            meltpath(I) = 1
          ENDIF
        ELSE
c     we have a problem
          print *, 'There is a problem with the snow accumulation '
          print *, 'algorithm. Check classa.f.'
          STOP
        ENDIF
      ENDIF
      endif
      IF(COSZS(I).GT.0.0.AND.(QSWV(I)+QSWI(I)).GT.0.0) THEN
        FCLOUD(I)=MAX(0.0,MIN(1.0,QSWD(I)/(QSWV(I)+QSWI(I))))
      ELSE
        FCLOUD(I)=0.
      ENDIF
      ALVSCN(I)=0.0
      ALIRCN(I)=0.0
      ALVSCS(I)=0.0
      ALIRCS(I)=0.0
      TRVSCN(I)=0.0
      TRIRCN(I)=0.0
      TRVSCS(I)=0.0
      TRIRCS(I)=0.0
      ALVSSN(I)=0.0
      ALIRSN(I)=0.0
```
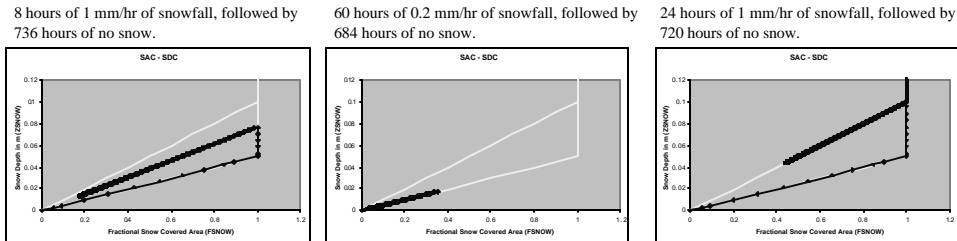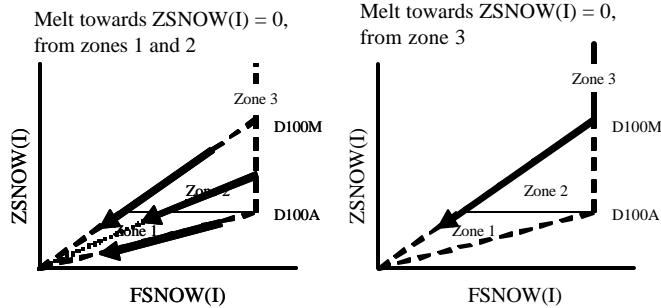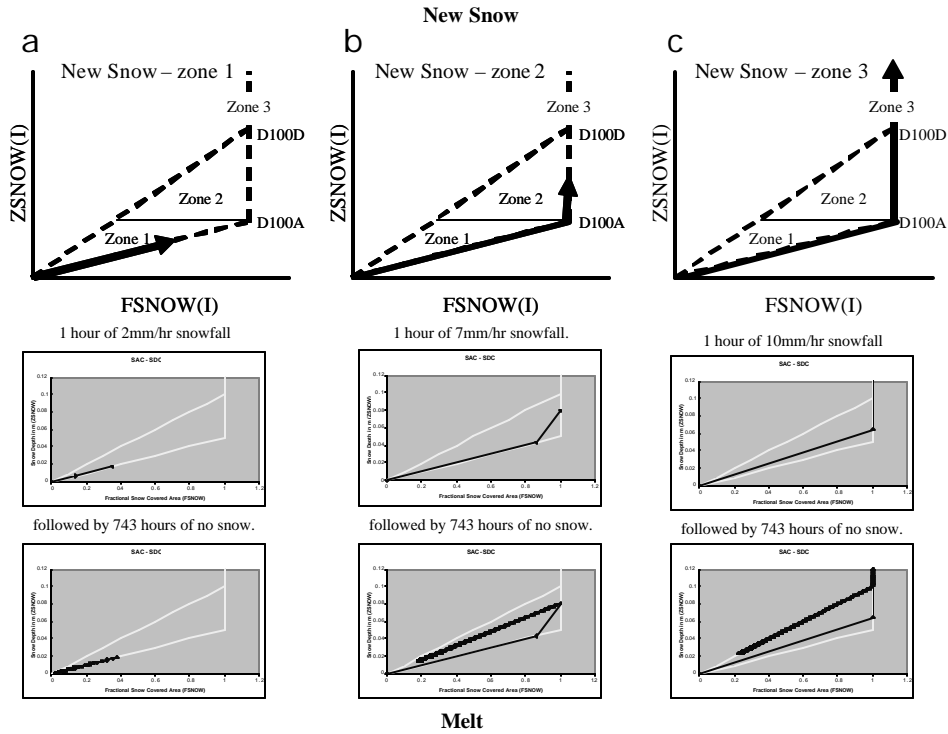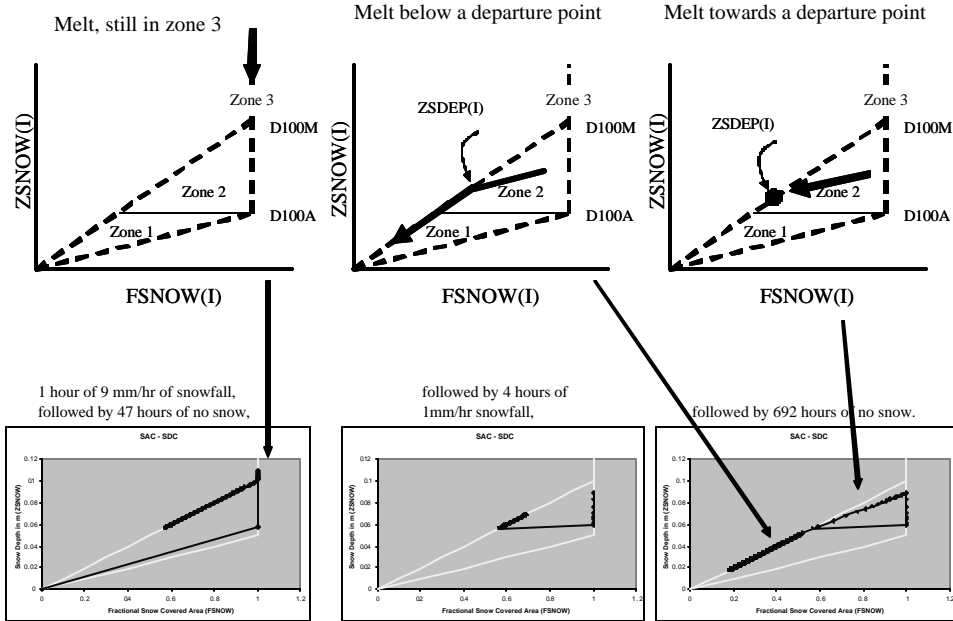
```
      ALVSG (I)=0.0
      ALIRG (I)=0.0
      TRSNOW(I)=0.0
100 CONTINUE
```
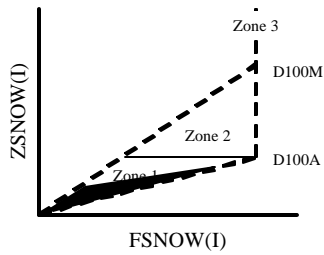
Appendix C.   SAC-SDC Testing

New Snow

a
New Snow – zone 1

1 hour of 2mm/hr snowfall

followed by 743 hours of no snow.

b
New Snow – zone 2

1 hour of 7mm/hr snowfall.

followed by 743 hours of no snow.

c
New Snow – zone 3

1 hour of 10mm/hr snowfall

followed by 743 hours of no snow.

Melt

Melt towards ZSNOW(I) = 0,
from zones 1 and 2

Melt towards ZSNOW(I) = 0,
from zone 3

8 hours of 1 mm/hr of snowfall, followed by 736 hours of no snow.

60 hours of 0.2 mm/hr of snowfall, followed by 684 hours of no snow.

24 hours of 1 mm/hr of snowfall, followed by 720 hours of no snow.

114

Melt

Melt, still in zone 3

Melt below a departure point

Melt towards a departure point

1 hour of 9 mm/hr of snowfall, followed by 47 hours of no snow,

followed by 4 hours of 1mm/hr snowfall,

followed by 692 hours of no snow.
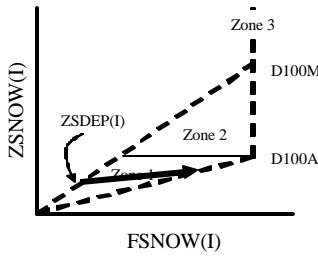

Snowfall – Zone 1

Snow on Snow

Setting the stage: 8 hours of 1 mm/hr of snowfall, followed by 736 hours of no snow.

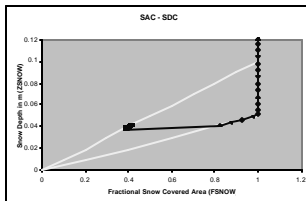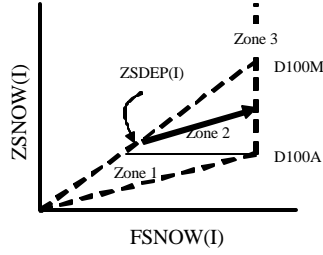This piece of the SAC-SDC: a humidity value of 3e-03 for the last four hours of the simulation.
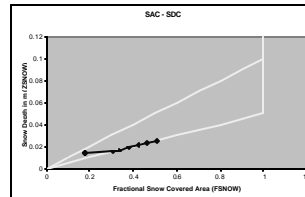
Setting the stage: 8 hours of 1 mm/hr of snowfall, followed by 736 hours of no snow.

This piece of the SAC-SDC: a humidity value of 7e-03 for the last three hours of the simulation.
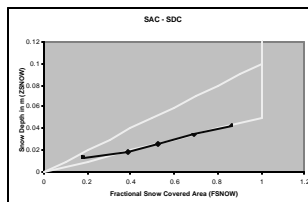
Setting the stage: 8 hours of 1 mm/hr of snowfall, followed by 736 hours of no snow.

This piece of the SAC-SDC: a humidity value of 2e-03 for the last four hours of the simulation.
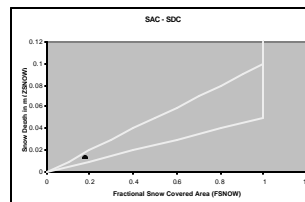
Snow on Snow

Departure Snowfall – Zone 1

Setting the stage: 20 hours of 1 mm/hr of snowfall, followed by 699 hours of no snow.

This piece of the SAC-SDC: the melt path of the first snowfall, followed by 10 hours of 1mm/hr of snowfall from hours 720 to 729.
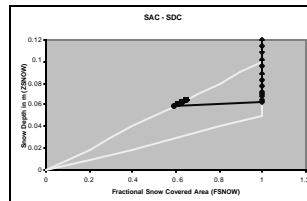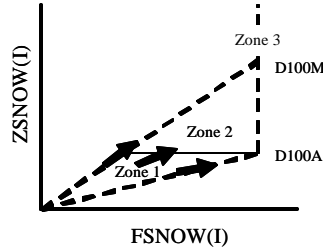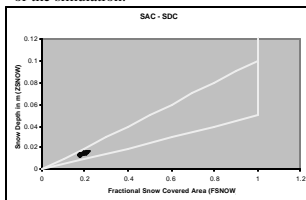

Departure Snowfall – Zone 2

Setting the stage: 30 hours of 1 mm/hr of snowfall, followed by 689 hours of no snow.

This piece of the SAC-SDC: the melt path of the first snowfall, followed by 10 hours of 1mm/hr of snowfall from hours 720 to 729.

Snow on Snow
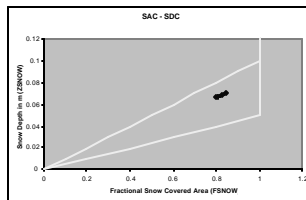
Extremely small snowfall,
Zones 1 and 2 (no overshoot)

Setting the stage: 8 hours of 1 mm/hr of snowfall, followed by 736 hours of no snow.

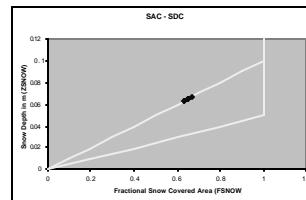This piece of the SAC-SDC: a humidity value of 2.5e-03 for the last four hours of the simulation.

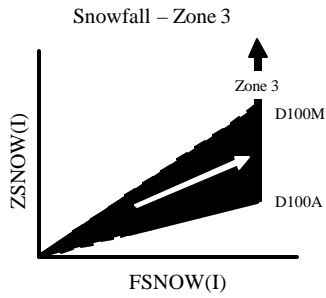Setting the stage: 1 hour of 7mm/hr snowfall during hour 730.

This piece of the SAC-SDC: a humidity value of 2.8e-03 for the last four hours of the simulation.

Setting the stage: 1 hour of 10mm/hr snowfall during hour 700.

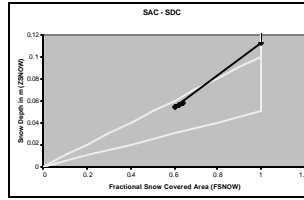This piece of the SAC-SDC: a humidity value of 2.7e-03 for the last four hours of the simulation.
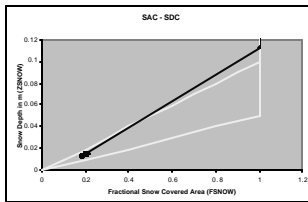

116

Snow on Snow

Snowfall – Zone 3

Setting the stage: 1 hour of 1 mm/hr of snowfall, followed by 10 hours of 1mm/hr snowfall during hours 700 to 709.

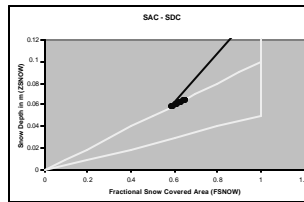This piece of the SAC-SDC: a 10mm/hr snowfall during hour 740.

8 hours of 1 mm/hr of snowfall, followed by 731 hours of no snow.

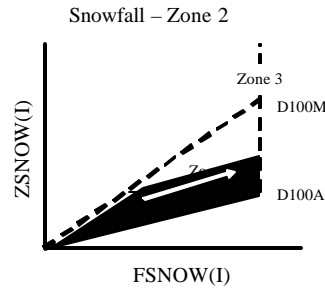This piece of the SAC-SDC: 15 mm/hr of snowfall on hour 740.

30 hours of 1 mm/hr of snowfall, followed by 709 hours of no snow.

This piece of the SAC-SDC: 15 mm/hr of snowfall on hour 740.

Snow on Snow

Snowfall – Zone 1

Snowfall – Zone 2

8 hours of 1 mm/hr of snowfall, followed by 731 hours of no snow.

This piece of the SAC-SDC: 2 mm/hr of snowfall on hour 740.
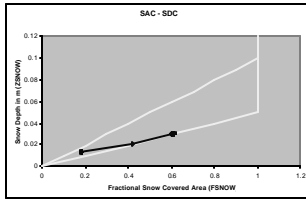
8 hours of 1 mm/hr of snowfall, followed by 731 hours of no snow.

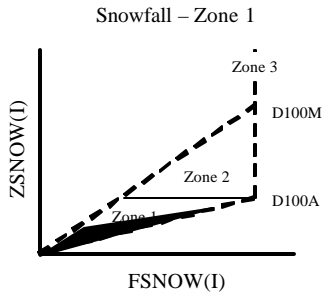This piece of the SAC-SDC: 6.8 mm/hr of snowfall on hour 740.
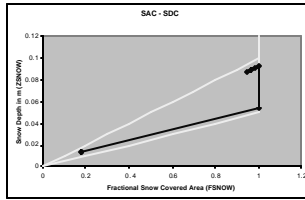
Setting the stage: 1 hour of 1 mm/hr of snowfall, followed by 10 hours of 1mm/hr snowfall during hours 700 to 709.

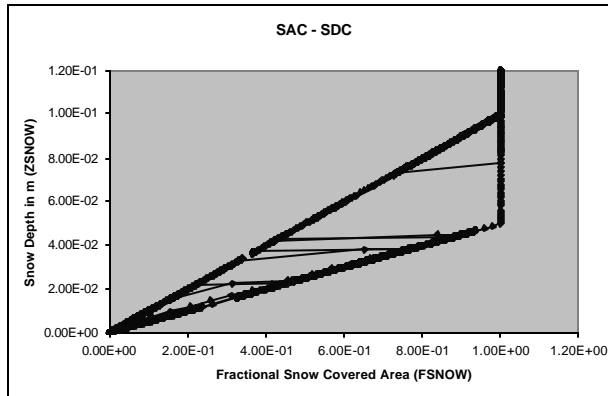This piece of the SAC-SDC: a snowfall of 2.8 mm/hr on hour 740.
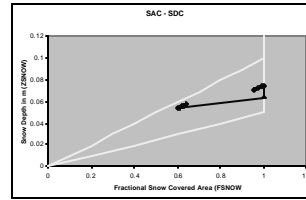
This is what the SAC-SDC looks like for the three year NSA run. It would be nice to collect some data showing if this is typical hysteresis for this area… maybe later.

References

Adam KM. 1981. Travel Over Snow. In *Handbook of Snow – Principles, Processes, Management & Use*. DM Gray and DH Male (Eds). Pergamon Press: Oxford, England; pp 648 - 670.

Aguado E. 1985. Radiation balances of melting snow covers at an open site in the central Sierra Nevada, California. *Water Resources Research.* **21**: 1649 – 1654.

Aitchison CW. 2001. The Effect of Snow Cover on Small Animals. In *Snow Ecology: An Interdisciplinary Examination of Snow-covered Ecosystems*. Jones HG, Pomeroy JW, Walker DA, Hoham RW (Eds). Cambridge University Press: Cambridge; pp 229 – 265.

Auer AH Jr. 1974. The rain vesus snow threshold temperatures. *Weatherwise.* **27**: 67.

Barnett TP, Dumenil L, Schlese U, Roeckner E, Latif M. 1989. The effect of Eurasian snow cover on regional and global climate variations. *Journal of Atmospheric Science* **46:** 661-685.

Bear J. 1972. *Dynamics of Fluids in Porous Media*. Dover Publications, Inc., New York, 764 pp.

Benson CS. 1969. *The Seasonal Snow Cover in Arctic Alaska*. Report 51, The Arctic Institute of North America, Calgary, Canada.

Betts AK, Ball JH, Beljaars ACM, Miller MJ, Viterbo P. 1994. Coupling between land-surface boundary-layer parameterizations and rainfall on local and regional scales: Lessons from the wet summer of 1993. In: *Proceedings of the Fifth Conference of Global Change Studies*, Nashville TN, 23 – 28 January 1994. American Meteorological Society, Boston, Massachusetts. Pp. 174 – 181.

Biswas AK. 1970. *History of Hydrology*. Amsterdam: North-Holland Publishing Co.

Boer GJ, McFarlane NA, Labrise R, Henderson JD, Blanchet JP. 1984. The Canadian Climate Centre spectral atmospheric general circulation model. *Journal of Climatology*. Vol. 5: 1045 – 1077.

Bowling LC, Lettenmaier DP, Nijssen B, Graham LP, Clark DB, Maayar ME, Essery R, Goers S, Gusev M, Habets F, van den Hurk B, Jin J, Kahan D, Lohmann D, Mahanama S, Mocko D, Nasonova O, Niu Y, Samuelsson P, Shmakin AB, Takata K, Verseghy D, Viterbo P, Xia Y, Ma X, Xue Y, Yang ZL. Simulation of high latitude hydrological processes in the Torne-Kalix basin: PILPS Phase 2(e) 1: Experiment description and summary intercomparisons. In Press [a]. *Global and Planetary Change*.

Bowling LC, Lettenmaier DP, Nijssen B, Polcher J, Koster RD, Lohmann D. Simulation of high-latitude hydrological processes in the Torne-Kalix basin: PILPS Phase 2(e) 3: Equivalent model representation and sensitivity experiments. In Press [b]. *Global and Planetary Change*.

Canadian Hydraulics Centre. July 2003. *Ensim Hydrologic Reference Manual*. National Research Council Canada.: Ottawa, Ontario.

Carson DJ. 1982. Current parameterizations of land-surface processes in atmospheric general circulation models. In: *Land Surface Processes in Atmospheric General Circulation Models*, Eagleson PS. (Ed.), Cambridge University Press, Cambridge, 560 pp.

Chow VT, Maidment DR, Mays LW, 1988. *Applied Hydrology*. McGraw-Hill, New York.

Church M. 1974. Hydrology and permafrost with reference to northern North America. In – Permafrost Hydrology, Proceedings of Workshop Seminar 1974, Canadian National Committee for the International Hydrological Decade, Ottawa, Ontario, pp 7 – 20.

Colbeck SC. 1978. *Adv. Hydrosci.* **11** 165 – 206.

Cox LM, Zuzel JF. 1976. A method for determining sensible heat transfer to late-lying snowdrifts. *Proceedings of the 44th Annual Meeting of the Western Snow Conference*: Calgary, Alberta. 1976. pp 23-28.

Cuenca RH, Stangel D, Kelly S. 1999. *BOREAS HYD-1 Volumetric Soil Moisture Data*. Data Set "HYD01_VOL_SOIL_MOIST" from the BOREAS Study.

Deardorff JW. 1972. Parameterization of the planetary boundary layer for use in general circulation models. *Monthly Weather Review*. **100**: 93 – 106.

Deardorff JW. 1978. Efficient prediction of ground surface temperature and moisture, with inclusion of a layer of vegetation. *Journal of Geophysical Resources*. **83**: 1889 – 1903.

Diamond M, Lowry WP. 1953. Correlation of density of new snow with 700mb temperature. *Research Paper 1, Snow, Ice and Permafrost Research Establishment*. US Army Corps of Engineers, 3pp.

Dickinson RE. 1984. Modeling evapotranspiration for three-dimensional global climate models. In *Climate Processes and Climate Sensitivity.* Hanson JE and Takahashi K (Eds.), Geophysical Monograph 2a, Maurice Ewing Vol. 5, American Geophysical Union, Washington, DC, pp 58 – 72.

Dickinson RE, Henderson-Sellers A, Kennedy PJ, Wilson MF. 1986. *Biosphere-Atmosphere Transfer Scheme (BATS) for the NCAR Community Climate Model.* National Center for Atmospheric Research, Boulder, Colorado, NCAR/TN-275+STR, 69 pp.

Dingman SL. 1994. Snow and Snowmelt. In *Physical Hydrology*, Prentice Hall Englewood Cliffs, New Jersey; pp 159 – 209.

Dirmhirn L, Eaton FD. 1975. Some characteristics of the albedo of snow. *Journal of Applied Meteorology.* **14**: 375 – 379.

Donald JR 1992. Snowcover Depletion Curves and Satellite Snowcover Estimates for Snowmelt Runoff Modelling. *PhD Thesis*, Civil Engineering, University of Waterloo.

Donald JR, Soulis ED, Kouwen N, Pietroniro A. 1995. A land cover-based snow cover representation for distributed hydrologic models. *Water Resources Research.* 31**,** No. 4: pp. 995 – 1009.

Environment Canada. 2003. Environment Canada's online climate data information archive. *Climate Normals and Averages*. http://www.climate.weather office.ec.gc.ca/Welcome_e.html, Accessed 12 Oct. 2003.

Essery R. 1997. Modelling fluxes of momentum, sensible heat and latent heat over heterogeneous snow cover. *Q. J. R. Meteorol. Soc..* 123:1867-1883 1997.

Essery R, Yang ZL. 2001. *An Overview of Models Participating in the Snow Model Intercomparison Project (SNOWMIP).* SnowMIP Workshop 11 July 2001. 8th Scientific Assembly of IAMAS. Innsbruck.

Etchevers P, Martin E, Brown R, Fierz C, Lejeune Y, Bazile E, Boone A, Dai YJ, Essery R, Fernanadez A, Gusev Y, Jordan R, Koren V, Kowalczyk E, Pyles RD, Schlosser A, Shmakin AB, Smirnova TG, Strasser U, Verseghy D, Yamazaki T, Yang ZL. 2002. *SnowMIP, an intercomparison of snow models: first results.* International Snow Science Workshop, Penticton, BC Canada.

Fassnacht SR. 2000. Distributed Snowpack Simulation Using Weather Radar with an Hydrologic – Land Surface Scheme Model. *PhD Thesis.* University of Waterloo.

Fassnacht SR, Soulis ED. 2002. Implications during Transitional Periods of Improvements to the Snow Processes in the Land Surface Scheme – Hydrological Model WATCLASS. *Atmosphere – Ocean.* **40,** No. 4: pp. 389 – 403.

Formosov AN. 1946. Snow cover as an integral factor of the environment and its importance in the ecology of mammals and birds. *Materials for Fauna and Flora of the USSR. New Series, Zoology.* (English edition published by Boreal Institute, University of Alberta, Edmonton, Canada Occasional Paper 1), 5 1 – 152.

Frank LA, Sigwarth JB 2001. "Detections of small comets into the Earth's upper atmosphere. I. Observations. II. Interpretation." Geophysical Resource Letters, Vol. 13, No. 303, pp. 303-7.

Franklin BA, Bonzheim K, Gordon S, Timmins GC. Snow shoveling: a trigger for acute myocardial infarction and sudden coronary death. *Am J Cardiol* 1996; **77**:855-858.

Gleick P 2002. Environment and Security Water Conflict Chronology Version 2002. In *The World's Water - The Biennial Report on Freshwater Resources 2002 - 2003*. P Gleick (Ed.) Island Press. Washington D.C. pp. 194-208.

Gold LW. 1958. Changes in a shallow snow cover subject to a temperate climate. *Journal of Glaciology.* **3 2**18 – 222.

Goodison BE, Ferguson HL, McKay GA. 1981. Measurement and data analysis. In *Handbook of Snow – Principles, Processes, Management & Use*. DM Gray and DH Male (Eds). Pergamon Press: Oxford, England; pp 191 - 274.

Gray DM, Landine PG. 1987. Albedo model for shallow prairie snow covers. *Canadian Journal of Earth Sciences.* **24:** pp. 1760 – 1768.

Gray DM, Male DH. (Eds.) 1981. *Handbook of Snow: Principles, Processes, Management & Use.* Pergamon Press. Toronto.

Gray DM, Prowse TD. 1993. Snow and Floating Ice. In *Handbook of Hydrology*. DR Maidment (Ed).McGraw-Hill: Toronto, Ontario.

Groisman PY, Karl TR, Knight RW, Stenchikov GL. 1994. Changes of snow cover, temperature, and the radiative heat balance over the Northern Hemisphere. *Journal of Climate* **7:** 1633 – 1656.

Groisman PY, and Davies DD. 2001. Snow Cover and the Climate System. In *Snow Ecology: An Interdisciplinary Examination of Snow-covered Ecosystems*. Jones HG, Pomeroy JW, Walker DA, Hoham RW (Eds). Cambridge University Press: Cambridge; pp 1 – 44.

Gupta HV, Sorooshian S, Hogue TS, Boyle DP. 2003. Advances in Automatic Calibration of Watershed Models. In: *Calibration of Watershed Models, Water Science and Application*. Vol. 6. American Geophysical Union. Washington DC.

Hedstrom NR, Pomeroy JW 1997. Accumulation of intercepted snow in the Boreal Forest: Measurements and modelling. *Proceedings of the Eastern Snow Conference,* Banff, Alberta, **54**: 130 – 141.

Hedstrom NR, Pomeroy JW 1998. Measurements and modelling of snow interception in the boreal forest. *Hydrological Processes* 1**2**(10-11): 1611 – 1625.

Hoham RW, and Duval B. 2001. Microbial Ecology of Snow and Freshwater Ice with Emphasis on Snow Algae. In *Snow Ecology: An Interdisciplinary Examination of Snow-covered Ecosystems*. Jones HG, Pomeroy JW, Walker DA, Hoham RW (Eds). Cambridge University Press: Cambridge; pp 168 – 228.

Jones HG. 1999. The Ecology of Snow-covered Systems: A Brief Overview of Nutrient Cycling and Life in the Cold. *Hydrological Processes* **13:** 2135 – 2147.

Jones PB, Walker GD, Harden RW, McDaniels LL. 1963. *The Development of the Science of Hydrology.* Circ. No. 63-03, Texas Water Commission.

Kavetski D, Franks SW, Kuczera G. 2003. Confronting Input Uncertainty in Environmental Modelling. In: *Calibration of Watershed Models, Water Science and Application*. Vol. 6. American Geophysical Union. Washington DC.

Kluger J 1997. Spots confirmed, tiny comets spurned. *Science* Vol. 276, No. 5,317, May 30, p. 1,333.

Kouwen N, Mousavi SF. 2002. WATFLOOD/SPL9 Hydrological Model & Flood Forecasting System. In *Mathematical Models of Large Watershed Hydrology*. VP Singh and DK Frevert (Eds).Water Resources Publications, LLC: Colorado, USA; pp 649 - 685.

Kouwen N, Soulis ED, Pietroniro A, Donald J, Harrington RA 1993. Grouped Response Units for Distributed Hydrologic Modeling. *Journal of Water Resources Planning and Management.* Vol. 119, No. 3: 289 – 305.

Krynine PD. 1960. On the Antiquity of Sedimentation and Hydrology. New York: *Bull. Geol. Soc. Am.* **70** 1721-1726.

Kung EC, Bryson RA, Lenschow DH. 1964. Study of a Continental Surface Albedo on the Basis of Flight Measurements and Structure of the Earth's Surface Cover Over North America. *Monthly Weather Review*. Vol 92, Number 12: 543 – 564.

La Chapelle E. 1961. *Snow Layer Densification.* Alta Avalanche Study Center, Project F, Progress Report No. 1, US Department of Agriculture Forest Service, Wasatch National Forest.

Leavesley GH, Stannard LG 1990. Application of remotely sensed data in a distributed-parameter watershed model. *Proc. Workshop on Applications of Remote Sensing in Hydrol.,* Feb., 47 – 68.

Leonard RE, Eschner AR. 1968. Albedo of intercepted snow. *Water Resources Research.* **4**: 931 – 935.

Li P. 1989. Recent trends and regional differentiation of snow variation in China. In *Glacier and Snow Cover Variations.* IAHS public. No. 183: pp. 3 – 10.

Liston GE. 1995. Local Advection of Momentum, Heat, and Moisture during the Melt of Patchy Snow Covers. *Journal of Applied Meteorology.* 1995. Vol. 34, pp. 1705 – 1715.

Liston GE. 1999. Interrelationships among Snow Distribution, Snowmelt, and Snow Cover Depletion: Implications for Atmospheric, Hydrologic, and Ecologic Modeling. *Journal of Applied Meteorology.* 1995. Vol. 38, pp. 1474 – 1487.

Longley RW. 1960. Snow depth and snow density at Resolute, Northwest Territories. *Journal of Glaciology.* **3,** 733 – 738.

Luce CH, Tarboton DG, Cooley KR. 1999. Sub-grid parameterization of snow distribution for an energy and mass balance snow cover model. *Hydrological Processes* **13:** 1921-1933.

Male DH. 1980. The Seasonal Snowcover. In *Dynamics of Snow and Ice Masses*. SC Colbeck (Ed). Academic Press: New York, U.S.A.; pp 305 – 395.

Male DH and Gray DM. 1981. Snowcover Ablation and Runoff. In *Handbook of Snow – Principles, Processes, Management & Use*. DM Gray and DH Male (Eds). Pergamon Press: Oxford, England; pp 360 - 436.

Manabe S. 1969. Climate and the ocean circulation, I. The atmospheric circulation and the hydrology of the Earth's surface. *Monthly Weather Review.* **97**: 739-774.

Manning S. 2003. Roof Collapse Injures Nine. *The San Francisco Examiner* Feb. 24 2003. http://www.examiner.com/headlines/default.jsp?story=n.toys.0224w . Accessed 17 May 2003. Associated Press.

Marsh P. 1990. Snow Hydrology. In *Northern Hydrology – Canadian Perspectives*. Prowse TD, Ommanney CSL (Eds). NHRI Science Report No. 1: Environment Canada, Saskatoon; pp 37 - 62.

Marsh P, Neumann NN, Essery RLH, Pomeroy JW. 1999. Model estimates of local advection of sensible heat over a patchy snow cover. *Interactions Between the Cryoshere, Climate and Greenhouse Gases.* Proceedings of the IUGG 99 Symposium HS2, Birmingham, July 1999. IAHS Publ. no. 256 1999.

McKay GA, Gray DM. 1981. The Distribution of Snowcover. In *Handbook of Snow – Principles, Processes, Management & Use*. DM Gray and DH Male (Eds).Pergamon Press: Oxford, England; pp 153 - 190.

Meinzer OE. 1949. Hydrology. In *Physics of the Earth*. McGraw-Hill: New York, New York 1942. Reprinted by Dover, New York 1949.

Mulvany TJ. 1850. On the use of self-registering rain and flood gauges. *Proeedings of the Insitute of Civil Engineers of Ireland*, Session 1850-1, v. IV, pt. II, 1 – 8, Dublin.

Nace RL. 1974. General evolution of the concept of the hydrological cycle. *Three Centruies of Scientific Hydrology*, Paris: UNESCO-World Meteorological Organization-International Association of Hydrological Sciences, pp. 40-48.

Natural Resources Canada. 2003. Environment-Land-Permafrost map. *The Atlas of Canada*. http://atlas.gc.ca/site/english/maps/environment/land/permafrost, Accessed 12 Oct. 2003.

Nijssen B, Bowling LC, Lettenmaier DP, Clark DB, Maayar ME, Essery R, Goers S, Gusev YM, Habets F, van den Hurk B, Jin J, Kahan D, Lohmann D, Ma X, Mahanama S, Mocko D, Nasonova O, Niu GY, Samuelsson P, Shmakin AB, Takata K, Verseghy D, Viterbo P, Xia Y, Xue Y, Yang ZL. Simulation of high latitude hydrological processes in the Torne-Kalix basin: PILPS Phase 2(e) 2: Comparison of model results with observations. In Press. *Global and Planetary Change.*

Neumann NN, Marsh P. 1998. Local advection of sensible heat in the snowmelt landscape of Arctic tundra. *Hydrological Processes.* **12**. 1547 – 1560.

Payton B. 2003. Showdown at the Summit. *Canadian Geographic* May/June 2003 Issue, pp 54 – 68.

Piersol J 2000. Modelling Snowcover Depletion Using WATCLASS. *BSc Thesis*, Earth Sciences. University of Waterloo.

Pomeroy JW, and Li L. 1997. Development of the Prairie Blowing Snow Model for application in climatological and hydrological models. *Proceedings of the Western Snow Conference* 65: 186 – 197.

Pomeroy JW, Gray DM, Shook KR, Toth B, Essery RLH, Pietroniro A, Hedstrom N. 1998. An evaluation of snow accumulation and ablation processes for land surface modelling. *Hydrological Processes* 1**2** 2339-2367.

Pomeroy JW, and Brun E. 2001. Physical Properties of Snow. In *Snow Ecology: An Interdisciplinary Examination of Snow-covered Ecosystems*. Jones HG, Pomeroy JW, Walker DA, Hoham RW (Eds). Cambridge University Press: Cambridge; pp 45 – 126.

Pomeroy JW, Essery R, Toth B. 2003. Implications of spatial distributions of snow mass and melt rate on snowcover depletion: observations in a sub-arctic mountain catchment. *International Glaciological Society*, Davos, June 2003.

Postel S. 1999. *Pillar of Sand. Can the Irrigation Miracle Last?* Worldwatch Institute: New York, New York.

Prowse TD, Ommanney CSL (Eds). 1990. *Northern Hydrology – Canadian Perspectives*. NHRI Science Report No. 1: Environment Canada, Saskatoon.

Pruitt WO. 1984. Snow and living things. *Northern Ecology and Resource Management,* R Olson (Ed.). University of Alberta Press, pp 51 – 77.

Rango A, Martinec J, Foster J, and Marks D 1983: Resolution in operational remote sensing of snow cover. *Hydrological Applications of Remote Sensing and Remote Data Transmission*, (Proceedings of the Hamburg Symposium, August 1983). IAHS Publ. no 145.

Reisner M. 1986. *Cadillac Desert. The American West and its Disappearing Water.* Viking Penguin Inc.: New York, New York.

Richter GD. 1954. *Snow Cover, Its Formation and Properties.* U.S. Army Cold Regions Research and Engineering Laboratory, Transl. 6, NTIS AD 045950, Hanover, NH.

Robinson DA, Kukla G. 1984. Albedo of a dissipating snow cover. *Journal of Climate and Applied Meteorology.* **23**: 1626 – 1634.

Rohrer MB. 1989. Determination of the transition air temperature from snow to rain and intensity of precipitation. *WMO TD No. 328, International Workshop on Precipitation Measurement.* (Ed. B Sevruk) St. Moritz, Switzerland, (Instruments and Observing Methods Report No. 48), 475 – 482.

Rouse H Ince S. 1957. *History of Hydraulics.* Iowa Institute of Hydraulic Research: State University of Iowa.

Schmidt RA Jr, Gluns DR. 1991. Snowfall interception on branches of three conifer species. *Canadian Journal of Forest Research.* **21**:1262 – 1269.

Sellers PJ, Mintz Y, Sud YC, Dalcher A. 1986. A simple biosphere model (SiB) for use within general circulation models. *Journal of Atmospheric Science.* 43:505 – 531.

[a]Sellers PJ, Dickinson RE, Randall DA, Betts AK, Hall FG, Berry JA, Collatz GJ, Denning AS, Mooney HA, Nobre CA, Sato N, Field CB, Henderson-Sellers A. 1997. Modeling the exchange of energy, water and carbon between continents and the atmosphere. *Science.* 275:502 – 509.

[b]Sellers PJ, Hall FG, Kelly RD, Black A, Baldocchi D, Berry JA, Ryan M, Ranson KJ, Crill PM, Lettenmaier DP, Margolis H, Cihlar J, Newcomer J, Fitzjarrald D, Jarvis PG, Gower ST, Halliwell D, Williams D, Goodison B, Wickland DE, Guertin FE. 1997. BOREAS in 1997: Experiment Overview, Scientific Results and Future Directions. *Journal of Geophysical Research.* 28731 – 28770.

Shiklomanov IA 1993. World fresh water resources. In *Water in Crisis: A Guide to the World's Fresh Water Resources*. P.H. Gleick (Ed.): Oxford University Press, New York, pp. 13 – 24.

Shook KR 1995. Simulation of the Ablation of Prairie Snowcovers. *PhD Thesis*, University of Saskatchewan.

[a]Singh VP, Frevert DK (Eds). 2002. *Mathematical Models of Small Watershed Hydrology and Applications.* Water Resources Publications, LCC: Chelsea, Michigan.

[b]Singh VP, Frevert DK (Eds). 2002. *Mathematical Models of Large Watershed Hydrology and Applications.* Water Resources Publications, LCC: Chelsea, Michigan.

Singh VP, Woolhis er DA. 2002. Mathematical Modeling of Watershed Hydrology. *Journal of Hydrologic Engineering*, Vol. 4: pp. 270-292.

Snelgrove KR 2002. Implications of Lateral Flow Generation on Land-Surface Scheme Fluxes. *PhD Thesis*, University of Waterloo.

Soulis ED, Snelgrove KR, Kouwen N, Seglenieks F, Verseghy DL. 2000. Towards Closing the Vertical Water Balance in Canadian Atmospheric Models: Coupling of the Land Surface Scheme CLASS with the Distributed Hydrological Model WATFLOOD. *Atmosphere-Ocean*, **38**, No. 1: pp. 251 – 269.

Steppuhn H. 1981. Snow and Agriculture. In *Handbook of Snow – Principles, Processes, Management & Use*. DM Gray and DH Male (Eds). Pergamon Press: Oxford, England; pp 60 - 125.

Stevens WK. 1999. *The Change in the Weather-People, Weather, and the Science of Climate.* Random House: New York, New York.

Sturm M, Holmgren J, Liston GE. 1995. A seasonal snow cover classification system for local to global applications. *Journal of Climate*, 8 1261-1283.

Tieri N. 1999. Snow Taunts add to Toronto's Misery. *The Kitchener Waterloo Record.* Tuesday, January 19 1999 A2. Canadian Press.

Townsend AA. 1964. Natural convection in water over an ice surface. *Quarterly Journal of the Royal Meteorological Society.* **103**: 345 – 357.

US Army Corps of Engineers 1956. *Snow Hydrology: Summary Report of the Snow Investigations.* North Pacific Division, Portland, OR, 437p. (Available through the US Department of Commerce, Washington, DC).

Verseghy DL. 1991. CLASS – A Canadian Land Surface Scheme for GCMs. I. Soil Model. *International Journal of Climatology*, Vol. 11: pp. 111-133.

Verseghy DL, McFarlane NA, Lazare M. 1993. CLASS – A Canadian Land Surface Scheme for GCMs. II. Vegetation Model and Coupled Runs. *International Journal of Climatology*, Vol. 13: pp. 347-370.

Verseghy DL. 1996. Local climates simulated by two generations of Canadian GCM land surface schemes. *Atmosphere-Ocean*, Vol. 34: pp. 435 – 456.

Verseghy DL. 2000. The Canadian Land Surface Scheme (CLASS): Its History and Future. *Atmosphere-Ocean*, **38**, No. 1: pp. 1-13.

Vörösmarty CJ, Gutowski WJ, Person M, Chen TC, Case D. 1993. Linked atmosphere-hydrology models at the macroscale. *Macroscale Modelling of the Hydrosphere*. Proceedings of the Yokohama Symposium, July 1993. IAHS Publ. no. 214, 1993.

Vörösmarty CJ, Hinzman LD, Peterson BJ, Bromwich DH, Hamilton LC, Morison J, Romanovsky VE, Sturm M, Webb RS. 2001. *The Hydrologic Cycle and its Role in Arctic and Global Environmental Change: A Rationale and Strategy for Synthesis Study*. Fairbanks, Alaska: Arctic Research Consortium of the U.S., 84 pp.

Wakahama G. 1968. *Int. Assoc. Sci. Hydrol., Publ.* **79,** 370 – 379.

Viessman W, Lewis GL. 1996. *Introduction to Hydrology – 4th Edition*, Harper Collines College Publishers, New York, New York.

Whidden EA 1999. Distributed hydrological modelling in the Canadian Boreal Forests: subsurface model development, land surface model improvement and modelling results. *MASc Thesis*, University of Waterloo.

Whittaker RH, Linkins GE. 1975. *Primary Production of the Biosphere*. Springer-Verlag: New York.

Weisman RN. 1977. Snowmelt: A two-dimensional turbulent diffusion model. *Water Resources Research.* 13**,** No. 2: pp. 337 – 342.

Woo M, Marsh P, Pomeroy JW. 2000. Snow, frozen soils and permafrost hydrology in Canada 1995 – 1998. *Hydrological Processes* 1**4** 1591-1611.

Wood EF, Sivapalan M, Bevan K, Band L 1988. Effects of spatial variability and scale with implications to hydrologic modeling. *J. Hydrol.* 102 29 – 47.